Isotope measurements of atmospheric carbon monoxide at a remote site in East Asia and in urban areas

(東アジアの清浄大気および都市大気における一酸化炭素の同位体比測定)

KATO Shungo
加藤 俊吾

Isotope measurements of atmospheric carbon monoxide at a remote site in East Asia and in urban areas

東アジアの清浄大気および都市大気における一酸化炭素の同位体比測定

KATO Shungo

加藤 俊吾

Thesis submitted to the University of Tokyo

for a degree of Doctor of Philosophy

in

Interdisciplinary Course on Advanced Science and Technology

Graduate School, Division of Engineering

Table of contents

Abstract

CO is one of the important species in the atmospheric chemistry, since it reacts most of OH radicals and influences the oxidation capacity in the atmosphere. In spite of its importance, source and sink fluxes of atmospheric CO have large uncertainties. There is another question about seasonal variation of CO. Some atmospheric CO measurements at remote sites show "spring peak", maximum concentration appears in April delaying from the expected results determined by OH radical concentration. Isotopic measurement is a useful tool to estimate source, and expected to help more understanding of these questions.

In this work measurements of stable and radio isotopes on atmospheric CO are carried out at Happo, a remote site in Japan. This is the first isotopic measurements of CO in Asia. From the analyzed results, it is expected that northern mid-latitude is affected by CO from fossil fuel combustion considerably. Using a box model calculation, observed isotopic values and its seasonal variations are reproduced. In spring, CO from fossil fuel combustion would make "spring peak".

To obtain the basic data for isotopic analysis on CO, stable isotopic compositions of CO from fossil fuel combustion and biomass burning are measured. Urban air is also measured and it is shown that $\delta^{18}O$ measurements is a good indicator to assess pollution from fossil fuel combustion.

In **chapter 1**, features of atmospheric CO are explained; sink, source, latitudinal distribution, seasonal variation and recent trend. CO measurements in East Asia are also explained. In **chapter 2**, isotopic measurements of CO are summarized. There are four isotopomers for CO; ^{13}CO, $C^{18}O$, $C^{17}O$ and ^{14}CO. The units used for isotopic measurements and kinetic isotope effect, which is very important to discuss about atmospheric CO, are also explained. In **chapter 3**, the experimental set up, CO extraction line, CO sampling compressor and some information about the isotope mass spectrometer are explained. In **chapter 4**, stable isotopic compositions of CO from car

exhaust, which is one of the main CO sources especially in the northern hemisphere, are measured. In **chapter 5**, stable isotopic compositions of CO from biomass burning, which is also an important CO source especially in the southern hemisphere, are measured. Controlled cigarette burning experiments are also done. This is more simple and easier measurement of burning material under controlled condition. These kinds of basic measurements on CO sources are almost not yet done. In **chapter 6**, CO measurements in urban areas, Mainz and Tokyo, have been carried out and it is demonstrated that isotopic measurement is a very good indicator to estimate the contribution of CO pollution by car exhaust, especially using $\delta^{18}O$ values. In **chapter 7**, measurement of ambient air at Happo is explained. There is no report for isotopic measurement on CO in Asia and in a clean site in the northern mid-hemisphere for stable isotopic compositions of CO. Results are compared with isotopic measurements on CO at various places over the world reported by other researchers. There are characters of isotopic compositions at different sites. A box model calculation for CO concentration, $\delta^{18}O$, $\delta^{13}C$ and ^{14}CO simulating northern mid-hemisphere is performed. There is no trial of these kinds of model calculation for stable isotopes in the northern hemisphere. In **chapter 8**, Happo data affected by pollution are examined using dilution plot. Also backward trajectory analysis is performed.

Chapter 1

Review of CO measurements and purpose of this study

In this chapter general information on atmospheric CO is summarized; sink and source, seasonal variation and latitudinal variation. CO measurements in East Asia are also explained with the interest of ozone increasing trend. Also the purpose of this study is documented.

1-1 General introduction

Carbon monoxide (CO) is one of the important trace components in the atmosphere. CO itself is known as a toxic gas combining strongly with hemoglobin, but CO concentration in usual atmosphere is too low to work as toxic gas. The importance of CO in the clean atmosphere is reaction with OH radicals, which have high reactivity and oxidize most of the trace components in the atmosphere. For example, some global warming gases (CH_4, SF_6 etc.) are removed almost only by OH radicals. In the clean atmosphere the main sink of OH radical is the reaction with CO [*Thompson*, 1992; *Crutzen and Zimmermann*, 1991]. Therefore change of CO concentration will affect indirectly the oxidation capacity of the atmosphere. Atmospheric CO is removed 90-95 % by the oxidation reaction with OH radicals (R1) [*Logan et al.*, 1981]. CO uptake to soil is proposed as a miner CO sink process. The resulted H atom in reaction (R1) reacts with O_2 immediately and forms HO_2 radical in the reaction (R2). HO_2 radical plays an important role in the chain reaction of O_3 production connecting with NO_x (R3-R5).

$$CO + OH \rightarrow CO_2 + H \quad (R1)$$

$$H + O_2 + M \rightarrow HO_2 + M \quad (R2)$$

$$NO + HO_2 \rightarrow NO_2 + OH \quad (R3)$$

$$NO_2 + h\nu \rightarrow NO + O \quad (R4)$$

$$O + O_2 + M \rightarrow O_3 + M \quad (R5)$$

There are four main CO sources: fossil fuel combustion, biomass burning, CH_4 oxidation by OH and oxidation of nonmethane hydrocarbons (NMHC). Other minor CO sources are emission from ocean [*Springer-Young et al.*, 1996; *Johnson and Bates*, 1996; *Bates et al.*, 1995] and direct emission from plants. The first two main sources are induced by human activities. CO from fossil fuel combustion is mainly emitted as automobile exhaust, therefore this CO source is important in the northern hemisphere, where about 90 % of the human activity takes place. Biomass burning is the agricultural conduct or natural forest fires, and is an important CO source especially in the southern hemisphere [*Crutzen et al.*, 1979; *Crutzen and Andreae*, 1990]. Reaction mechanism of CO production from CH_4 oxidation is shown (R6-R12) omitting some minor branch reaction paths. After the initial oxidation step (R6), reactions progress in a short time scale and form HCHO, which life time is about 15 hour. HCHO has two passes to form CO: reaction with OH (R10-R11) and photolysis (R12). CO production from NMHC oxidation is mainly oxidation of terpenes and isoprene, which are emitted by plants and oxidized in a few hours [*Zimmerman et al.*, 1978; *Guenther et al.*, 1995]. Anthropogenic NMHC produced by industrial activities is not important as a CO source in a global scale. The budget of these CO sources and sink is estimated but still has considerable uncertainty. In Table 1-1 estimated budgets by some researchers are summarized. Roughly the main four sources are comparable contribution and they are not negligible.

$$CH_4 + OH \rightarrow CH_3 + H_2O \quad (R6)$$

$$CH_3 + O_2 \rightarrow CH_3O_2 \quad (R7)$$

$$CH_3O_2 + NO \rightarrow CH_3O + NO_2 \quad (R8)$$

$$CH_3O + O_2 \rightarrow HCHO + HO_2 \quad (R9)$$

$$HCHO + OH \rightarrow CHO + H_2O \quad (R10)$$

$$CHO + O_2 \rightarrow \boxed{CO} + HO_2 \quad (R11)$$

$$HCHO + h\nu \rightarrow \boxed{CO} + H_2 \quad (R12)$$

Table 1-1. CO budgets estimated by several researchers

(NH/SH)	LPWM	VED	SC	PG
SOURCE				
Fossil Fuel	450 (425/25)	640	640±200	440±150
Biomass Burning	655 (415/240)	1250±950	1000±600	700±200
NMHC oxidation	650 (465/185)	1000±800	900±500	800±400
CH_4 oxidation	810 (405/405)	950±350	600±300	600±200
Ocean	40 (13/27)	100	100±90	50±40
Vegetation	130 (90/40)	50	75±25	75±25
TOTAL	2735	3990±2100	3315±1700	2700±1000
SINK				
Reaction with OH	3170 (1890/1280)	2600±950	2000±600	
Uptake to soil	250 (210/40)	320	390±140	

Unit is [TgCO yr^{-1}]. LPWM: *Logan et al.* [1981], VED: *Volz et al.* [1981], SC: *Seiler and Conrad* [1987], PG: *Pacyna and Graedel* [1995]. NH and SH means the northern hemisphere and the southern hemisphere.

The lifetime of CO in the atmosphere is about 1-2 months, which is not enough long to homogenize in a hemisphere and much shorter than the time scale of interhemispheric exchange. Therefore there is a wide range of local and interhemispheric concentration variation. Lower concentrations are found in marine air and higher concentrations are found near industrial, polluted area. Also, CO concentration is higher in the northern hemisphere (about 150 ppb) and lower in the southern hemisphere (about 50 ppb). This interhemispheric gradient shown in Figure 1-1 [*Novelli et al.*, 1998] is considerably large since CO from fossil fuel combustion is produced mostly in the northern hemisphere. Even within the northern hemisphere there is a latitudinal gradient; higher CO concentration at higher latitude and lower CO at lower latitude.

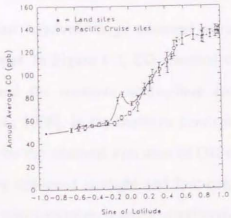

Figure 1-1. Average annual interhemispheric gradient, 1992-1995 [*Novelli et al.*, 1998]. Solid circles are land sites, and open circles are from the Pacific shipboard sampling program. Error bars are 1σ of four annual mean CO mixing ratios.

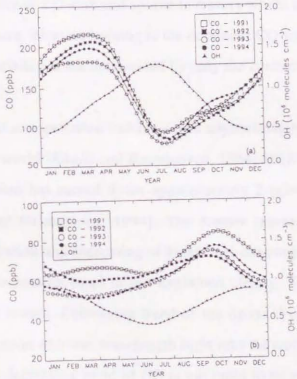

Figure 1-2. Overlay of smoothed CO and OH in the northern hemisphere (a) and southern hemisphere (b) [*Novelli et al.*, 1998]. OH concentrations were taken from a curve fit to the monthly concentrations at 950 mbar provided by *Spivakovsky et al.* [1990].

CO concentration has also relatively large seasonal variation; high during winter-spring and low during summer. In Figure 1-2, CO seasonal variations at remote sites in the northern hemisphere and the southern hemisphere are shown with OH radical concentrations [*Novelli et al.*, 1998]. In the northern hemisphere, the seasonal variation of CO is explained roughly by the seasonal variation of OH radicals; high concentration during summer is caused by enhanced sunlight and low concentration during winter is due to less sunlight. CO concentration reaches maximum in February-March, then decreases steeply and reaches minimum in July-August. After minimum, CO concentration increases gradually until next maximum. Seasonal cycle of CO concentration is not symmetric. Some measurements show "spring peak", the period of highest CO concentration shifts later and appears in March to April. These seasonal cycles indicate complexity of CO sink and source inventory which changes over seasons. In the southern hemisphere, biomass burning is the dominant CO source and the seasonal cycle of CO seasonal variation is not determined by only the concentration of OH radical.

Until early 1980s, CO concentration had increased approximately 2 ppbv yr^{-1} at many sampling sites over the world [*Khalil and Rasmusssen*, 1984; 1988]. But from 1986, the trend of CO concentration has turned down approximately 2 ppbv yr^{-1} [*Novelli et al.*, 1998; 1994; *Khalil and Rasmusssen*, 1994]. The former increasing trend had been explained as industrialization and increasing of fossil fuel consumption. There are some explanations, but the decreasing trend is not explained clearly. The increasing of OH concentration may be a reason. Decreasing trend of the ozone layer in the stratosphere will permit more penetration of lower wavelength light into the troposphere and enhance OH production. But the decreasing trend of CO is too rapid to be explained in this way. The control of CO emission from anthropogenic activities, car exhaust in the northern hemisphere is also thought as one reason. But this explanation is not enough for CO decrease in the southern hemisphere. The decreasing emission from biomass burning would be the persuasive reason [*Khalil and Rasmusssen*, 1994]. To investigate atmospheric CO concentration change in recent centuries, ice core had been analyzed by

Haan et al. [1996]. After 1850 CO began to increase in Greenland, but it remains constant in Antarctica. Now NOAA/CMDL flask sampling network covers world wide and monitors CO concentration changes at remote sites and at some locally effected sites [*Novelli et al.*, 1998; 1992].

Comparing with other typical pollutant (SO_x and NO_x) in urban and industrial areas, which cause acid rain and tropospheric ozone production, CO has longer lifetime and can be used as a good indicator for long-range transport of polluted air mass [*Jaffe et al.*, 1997; *Derwent et al.*, 1998]. When there is a good correlation between CO and ozone concentrations, this suggests that ozone is produced photochemically by NO_x (R3-R5), which is emitted concomitantly with CO in an industrial area. Nitrogen compounds are transported as PAN and HNO_3, which have longer lifetime than NO_x, and produce ozone photochemically or cause acidification, but they are more difficult to measure than CO.

1-2 CO measurements in East Asia

Asia is one of the most populated area in the world and expected more rapid development in the future, with concern for air pollution in large regional scale, as well as local pollution [*Kato and Akimoto*, 1992]. But comparing to other activated areas, i.e. North America and Europe, atmospheric measurements are poor in Asia. Recent measurements at rural sites in Japan show increasing trend (approximate 2 % yr^{-1}) of the ozone concentration [*Akimoto et al.*, 1994; *Lee et al.*, 1998], which indicates that large scale pollution is progressing in East Asia. In Japan, westerly wind is dominant and the Siberian continental air is transported during winter. Such air mass can be influenced by pollutants emitted in China and Korea. On the other hand, clean Pacific marine air mass with low CO concentration is dominant during summer, and the pollutants emitted in Japan may influence to China and Korea. In the case of Happo, the air comes across Japan in some case and is polluted, especially during summer.

In PEM-West A campaign carried out in the period of September-October, 1991, ozone measurements at three remote islands in East Asia (Oki, Okinawa and Kenting) were

categorized by air mass origin. This revealed higher ozone concentration in the air mass transported from northwesterly continent [*Akimoto et al.*, 1996; *Akimoto*, 1997].

Jaffe et al. [1996] measured NO, NO_y, CO and O_3 at Oki island in Japan during PEM-WEST A campaign and found good correlation between NO_y, CO and O_3 during daytime, which indicates photochemical production of O_3. In successive PEM-West B campaign during February-March, 1994, *Kajii et al.* [1997] measured CO and other trace components at Oki island, and categorized CO concentration by air mass origin. In figure 1-3 average ozone and CO concentration measured during PEM-West A (open circle) and PEM-West B (solid circle) are plotted for 4 air mass origins (N/NE, NW, WNW and W) [*Kajii et al.*, 1997]. Among continental air mass, CO concentration and ozone concentration are the lowest when air mass arrived from N/NE, where is less populated area in Siberia, and the highest from W, where is populated area in China. CO concentration of PEM-West B is higher than PEM-West A, because the measurements were carried out in different season; CO concentration is higher during February-March than during September-October. *Kajii et al.* [1998] measured CO (1996) and O_3 (1994-1996) at Happo. CO and ozone concentration maximum appear in April, and explained that the spring maximum of ozone concentration is caused by photochemical production since good correlation of CO and ozone was observed during April-July. In Figure 1-4, continuous CO measurements by NDIR (non dispersed infrared) method at Happo are shown (median of 1996-1998). The CO concentration is higher than those in the northern high-latitude over year. To reduce the influence of pollution in Japan, median is used rather than average. *Zhao et al.* [1997] observed atmospheric CO by infrared solar spectra over Japan (Rikubetsu) and found the maximum of 219 ± 26 ppb in April and the minimum of 115 ± 7 ppb in September at 0-3 km average. The data also show that CO concentrations and seasonal amplitude decrease with altitude.

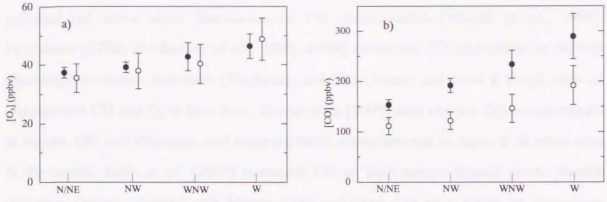

Figure 1-3. Mean ozone (a) and mean CO (b) concentration plots observed during PEM-WEST A (open circle) and PEM-WEST B (solid circle) for the four air mass patterns. [*Kajii et at.,* 1997]. Error bars show single standard deviation.

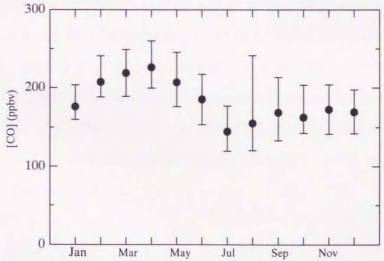

Figure 1-4. CO measurements at Happo by NDIR method. It is given as median of measurements during 1996-1998 and error bars are 25 %and 75 % deviation.

The flask sampling network of NOAA has sampling stations in East Asia at Tae-ahn peninsula (Korea) and Ulaan Uul (Mongolia). Those sites are thought to be regionally polluted and show some fluctuation of CO concentration [*Novelli et al.*, 1998]. *Pochanart* [1998; *Pochanart et al.*, 1996; 1999] measured CO and ozone in Mondy (Russia), Srinakarin, Inthanon (Thailand), and Oki (Japan) and built a rough view of atmospheric CO and O_3 in East Asia. *Narita et al.* [1999] also explain CO measurements at Happo, Oki and Okinawa, and compare these measurements in Japan with other sites in the world. *Jaffe et al.* [1997] measured CO at four remote islands in the Pacific (Shemya, Guam, Midway and Mauna Loa) and used CO as a tracer of long-range transport of polluted air mass combining with backward trajectory calculation. When CO concentration at these islands is higher (> 5 ppb) than average seasonal cycle, the air mass comes from the source region (East Asia) in many cases.

1-3 Purpose of this study

The spring maximum of ozone in Japan is explained as photochemical production but still there is a question. Why the CO maximum appears in spring? Isotopic measurements offer more information about CO sources and will lead better understanding of CO behavior.

To discuss the isotopic compositions of atmospheric CO, it is strongly desired to know the isotopic compositions of CO sources. In spite of some atmospheric measurements at remote sites, isotopic measurements of CO sources are relatively poor. One purpose of this work is to know the isotopic compositions of CO from car exhaust and biomass burning. CO from urban area is an important source when discussing about the northern hemisphere. The measurements of isotopic composition in urban area are interesting to see the influence of CO pollution from car exhaust. There are some isotopic CO measurements of the clean atmosphere; at high and mid latitude in the clean southern hemisphere and at high latitude in the northern hemisphere. However, in the northern mid-hemisphere where CO emission from human activity is intensive, there is no report of isotopic measurements of CO in the clean atmosphere at remote sites. The other purpose of this work is to see the CO isotopic compositions in middle latitude and to make more understanding of CO budget and to see the influence of human activity in the northern hemisphere. Also this work is the first measurements of isotopic compositions on CO in East Asia and it is interesting to see the characters in this region, including the cause of the spring maximum.

Chapter 2

Review of isotope measurements on CO

Isotopic measurements of carbon and oxygen on atmospheric CO are reviewed in this chapter with the information about δ notation and kinetic isotope effect. There are four isotopomers for CO; ^{13}CO, $C^{18}O$, $C^{17}O$ and ^{14}CO. ^{13}CO and $C^{18}O$ have been analyzed most frequently. $C^{17}O$ is interested recently since it involves Mass Independent Fractionation. ^{14}CO is radio-isotope and offers unique information about average concentration of OH radical in the atmosphere. The results are reviewed by *Conny* [1998] and *Brenninkmeijer et al.* [1999]. *Keya* [1987] also reviewed CO isotopic measurements with other atmospheric species.

2-1 δ notation

Isotopic compositions of carbon and oxygen are roughly constant in nature. $^{13}C/^{12}C$ is about 0.011 and $^{18}O/^{16}O$ is about 0.002. But there are slight fluctuations because of the difference of reactivity or other physical properties in each isotope, especially in biological processes. Usually light isotope reacts faster than heavy isotope. For expressing these slight differences of isotopic compositions, δ notation is employed in general. The difference of isotopic composition of samples is compared with standard in the unit of "‰" (per mil; 1/1000). Here the relationship is shown in the case of $^{13}C/^{12}C$, for example.

$$\delta^{13}C = \{(^{13}C/^{12}C)_{sample} / (^{13}C/^{12}C)_{standard} - 1\} \times 1000\ ‰ \qquad \text{(Eq.2-1)}$$

Standards are used V-PDB (Vinna Pee Dee Beremnite, $^{13}C/^{12}C = 0.0112372$) [*Craig*, 1957] for carbon and V-SMOW (Vinna Standard Mean Ocean Water, $^{18}O/^{16}O = 2005.20\pm0.45 \times 10^{-6}$) [*Gonfiantini*, 1978] for oxygen. In some cases, for example in the case of CO_2, oxygen isotopic compositions are expressed in V-PDB unit. The

relationship between V-SMOW and V-PDB is as follows [Brenninkmeijer, 1993].

$$\delta\,^{18}O_{V\text{-}SMOW} = 1.04145\times\delta^{18}O_{V\text{-}PDB} + 41.46 \qquad \text{(Eq.2-2)}$$

When explaining the isotopic compositions, expression of "heavy" or "light" are often used. Those mean "enriched in heavier isotope" or "less containing heavier isotope", respectively. More positive or less negative values indicate "heavy" isotopic compositions.

In the case of ^{14}CO, the abundance in the atmosphere is too small to use δ notation. The results of ^{14}CO measurements by an accelerator mass spectrometer are expressed in the unit of percent of Modern Carbon (pMC); the ^{14}C abundance of sample is compared with Modern Carbon ($^{14}C/C_{toatal} = 1.189\times10^{-12}$; C_{total} denotes $^{13}C+^{12}C$) in % unit. It is preferred to express ^{14}CO in the unit of molecules cm^{-3} at standard condition (273.15K, 1013.25hPa). The relationship between this molecules cm^{-3} unit and pMC is as follows [Brenninkmeijer, 1993].

$$[^{14}CO] = pMC/100 \times \{(1000+\delta^{13}C)/975\}^{2} \times 1.189\times10^{-12} \times \{^{12}CO/(^{12}CO+^{13}CO)\} \times [CO] \qquad \text{(Eq.2-3)}$$

2-2 ^{13}CO and $C^{18}O$

The first measurements of atmospheric ^{13}CO and $C^{18}O$ were performed by *Stevens et al.* [1972] and *Stevens and Krout* [1972]. They measured some urban atmosphere over the world and estimated the average isotopic compositions of CO from car exhaust, $\delta^{13}C = -27.4 \pm 0.3$ ‰ and $\delta^{18}O = 24.6$ ‰. The carbon isotopic composition is close to that of petroleum and the oxygen isotopic composition is close to that of atmospheric oxygen (23.5 ‰ [*Kroopnick and Craig*, 1972]). They also measured atmospheric CO in suburb Illinois during 1970 to 1971. The isotopic compositions show seasonal variation and they estimated CO sources for each season. The high CO concentration and heavy $\delta^{18}O$ value especially during winter seem to be influenced by urban air (car exhaust). *Stevens and*

Wagner [1989] discussed isotopic compositions of CO source using unpolluted data (< 200 ppb in CO) in this Illinois measurements during summer. The estimated CO source in clean air (unpolluted by car exhaust) have $\delta^{13}C$ = -32 ‰ and $\delta^{18}O$ = 15 ‰, and they adopted those values to the $\delta^{13}C$ value of CO from oxidized nonmethane hydrocarbons, and to the $\delta^{18}O$ value of CO from oxidized methane and nonmethane hydrocarbons. They also mentioned about the kinetic isotope effect (KIE) of CO uptake by soil bacteria, -6 ‰ for carbon and -11 ‰ for oxygen.

Brenninkmeijer [1993] reported isotopic compositions of atmospheric CO in Scott Base (78°S), Antarctica during July 1991 to March 1992. The results show clear seasonal variations, but they are quite lighter isotopic compositions than the Illinois measurements both in carbon and oxygen. For $\delta^{13}C$, the maximum is about -27 ‰ at November-December and the minimum is less than -31 ‰ during summer. $\delta^{18}O$ show the maximum -2 ‰ around October and the minimum less than -7 ‰ during summer.

The measurements at Baring Head (41°S), New Zealand have shown CO concentration and $\delta^{13}C$ during the period June 1989 to June 1995 [*Manning et al.*, 1997]. $\delta^{13}C$ shows the maximum -27.3 ‰ in December and the minimum -31.6 ‰ in March. In spite of latitudinal difference, CO concentration and isotopic value are close in Scott Base and Baring Head. This means well-mixing of air in the southern hemisphere. In that report they used zonally averaged atmospheric model to fit the amount of CO sources to the observed CO concentration and $\delta^{13}C$ seasonal cycles in the southern hemisphere.

The measurements at Spitsbergen (79°N) during polar sunrise period in 1995 (ARCTOC Champaign) are explained by *Röckmann and Brenninkmeijer* [1997]. The $^{13}C/^{12}C$ ratio changes very rapidly in 6 weeks; from -25.7 ‰ to -23.4 ‰ . This is the heaviest $\delta^{13}C$ found in atmospheric CO measurements. $\delta^{18}O$ decreased from 8.5 ‰ to 2.5 ‰. They explained these rapid isotopic composition changes by the kinetic isotope effect of CO + OH (chapter 2-3). *Röckmann et al.* [1999] also reported the $\delta^{13}C$ of CO in spring at Spitsbergen and observed slight decrease of $\delta^{13}C$ caused by CO production from CH_4 + Cl during the ozone depression events.

There are also figures of $\delta^{18}O$ value measured at Spitsbergen (79°N), Alert (81°N) and Izaña (28°N) [*Röckmann et al.*, 1998a; 1998b], but these reports mainly focused on $C^{17}O$

measurements. At high latitude in the northern hemisphere (Spitsbergen and Alert), they show almost same seasonal change in CO concentration and isotopic ratios. The maximum $\delta^{18}O$ is about 10 ‰ in February to March, and the minimum $\delta^{18}O$ is less than 4 ‰ in summer. On the other hand, $\delta^{18}O$ values in Izaña show only small seasonal variation.

There are also some reports about measurements using an aircraft. *Mak and Brenninkmeijer* [1998] show latitudinal variation of $\delta^{13}C$ and $\delta^{18}O$ in several flights during 1991 to 1993. In August, it is not found that clear latitudinal trend of $\delta^{13}C$, but $\delta^{18}O$ is light around equator. In February, there is a large latitudinal gradient both carbon and oxygen; heavier in the northern hemisphere and lighter in the southern hemisphere.

Brenninkmeijer et al. [1995, 1996] and *Brenninkmeijer and Robert*, [1994] measured CO isotopes in the lower stratosphere. They found very light $\delta^{13}C$ value of about -43 ‰ as altitude increase and explained the effect by very light CO produced by large kinetic isotope effect of CH_4 oxidation by Cl atoms [*Müller et al.*, 1996].

$$CH_4 + Cl \rightarrow CH_3 + HCl \quad (R13)$$

Sakugawa and Kaplan [1997] reported urban atmospheric CO measurements in Los Angeles, where CO concentration is high and $C^{18}O$ shows urban isotopic compositions. *Bergamaschi et al.* [1998] and *Crutzen et al.* [1998] reported CO and CH_4 isotopic measurements using Siberian railway in August, 1996. They attributed high CO concentration in same samples to biomass burning based on the isotopic analysis. *Conny et al.* [1997] conducted model calculation on $\delta^{13}C$ in Brazil during biomass fire periods and estimated CO concentration and $\delta^{13}C$ in the biomass burning area and its surrounding.

2-3 Kinetic Isotope Effect (KIE)

In general, the lighter isotope reacts faster than the heavier isotope, so in the case of sink reaction, the isotopic composition of the interested species become heavier as the

sink reaction progresses. In the case of CO, the sink reaction, CO + OH (R1), is affected by a KIE and it shows interesting features; totally different KIE in carbon and oxygen. Figure 2-1 and 2-2 are results of the KIE measurements reported by *Stevens et al.* [1980] and *Stevens and Wagner* [1989]. Similar results have been obtained by other researchers [*Smit et al.*, 1982; *Röckmann et al.*, 1998b]. In the case of carbon the extent of the KIE depends strongly on pressure. At atmospheric pressure, α=1.006 and it decreases less than unity at low pressure (here $\alpha = k_{12CO+OH} / k_{13CO+OH}$ or $k_{C16O+OH} / k_{C18O+OH}$). In the case of oxygen, the KIE is almost independent from pressure, but it is inverse (α=0.990), i.e. heavier isotope reacts faster and $\delta^{18}O$ becomes lighter as the sink reaction progresses.

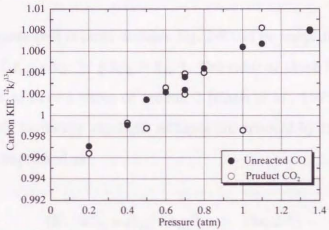

Figure 2-1. KIE for carbon isotopes vs. pressure of air for the reaction CO+OH+M [Stevens and Wagner, 1989]

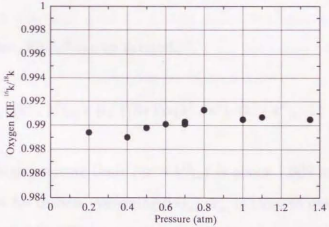

Figure 2-2. KIE for oxygen isotopes vs. pressure of air for the reaction CO+OH+M [Stevens and Wagner, 1989]

The reaction mechanism is explained as follows [*Stevens et al.*, 1980].

$$CO + OH \overset{(a)}{\rightarrow} \overset{(-a)}{\leftarrow} HOCO^* \overset{(b)}{\rightarrow} CO_2 + H$$
$$\downarrow (c) + M$$
$$HOCO + X \rightarrow \text{products}$$

HOCO* is an activated complex and step (-a) is a reverse reaction from activated complex. The overall rate constant of reaction CO + OH (R1) is expressed as following.

$$k = k_{(a)} \times \{ k_{(b)} + k_{(c)} \times [M] \} / \{ k_{(-a)} + k_{(b)} + k_{(c)} \times [M] \} \quad \text{(Eq. 2-4)}$$

At high pressure where [M] is large enough, Eq. 2-4 can be simplified as $k_\infty = k_{(a)}$, and at low pressure $k_0 = \{ k_{(a)} \times k_{(b)} \} / \{ k_{(-a)} + k_{(b)} \}$. The ratio of these limiting rates, $k_\infty/k_0 = 1+k_{(-a)}/k_{(b)}$, appears to have a value of around 2 [*Chan et al.*, 1977], thus $k_{(-a)}/k_{(b)}$ (β) is close to unity. When the heavy and light isotopes are denoted by H and L, high and low pressure limits are expressed as

$$(k^L / k^H)_\infty = (k_{(a)}{}^L / k_{(a)}{}^H) \quad \text{(Eq.2-5)}$$

$$(k^L / k^H)_0 = (k_{(a)}{}^L \times k_{(b)}{}^L) / (k_{(a)}{}^H \times k_{(b)}{}^H) \times (k_{(-a)}{}^H + k_{(b)}{}^H) / (k_{(-a)}{}^L + k_{(b)}{}^L) \quad \text{(Eq.2-6).}$$

From these equations, Eq.2-7 can be derived.

$$(k^L / k^H)_{(-a)} / (k^L / k^H)_{(b)} = \beta / \{(\beta+1) \times (k^L / k^H)_0 / (k^L / k^H)_\infty - 1\} \quad \text{(Eq.2-7)}$$

From Figure 2-1, high pressure limit $\{(k^L / k^H)_\infty\}$ is about 1.009 and low pressure limit $\{(k^L / k^H)_0\}$ is 0.994 for carbon. Assuming $\beta = k_{(-a)}/k_{(b)}$ is close to unity, $(k^{12} / k^{13})_{(-a)} / (k^{12} / k^{13})_{(b)} = 1.03$. Most of this KIE is associated with the rupture of the C-O bond in the reversion of the activated HOCO to reactants (step -a). The Positive KIE of ^{13}C and the negative KIE of ^{18}O are caused by initial step (step a) because they are independent on pressure.

The isotopic change as the reaction proceeds can be calculated by Rayleigh's Equation.

$$\delta_{fin} = \delta_{ini} + (1000 + \delta_{ini}) \times (1/\alpha - 1) \times \log([CO]_{fin}/[CO]_{ini}) \quad \text{(Eq.2-8)}$$

where δ is isotopic composition denoted δ notation and α is the ratio of reaction rate for light and heavy isotopes, and "fin" and "ini" mean final and initial, respectively. In Figure 2-3 and 2-4, calculated δ values using Eq.2-8 are plotted against reacted proportion $(1 - [CO]_{fin}/[CO]_{ini})$ for ^{13}CO and $C^{18}O$, respectively. The initial δ values are set zero in both case, and α values are 1.006 and 1.003 for carbon and α = 0.990 for oxygen. 1.003 is deduced as the average KIE of tropospheric CO because of its pressure dependence [*Manning et al.*, 1997]. Here one can see $\delta^{13}C$ increase and $\delta^{18}O$ decrease as the reaction CO + OH (R1) progresses.

The CO producing reaction, CH_4 + OH (R6), also involves a KIE in carbon. *Cantrell et al.* [1990] reported α=1.0054±0.0009 and *Davidson et al.* [1987] reported α=1.010±0.007, therefore CO from CH_4 oxidation becomes lighter than original CH_4. In the case of CH_4 + Cl (R13), which is interesting under ozone hole condition as a very depleted CO source and impact for $^{13}C/^{12}C$ ratio of stratospheric CH_4 [*Bergamaschi et al.*, 1996], the KIE is very large (α=1.066±0.002 at 297K [*Saueressig et al.*, 1995]). In theoretical calculation [*Gupta et al.*, 1997], CH_4 + OH has a larger KIE (α=1.01) and CH_4 + Cl has a smaller KIE (α=1.034) than experimental results.

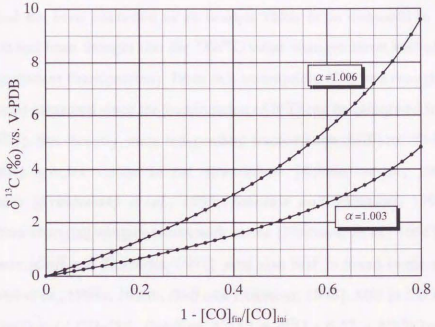

Figure 2-3. Calcurated $\delta^{13}C$ fractionatin of CO+OH by Rayleigh's equation

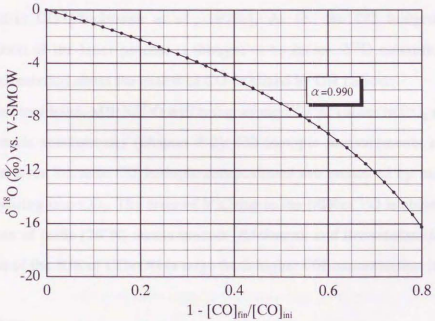

Figure 2-4. Calcurated $\delta^{18}O$ fractionatin of CO+OH by Rayleigh's equation

2-4 $C^{17}O$

$\delta^{17}O$ had not been interested as an isotopic value to be measured in the atmosphere, because it had been thought that the $^{17}O/^{16}O$ value changes about half of $^{18}O/^{16}O$ change (Mass Dependent Fractionation). From this assumption, $\delta^{17}O$ was thought that it was not needed to be measured since the fractionation of $\delta^{17}O$ can be calculated from $\delta^{18}O$ ($\delta^{17}O = 0.52 \times \delta^{18}O$). But recently, mass independent fractionation (MIF) of ^{17}O is found in some atmospheric species; ozone in the stratosphere [*Schüler et al.*, 1990] and in the troposphere [*Krankowsky et al.*, 1995; *Johnston and Thiemens*, 1997], CO_2 in the stratosphere changing oxygen atoms with ozone [*Thiemens et al.*, 1991] and N_2O in the troposphere [*Cliff and Thiemens*, 1997]. And also MIF is found in the tropospheric CO [*Röckmann et al.*, 1998a; 1998b; *Huff and Thiemens*, 1998]. MIF in CO is caused mainly by the reaction of CO+OH, therefore $\Delta^{17}O$ ($\equiv \delta^{17}O - 0.52 \times \delta^{18}O$) becomes larger in summer, when the OH concentration becomes higher. The oxidation of nonmethane hydrocarbon (isoprene) by ozone is also pointed out as a cause of $\delta^{17}O$ enrichment of atmospheric CO [*Röckmann et al.*, 1998a]. As for the CO budgets, however, the contribution of the latter process is thought to be minor. $\delta^{17}O$ measurements will offer useful information about the extent of CO oxidized by OH radicals.

On the other hand, MIF of ^{17}O will bring wrong $^{13}C/^{12}C$ values in CO_2 measurements in isotope mass spectrometer (chapter 3-2). CO isotopic measurements are also not free from this error, because CO isotopic compositions are measured by mass spectrometer after oxidizing into CO_2. The error of $\delta^{13}C$ due to the MIF of ^{17}O is about 0.08 to 0.25 ‰ in the case of Izaña (28°N) measurements [*Röckmann and Brenninkmeijer*, 1998], where the effect of the KIE of CO+OH is large from higher OH concentration in low latitude.

2-5 ^{14}CO

^{14}C is radio isotope and its lifetime is about 5730 years. Neutrons react with ^{14}N and produce ^{14}C and protons in the upper atmosphere. About 95 % of ^{14}C become ^{14}CO.

$$^{14}N\ (n,p)\ ^{14}C \qquad (R14)$$

$$^{14}C + O_2 \rightarrow {}^{14}CO + O \qquad (R15)$$

The production rate of ^{14}CO is dependent on altitude; the maximum production is at about 16 km and production of ^{14}CO takes place 50 % in the stratosphere and 50 % in the troposphere [*Jöckel et al.*, 1999]. The production of ^{14}CO is also influenced by the 11 year solar cycle. The recycled carbon (^{14}CO from biomass burning and oxidation of methane and nonmethane hydrocarbons) make some influence; about 0.03 molecules cm^{-3} per 1 ppb CO. The local CO pollution from biomass burning will influence ^{14}CO data [*Bergamaschi et al.*, 1998]. As the sink reaction of ^{14}CO is almost only $^{14}CO + OH$ and its production can be calculated from cosmic ray, ^{14}CO is a unique tool to assess the OH concentration in the atmosphere like CH_3CCl_3 [*Spivakovsky et al.*, 1990; *Primm et al.*, 1987].

The first measurement of ^{14}CO in the atmosphere was done by *MacKey et al.* [1963]. Then *Weinstock* [1969] estimated the lifetime of CO in the atmosphere about 0.1 year. *Weinstock and Niki* [1972] estimated tropospheric OH concentration as 2.3×10^6 molecule cm^{-3} from the ^{14}CO concentration. *Weinstock and Changi*, [1974] discussed the global balance of CO by using ^{14}CO and ^{13}CO, $C^{18}O$.

The progressive measurements took place by *Volz et al.* [1981] during 1977 to 1978 in Jülich (51°N), Germany. ^{14}CO has the maximum 25 ± 2 molecules cm^{-3} in January-February and minimum 11 ± 1 molecules cm^{-3} in July-August. Using a model calculation, they estimated average OH concentration in the troposphere, $(6.5\ ^{+3}_{-2}) \times 10^5$ molecules cm^{-3}.

Brenninkmeijer et al. [1992] reported the ^{14}C measurements at Baring Head (41°S) and found lower ^{14}CO concentration than in the northern hemisphere, which would suggest OH concentration is higher in the southern hemisphere. *Brenninkmeijer* [1993] also measured ^{14}CO at Scott Base (78°S) and found almost no differences from measurements at Baring Head. *Röckmann and Brenninkmeijer* [1997] showed ^{14}CO measurements at Spitsbergen (79°N) in the sunrise period of 1995. *Mak and Southon* [1998] measured

^{14}CO at Barbados (13°N) and mentioned that the higher ^{14}CO concentration in the tropics than the model calculation results would be caused by an enhanced air mass transport from mid latitude. Latitudinal gradient of ^{14}CO in the free troposphere is examined by aircraft measurements and comparison with model results suggested supplemental CO sink [*Mak and Brenninkmeijer*, 1992; *Mak et al.*, 1994]. *Brenninkmeijer et al.* [1995; 1996] and *Brenninkmeijer and Roberts*, [1994] measured ^{14}CO in the lower stratosphere. They found that ^{14}CO is enriched in the stratosphere and a very good indicator of stratospheric air .

Radioisotope measurement, ^{14}CO and $^{14}CH_4$, in polluted village had been carried out to reveal the CO pollution source [*Klouda et al.,* 1986; 1988]. *Currie et al.*, [1986] measured ^{14}C in aerosol and carbon containing species. *Sakugawa and Kaplan* [1997] measured ^{14}CO in a megacity (Los Angeles). Even such a very polluted city ^{14}CO data are not influenced by pollution and seasonal variation can be seen, because fossil fuel combustion contains no ^{14}CO. But there was a very high ^{14}CO measurement suspected contamination from biomass burning, which contains "recycled ^{14}C". *Bergamaschi et al.* [1998] also showed that ^{14}CO measurement works as a good indicator to assess the CO from biomass burning in the railway measurement in Siberia.

Felton et al. [1988; 1990] measured local OH concentration using an unique technique. ^{14}CO was injected to ambient air flow, and the reaction $^{14}CO+OH$ produced $^{14}CO_2$. From the $^{14}CO_2$ concentration, OH concentration in the ambient air can be deduced.

Chapter 3

Experimental set up

In this chapter, the CO extraction lines for isotopic analysis are explained together with information about an isotope mass spectrometer and an accelerator mass spectrometer. The air sampling compressor and cylinders are also explained.

3-1 CO extraction line

There are two types of CO extraction lines, made by glass and metal tubes. The glass line is used for clean ambient air samples at Happo. The metal line is used for other experiments (urban air, car exhaust and biomass burning measurements). The glass line is described in detail by *Brenninkmeijer* [1993]. The metal line, which is depicted in Figure 3-1, is simplified in purification parts and can be operated easily with the toughness of metal material, but there is limitation of processing air flow rate. During evacuating by a diaphragm pump, air in the sampled cylinder is introduced into the CO extraction line by a mass flow controller (MFC, max. 10 LM). At first, two very effective liquid nitrogen traps (named Russian doll trap) remove H_2O, CO_2, N_2O and hydrocarbons except for CH_4. This Russian doll trap contains glass thimbles in it and very large surface area is available [*Brenninkmeijer*, 1991; *Brenninkmeijer and Röckmann*, 1996]. In order to oxidize CO into CO_2, Schütze reagent, which contains I_2O_5 supported on silica gel [*Schütze*, 1949], are used. In the case of glass line, the reactor filled with Schütze reagent is kept at a constant temperature (about 30 °C) with a ribbon heater, as the isotope composition of additional oxygen from Schütze reagent may change with temperature. CO_2 oxidized from CO is trapped with another liquid nitrogen trap located down stream of the line. After processing desired sampled air volume, the valves were closed to isolate the purification part and the residual air in the line was pumped by a turbo drug pump. The resulted CO_2 was moved to a glass tube containing P_2O_5 by vacuum operation to remove H_2O perfectly, since small amount of H_2O may be emitted from Schütze reagent.

Then CO_2 derived from CO was closed in a small glass tube whose volume was calibrated (about 0.75 m litter). The amount of this CO_2 gas was calculated from pressure measured by a piezo resistive pressure sensor. The processed total air volume was measured by the domestic gas meter installed after the diaphragm pump, and CO concentration can be calculated from the extracted CO amount and processed total air volume. Then CO_2 gas oxidized from CO was moved to the sample tube, and was brought to the isotope mass spectrometer for $^{13}C/^{12}C$ and $^{18}O/^{16}O$ measurements. The oxygen isotopic composition of CO can be calculated from the isotopic composition of the oxidized CO_2 , since oxidation process by Schütze reagent is just an additional reaction of one oxygen atom onto CO. Also there is no isotopic exchange and original oxygen isotopic composition of CO is conserved [*Brenninkmeijer*, 1993; *Brenninkmeijer and Röckmann*, 1997].

To know the isotopic value of additional oxygen atom from Schütze reagent, regular measurements of isotopically known standard CO gas are required (calibration run). When flowing the air devoid of CO (zero gas) as a main flow, standard CO gas (269 ppm in He) is injected by another MFC (max. 10 ccM) through a thin 1/16 inch metal tube. Controlling the flow rate of two MFCs, desirable CO concentration can be obtained. The small MFC has a total flow integrator and the amount of injected CO can be calculated. The zero gas is generated from ambient air through heated Hopcalite (100 °C) with molecular sieve or Sofnocat catalyst (Molecular Product Ltd.), which removes CO at room temperature. The errors are estimated to be about 2 % for CO concentration, 0.2 ‰ for $\delta^{13}C$, 0.4 ‰ for $\delta^{18}O$.

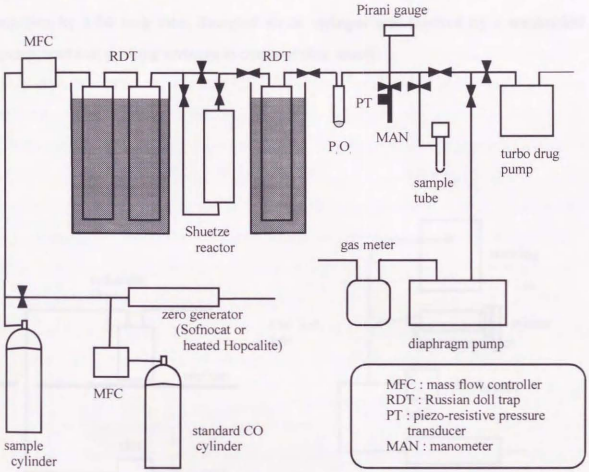

Figure 3-1. CO extraction line (metal line)

Figure 3-2a shows the set up of inlet in ambient air measurements in Mainz and Tokyo (chapter 6). Air taken from out side was introduced through molecular sieve, and injected into the CO extraction line with MFC. Figure 3-2b shows the inlet set up of car exhaust and biomass burning experiments (chapter 4, 5). Sampled air in tedra bag or syringe was injected slowly before MFC to mix with CO zero air. Tedra bag was just connected to the main line by 1/16 inch tube. Sampled air in syringes was injected by a mechanical injector machine, pushing syringes at constant slow speed.

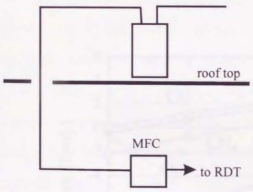

Figure 3-2a. Inlet for ambient air measurement

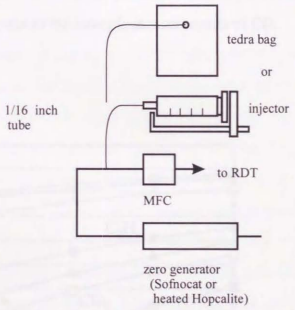

Figure 3-2b. Inlet for car exhausts and biomass measurements

It is important to remove trace gases which make interference before oxidation of CO. If first two liquid nitrogen cold traps do not work efficiently enough and CO_2 or N_2O contaminate into the extracted CO sample, the isotopic value of CO will be disturbed because CO is trapped as the form of CO_2, and N_2O has peak at mass 44 and 45. For example, CO_2 needs to be removed by the factor 10^{-6} when reducing 360 ppm to 0.36 ppb. Double Russian Doll traps can remove CO_2, and N_2O sufficiently enough to prevent their interference. In Figure 3-3, the vapor pressures of several molecules are plotted against temperature. Here one can see that CO, CH_4 and O_2 have much higher vapor pressure than other molecules found in typical atmosphere.

As C_2H_6 has relatively high vapor pressure, C_2H_6 was detected in the mass spectrum of the extracted CO (CO_2) sample in some measurements of urban air. However, when excess C_2H_6 was added during calibration run and mass peaks of C_2H_6 in the extracted sample were found, there was no interference to the isotopic measurements of CO.

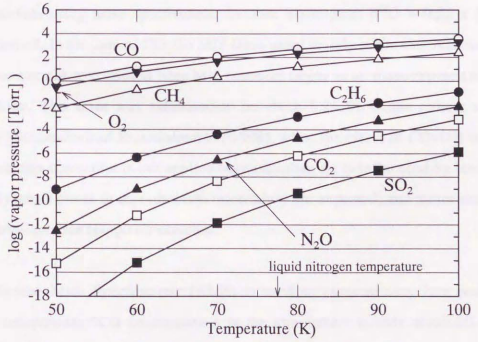

Figure 3-3. Vapor pressure of various atmospheric species

3-2 Isotope mass spectrometer and accelerator mass spectrometer

$^{13}C/^{12}C$ and $^{18}O/^{16}O$ ratios of CO_2 oxidized from CO were measured by isotope mass spectrometer. Finnigan MAT model 252 and Finnigan delta plus were used at Max Planck Institute in Mainz and at NIES (National Institute for Environmental studies, in Tsukuba), respectively.

From the intensity of mass 44, 45 and 46, $^{13}C/^{12}C$ and $^{18}O/^{16}O$ ratios are calculated. Mass 44 is only $^{12}C^{16}O_2$, mass 45 is $^{13}C^{16}O_2$ and $^{12}C^{17}O^{16}O$, and mass 46 is $^{13}C^{17}O^{16}O$, $^{12}C^{17}O^{17}O$ and $^{12}C^{18}O^{16}O$. Since $^{13}C^{17}O^{16}O$ and $^{12}C^{17}O^{17}O$ are very low concentration and can be negligible, the ratio (mass 46)/(mass 44) will be given by the ratio $(^{12}C^{18}O^{16}O)/(^{12}C^{16}O_2)$ and hence the $^{18}O/^{16}O$ ratio can be obtained. (Mass 45)/(mass 44) will be given by the ratio $(^{13}C^{16}O_2 + {}^{12}C^{17}O^{16}O)/(^{12}C^{16}O_2)$. From the assumption of mass dependent fractionation of ^{17}O ($\delta^{17}O = 0.52 \times \delta^{18}O$) and results of (mass 46)/(mass 44), $^{13}C/^{12}C$ ratio can be calculated using the ratio $(^{13}C^{16}O_2 + {}^{12}C^{17}O^{16}O)/(^{12}C^{16}O_2)$. But recently, as mentioned in Chapter 2-2-4, mass independent fractionation (MIF) of ^{17}O has been found in atmospheric species. The MIF will make wrong $^{13}C/^{12}C$ value in CO_2 measurements using mass spectrometer because assumption $\delta^{17}O = 0.52 \times \delta^{18}O$ is no longer correct. In the case of CO, the MIF takes place mainly in the sink reaction CO+OH. Therefore error of $\delta^{13}C$ caused from MIF becomes larger as air mass exposed to OH for a longer time. This error was estimated to be about 0.25 ‰ in the remote site during summer [*Röckmann and Brenninkmeijer*, 1998], when the effect of CO+OH is larger. In this thesis this correction is not applied because urban air is influenced by less MIF, and relatively small errors to measurement uncertainty are expected, and no measurement on $\delta^{17}O$ is available for Happo air samples.

Accelerator Mass Spectrometer (AMS) is used to measure very low concentration isotope component. ^{14}CO concentration in the atmosphere is only about 20 molecules cm^{-3}. After stable isotope measurement, the CO_2 samples from CO were frozen back to sample bottles again and diluted by ^{14}C free CO_2 about 10 times to make enough sample

size for ^{14}C analysis. Usually the results are obtained in the unit percent of Modern Carbon (pMC); ^{14}C concentration that is compared to the standard (Modern Carbon) in the unit of %. In this report, ^{14}CO concentration is expressed in the unit of molecules cm^{-3} (eq. 2-3).

3-3 Air compressor and cylinders

The air compressor for sampling is depicted in Figure 3-4. RIX compressor is modified for CO isotopic measurement to keep low CO production, less than 2 ppb. Details of modifications are described elsewhere [*Mak and Brenninkmeijer,* 1994]. At the inlet, air is dried using Drierite ($CaSO_4$), which makes no effect to CO (and CO_2) characters, since moisture will hinder stable reservation of low concentration CO in cylinders and may cause isotopic exchange [*Gemery et al., 1996; Brenninkmeijer et al.*, 1983]. The inlet pressure gauge #1 is useful to check whether the air flow is normal of not. If there is any resistance, the inlet pressure will indicate negative pressure. The three stage compressor is just using pistons, which have different diameters depending on the resulted pressure. Pistons are moved simply by a motor. Teflon spirals are used as o-ring to suppress the production of CO. Two cooling towers are mounted to remove liquefied water, but in this sampling procedure air is already dried at inlet by Drierite and no water should remain there. An air fan is added in front of the three stage piston compressor for a more effective cooling to prevent the production of CO due to high temperature. After pressured by three pistons, air goes through Drierite again in "High pressure dry tube" to confirm drying is perfect. The pressure gauge #2 is mounted before the pressure controller, which will operate over 50 bar. The pressure gauge #3 indicates the pressure on cylinder connected to the outlet. The hole system can keep over 200 bar, however, a safety valve is amounted and set 150 bar.

About 40 m 1/2 inch Teflon tube was connected to the compressor inlet and the ambient air was taken up in order to prevent very local CO contamination around the compressor. Before filling to the cylinder, air was taken to flash the inside of the black tube for three times, then sampling cylinder was filled until 5bar and was flashed for

three times. The cylinder was filled until about 100bar. As the volume of the cylinder is 5.9L, the sampled air is about 600L. It takes about 50 minutes for sampling (without preparation) and it is the time resolution of data in this sampling method.

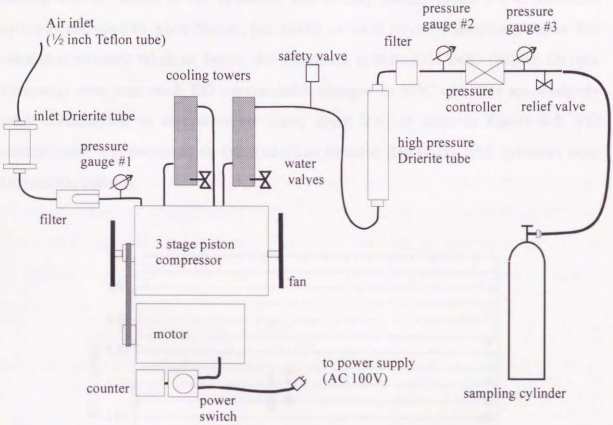

Figure 3-4. Schematic figure of modified RIX compressor

When the O-rings of the pistons are worn, there arises a problem at cold temperature; pressure does not rise at starting of the compressor. In this case, before starting compressor, compression parts need to be heated by a fan heater. Once the pressure rises, the compressor produces heat itself and keeps pressure rising.

Aluminum cylinders are used since they can keep CO stable for a long time [*Mak and Brenninkmeijer*, 1994]. Care is needed to prevent the ambient air, especially moisture, coming into the inside of the cylinders, and to keep surface clean. 5.9 L aluminum cylinders equipped by Scott-Marrin, Inc. (SMI) are used for most samples in Japan. For some first samples taken in Japan, the aluminum cylinders of BOC (British Oxygen Company) were also used. CO concentration changes in BOC cylinders are relatively small (comparable to measurements error; about 2%) as seen in Figure 3-5. CO concentration was measured by GC-Reduction detector (Hg-HgO). SMI cylinders have also similar stability.

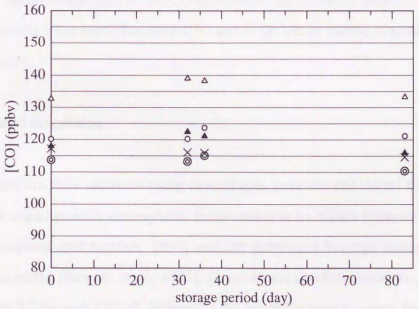

Figure 3-5. CO concentration change in cylinders

Chapter 4

Car exhaust experiments

Car exhaust is one of the main CO sources, especially in the northern hemisphere and it is dominant CO source in urban area. In spite of its importance, there are only a few measurements on isotopic compositions of CO in car exhausts. In this chapter, car exhausts using gasoline, diesel and natural gas as fuels are measured for stable isotopic compositions of CO. It is found that they emitted isotopically different CO.

4-1 Experiment

Gas samples of car exhaust were collected with 50 mL syringes or 6 L Tedlar bags from tail pipes. To fill Tedlar bags, a small membrane pump and a molecular sieve trap were used. During sampling, the cars were stationary and the accelerators were some what pushed down. The experimental setup for the isotopic measurements is explained in chapter 3-1. The injection part to the CO extraction line is shown previously in Figure 3-2b. Measurements were made for only $\delta^{13}C$ and $\delta^{18}O$. These measurements were done in Mainz, Germany.

4-2 Results and discussion

Results of automobile exhausts using natural gas, gasoline and diesel fuels are plotted in Figure 4-1 together with atmospheric measurements in Mainz (chapter 6) and in Los Angeles [*Sakugawa and Kaplan*, 1997] and the estimated average isotope ratio of car exhaust in the world [*Stevens et al.*, 1972]. Gasoline cars without catalytic converter give $\delta^{18}O$ of 22.3 ± 0.3 ‰ and $\delta^{13}C$ of -29.9 ± 0.3 ‰. No difference between just after starting the engine (cold engine) and after driving (hot engine) was observed. Gasoline cars with catalyst emit CO with the same isotopic compositions as the one with non-catalyst car for cold start. In hot engine condition, the CO concentration in the exhaust from the catalyst

car was too low to make isotopic analysis by the present sampling procedure. The oxygen isotopic composition from a gasoline fueled car is very close to the atmospheric oxygen isotopic composition ($\delta^{18}O$ = 23.5 ‰), implying that atmospheric oxygen is transmitted to CO in the combustion process without significant isotopic fractionation. *Brenninkmeijer and Röckmann* [1997] reported oxygen isotopic compositions of CO from hot engine ($\delta^{18}O$ = 19.5 ± 1 ‰) and cold engine ($\delta^{18}O$ = 6 ± 1 ‰). The former value is consistent with this work, however, the latter is very light compared to the present data. *Huff and Thiemens* [1998] also reported $\delta^{18}O$ and $\delta^{17}O$ from car exhaust. Their results are enriched (29 ‰) or depleted (11 ‰), and explained by effectiveness of the catalytic converter, e.g. well working converter make heavy oxygen. The extent of kinetic isotope effect may depend on various factors, especially under cold engine conditions. The world average isotopic composition of automobile exhausts estimated by Stevens *et al.* [1972] is also plotted in Figure 4-1. These values ($\delta^{13}C$ = -27.4 ± 0.3 ‰, $\delta^{18}O$ = 24.6 ‰) were estimated from the atmospheric measurements in some big cities over the world. They commented that $\delta^{13}C$ values of CO were different in each city, since urban atmospheric CO will inherit the $\delta^{13}C$ value from that of the fossil fuel used in that city. The $\delta^{13}C$ value of gasoline engine exhausts in this work is about 3 ‰ lighter than the average isotopic value estimated from atmospheric measurements in big cities. This may be explained by the isotopically light fossil fuels used in Mainz.

Diesel cars without catalyst give lighter oxygen and heavier carbon ($\delta^{18}O$ = 10.9 ± 0.8 ‰ and $\delta^{13}C$ = -22.2 ± 1.1 ‰) both for cold and hot engine condition. At first it is surprising to find this light $\delta^{18}O$ since diesel engine combustion works at higher temperature than gasoline engine and a very effective oxidation process is expected. In spite of high temperature, diesel engine emits carbon particles (soot) and this means incomplete combustion because diesel fuel is composed of higher molecular weight hydrocarbons than gasoline fuels. Since $\delta^{13}C$ value of diesel fuel in Mainz is not available, it is not clear whether the observed value (-22.2 ± 1.1 ‰) is affected by any isotopic fractionation or not. Generally diesel fuel is isotopically heavier than gasoline because the KIE during production process of petroleum prefer lighter isotopes. Diesel

fuel consists of higher carbon numbers than gasoline fuel. CO is produced from organic material (fuel) and atmospheric oxygen, and isotopically lighter isotopes will be preferred in this reaction. This would produce lighter CO. But at the same time, CO is oxidized to CO_2 and also isotopically lighter CO will be consumed faster. As the result, the remained CO would be heavier. Therefore the isotopic compositions of CO from the engine combustion could not be determined simply. In the case of the diesel fuel combustion, the resulted oxygen becomes lighter and carbon seems to become heavier. This phenomenon could not be explained by a simple KIE. But it is interesting to note that the shift from the gasoline fuel combustion to the diesel fuel combustion is almost the same as the amplitude of the KIE of CO + OH reaction; 6 ‰ for carbon and -10 ‰ for oxygen. If the produced CO is removed by OH in later period of diesel engine combustion, lighter oxygen and heavier carbon might be possible. But in this explanation the KIE need to be same extent even at higher temperature, where KIE will become smaller, and reaction progresses at equilibrium. Also gasoline and diesel fuels need to have similar isotopic values and there is no reason why gasoline engine does not show a similar fractionation. At a moment there is no suitable explanation about this large isotope fractionation for diesel fuel combustion.

Busses running with natural gas in cold and hot engine condition give nearly the same oxygen isotopic composition as gasoline engine cars but give much lighter carbon ($\delta^{18}O$ = 20.1 ± 1.0 ‰ and $\delta^{13}C$ = -51.3 ± 1.5 ‰). The proximity of the $\delta^{18}O$ value to that of atmospheric oxygen may be an indicator of a highly efficient combustion, which excludes fractionation process. Biogenically and thermogenically produced CH_4 in natural gas has very light carbon with wide variety ($\delta^{13}C$ = -44 ‰ in average [*Stevens and Engelkemeir*, 1988]), therefore the present results may reflect the light isotope composition of the fuel used. At a moment car exhaust from natural gas engine is not important as air pollution. But this measurement is interesting as a point of view of burning of natural gas.

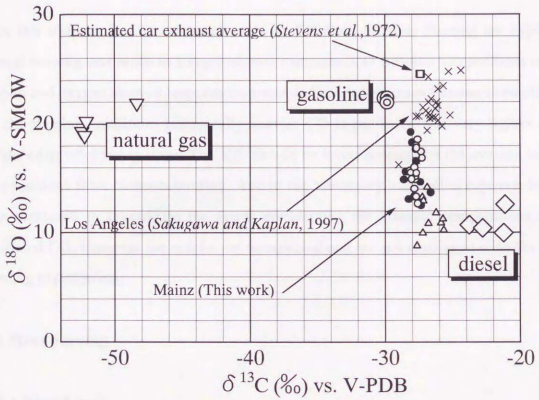

Figure 4-1. Isotopic compositions of car exhausts. $\delta^{18}O$ value of car exhausts fueled gasoline (◎), diesel (◇) and natural gas (▽) are plotted versus corresponding $\delta^{13}C$. They show quite different isotopic compositions. The atmospheric CO measurements in Mainz (chapter 6, △:summer ●: autumn ○:winter) and in Los Angeles (×, [*Sakugawa and Kaplan*, 1997]) are plotted together. The average isotopic composition of car exhausts estimated by *Stevens et al.* [1972] is also shown (□). $\delta^{18}O$ values of gasoline exhaust and big city (Los Angeles) are close to the isotopic composition of atmospheric oxygen (23.5 ‰).

Chapter 5

Biomass burning experiments

In this chapter, isotopic measurements on CO from biomass burning are explained. Actual burning was made in a experimental container. CO isotopic compositions of both carbon and oxygen showed large fractionation as burning becomes flaming to smoldering. At the flaming condition, isotopically heavier CO is produced and very lighter CO is produced at smoldering stage. The KIE should be taken account for the average isotopic compositions from biomass burning. And in the laboratory, controlled cigarette burning was measured to investigate the factor determining the isotopic compositions of the produced CO. However the results are unexpected and are not consistent with the plants burning experiments.

5-1 Plant burning

5-1-1 Experiment

Plant material was burned in an experimental container specially designed for biomass burning experiments [*Lobert et al.*, 1990]. A schematic of the experimental set up is shown in Figure 5-1. Above a burning stage there was a chimney with a fan to promote smoke extraction, and sample gas was collected from a sampling port mounted at the middle of the chimney. Using a diaphragm pump, air was drawn through a Teflon filter and a molecular sieve trap, then sampled into 6 L Tedlar bags. Burned plants were eucalyptus (big branches; 1.8 kg), eucalyptus (twigs; 1.1 kg), leaves (0.3 kg) and maize (0.3 kg). Eucalyptus and maize were shipped from Africa and had been dried. The leaves were mixture of broad-leaved trees and most of them were platane. They were collected from the university campus in Mainz and were dried before use. These leaves were not the proper plants for actual biomass burning, but it is meaningful to try different type of plants burning. As explained later, the burning process of leaves is different from that of

branches or twigs.

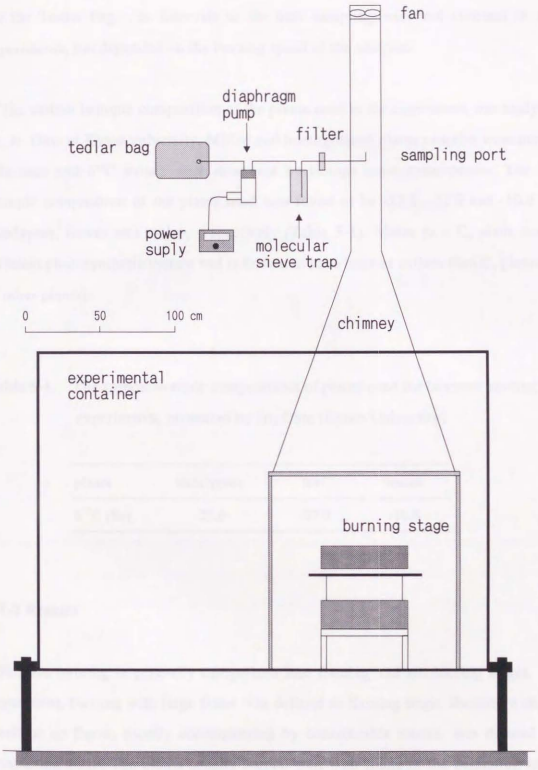

Figure 5-1. Experimental setup of plant burning experiments [*Lobert et al.* 1990]

On the burning stage, sample plants were ignited by a gas lighter and a piece of paper. After the fire was stabilized, air sampling was started. It took about one minute to fill the Tedlar bag. The intervals to the next sampling were not constant in all the experiments, but depended on the burning speed of the samples.

The carbon isotopic composition of the plants used in the experiment was analyzed by Dr. N. Ohte at Kyoto university. Milled and homogenized plants samples were burned in a furnace and $\delta^{13}C$ values were measured by isotope mass spectrometer. The carbon isotopic composition of the plants used was found to be -27.6, -27.0 and -10.8 ‰ for eucalyptus, leaves and maize, respectively (Table 5-1). Maize is a C_4 plant, having a different photosynthetic system and is known to have heavier carbon than C_3 plants (most of other plants).

Table 5-1. The carbon isotopic compositions of plants used for biomass burning experiments, measured by Dr. Ohte (Kyoto University)

plants	eucalyptus	leaf	maize
$\delta^{13}C$ (‰)	-27.6	-27.0	-10.8

5-1-2 Results

Biomass burning is generally categorized into flaming and smoldering stages. In this experiment, burning with large flame was defined as flaming stage. Burning with only a small or no flame, usually accompanying by considerable smoke, was defined as the smoldering stage. The plants usually burned well with flame in the beginning and then gradually started to smolder. All data can not be categorized clearly into flaming or smoldering, and transitional samples are categorized to "intermediate". In Figure 5-2,

$\delta^{13}C$ and $\delta^{18}O$ of CO from eucalyptus burning (big branches) were plotted against the time from ignition. There is a trend that both $\delta^{13}C$ and $\delta^{18}O$ become gradually lighter with time from ignition.

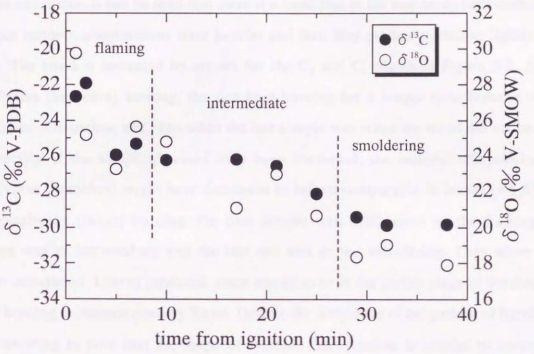

Figure 5-2. CO isotopic compositions from eucalyptus (branches) burning experiment as a function of time from ignition. The range of errors for the analysis are almost identical to the symbol size for $\delta^{13}C$ and less than the symbol size for $\delta^{18}O$.

The oxygen isotopic compositions of CO from burning plants are plotted against the corresponding carbon isotope ratios in Figure 5-3. The original carbon isotopic compositions of eucalyptus and leaves (average $\delta^{13}C$ = -27.3 ‰) and of maize ($\delta^{13}C$ = -10.8 ‰) are designated by dotted lines. The $\delta^{18}O$ value of atmospheric O_2 is also shown. The order of sampling in the burning experiments are numbered for eucalyptus (twigs), leaves and maize. It can be seen that there is a trend that at the beginning both carbon and oxygen isotopic compositions were heavier and then they gradually became lighter with time. The trend is indicated by arrows for the C_3 and C_4 plants in Figure 5-3. As for eucalyptus (branches) burning, the fire kept burning for a longer time because of the thickness of branches, and even when the last sample was taken the wood did not become ash totally. If the sampling would have been continued, the isotopic compositions of eucalyptus (branches) might have decreased to values comparable to leaves (4,5,6). For the eucalyptus (twigs) burning, the first sample was categorized as the flaming, the second was as intermediate and the last one was as the smoldering. They show clear linear correlation. Leaves produced much smoke even at the earlier stage of burning, but their burning is characterized by flame. Despite the difference of the pattern of burning, it is interesting to note that the slope of isotopic fractionation is similar to eucalyptus burning. As for Maize, the first three points correspond to samples at a flaming phase and the last three points to a smoldering phase. The results show heavier carbon than C_3 plants reflecting the heavy isotopic composition of the original biomass. Smoldering samples become isotopically lighter both for carbon and oxygen compared to flaming conditions. The slope of isotope ratio fractionation seems to be almost identical to the C_3 plants burning.

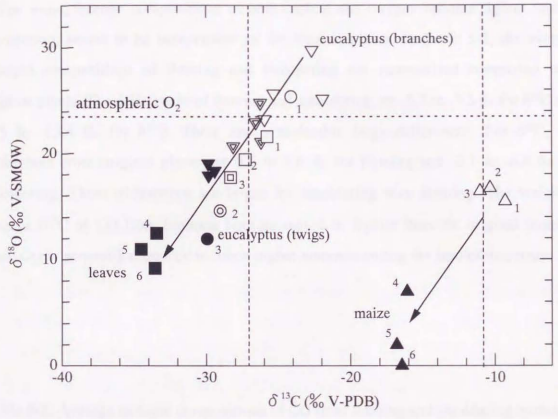

Figure 5-3. The isotopic compositions of CO from the plant burning experiments. Open symbols are samples at flaming stage, solid symbols are samples at smoldering stage and doubled symbols are sampled at their intermediate. Inverted triangles denote eucalyptus (branches), circles denote eucalyptus (twigs), squares denote leaves and triangle denote maize. The numbers indicate the orders of the sampling and arrows show the trends of CO isotopic composition change with time. The carbon isotopic compositions of eucalyptus and leaves (average $\delta^{13}C$ = -27.3 ‰) and of maize ($\delta^{13}C$ = -10.8 ‰) are plotted by dotted lines. The $\delta^{18}O$ value of atmospheric oxygen ($\delta^{18}O$ = 23.5 ‰) is also shown by a dotted line.

5-1-3 Discussion

The trend, isotope compositions of both carbon and oxygen become lighter toward smoldering, seems to be independent of the kind of plants. In Table 5-2, the average isotopic compositions of flaming and smoldering are summarized comparing with original plants. The differences of flaming and smoldering are -5.7 to -7.3 ‰ for $\delta^{13}C$ and -7.5 to -13.4 ‰ for $\delta^{18}O$. There are considerable large differences. For $\delta^{13}C$, the differences from original plants are 0.6 to 3.6 ‰ for flaming and -2.1 to -6.8 ‰ for smoldering. These differences are larger for smoldering than flaming. The weighted average $\delta^{13}C$ of CO from biomass burning would be lighter than the original biomass since CO is generally produced in much higher amounts during the smoldering stage.

Table 5-2. Average isotopic compositions of CO from flaming and smoldering burning.

	$\delta^{13}C$ (‰ V-PDB)						$\delta^{18}O$ (‰ V-SMOW)		
	P	F	S	Δ(S-F)	Δ(F-P)	Δ(S-P)	F	S	Δ(S-F)
eucalyptus (branches)	-27.6	-24.0	-29.7	-5.7	3.6	-2.1	26.0	18.4	-7.5
eucalyptus (twigs)	-27.6	-24.1	-29.9	-5.8	3.5	-2.3	25.4	12.0	-13.4
leaves	-27.0	-26.5	-33.8	-7.3	0.5	-6.8	20.5	10.9	-9.6
maize	-10.8	-10.2	-16.5	-6.2	0.6	-5.7	16.2	3.0	-13.2

P: isotopic composition of original plants, F: flaming, S: smoldering

Table 5-3. The carbon isotopic composition of CO and CO_2 emitted from burning biomass [*Stevens and Engelkemeir*, 1988]

plants	CO_2	CO	CO/CO_2
Field grass	-34 ‰	-29.4 ‰	38 %
Slash pine	NA	-23.6 ‰	NA
Brush, dried	-25.0 ‰	-27.2 ‰	2.2 %
Brush, green	-24.2 ‰	-23.6 ‰	10 %
Brush, damp after dying 6 months	-27.5 ‰	-14.3 ‰	26 %

NA indicates not analyzed

There has been only one report about isotopic compositions of CO from the burning of an agricultural field and unconfined bonfires of dried tree branches [*Stevens and Engelkemeir*, 1988]. The results of $\delta^{13}C$ are -29.4, -23.6, -27.2, -23.6 and -14.3 ‰ for field grass, slash pine, brush dried, brush green and brush damp after drying 6 month, respectively (Table 5-3). At the same time they measured carbon isotopic compositions of CO_2 , and the difference with CO and CO_2 for first four plants is ± 2 ‰. *Stevens and Wagner* [1989] noted that carbon in CO from biomass burning would be nearly the same or possibly more enriched than that of the original biomass. Their contention is consistent with this observation only when the burning is at the flaming stage.

Conny et al. [1997] performed a model calculation study on $\delta^{13}C$ of CO at biomass burning season in Brazil. To estimate the $\delta^{13}C$ values of CO from biomass burning, they burned C_3 and C_4 plants in a quartz tube and measured $\delta^{13}C$ of produced CO_2 (not CO). In this method oxidation progressed almost completely, which accompany little isotopic fractionation, and $\delta^{13}C$ of CO_2 was almost the same as original isotopic compositions of biomass. They adopted the mixture of these isotopic values to CO source in their calculation with consideration of C_3 and C_4 plants distribution, but assumed that no KIE was involved. *Manning et al.* [1997] reported model calculations for $\delta^{13}C$ of atmospheric

CO in the southern hemisphere, where biomass burning is relatively more important as a CO source. They employed -25 ‰ for forest burning and -12 ‰ for savanna burning separately, because typically C_4 plants are growing in savanna. Their values for CO from biomass burning were adopted without considering the KIE. If they would have incorporated this effect, modulated $\delta^{13}C$ values would have been lower. They needed however to assume low conversion factor (0.7) of CH_4 oxidation as a CO source in their model calculation, since this source produces very light CO in carbon. The consideration of the KIE in biomass burning will make this problem worse.

Only one report [*Stevens and Wagner*, 1989] gave the oxygen isotopic compositions of CO from actual biomass fires with an average of 18 ± 1 ‰. *Huff and Thiemens* [1998] reported that $\delta^{18}O$ measurements of CO at urban air condition (about 22 ‰) became lighter (about 18.5 ‰) when air from a wildfire area affected the measurements. This suggests $\delta^{18}O$ of CO from biomass burning is at least 18.5 ‰ or lighter. *Bergamaschi et al.* [1998] measured isotopic compositions of CO on the Siberian railroad and observed high CO concentration data which seemed to be affected by biomass burning. They estimated the $\delta^{18}O$ value of these samples were about 10 ‰. Present measurements are consistent with these reports if the values during smoldering phase were considered. The lighter value of *Bergamaschi et al.* [1998] can be explained by the larger KIE during late smoldering.

If the oxygen of CO from biomass burning inherits to the $\delta^{18}O$ value of atmospheric oxygen, $\delta^{18}O$ should be around 23.5 ‰. In Table 5-2, two eucalyptus burning samples during flaming conditions show heavier oxygen values than 23.5 ‰, but leaves and maize data in flaming are lighter than that. The values during smoldering are lighter than atmospheric oxygen for all plants. It seems as if $\delta^{18}O$ of CO from burning plants started at different oxygen isotopic ratios. The initial $\delta^{18}O$ value would be determined by the scale of fire and be affected by the $\delta^{18}O$ value of original biomass, since plants themselves have nearly the same amount of oxygen as carbon in cellulose ($C_6H_{12}O_6$). The oxygen isotopic composition of cellulose is determined only by the $\delta^{18}O$ value of the water around the plants living and it value is, for example, 26 ‰ [*Saurer et al.*, 1997]. The $\delta^{18}O$ value of oxygen in plant cellulose is dependent on that of the meteoric water

and depends strongly on the relative humidity [*Brenninkmeijer,* 1983]. Therefore the $\delta^{18}O$ value of the eucalyptus trees, which usually grow in dries area, would be relatively high.

Large isotopic fractionation of $\delta^{18}O$ and $\delta^{13}C$ in CO is observed in biomass burning experiments. At the flaming stage, isotopic compositions of CO are heavier than those of the carbon in the plants and atmospheric O_2. But they become lighter in smoldering stage. The average isotopic compositions from biomass burning could be derived if the contribution from flaming and smoldering, and their typical isotopic values are determined. However accurate estimation of these factors is difficult, the average of CO isotopic composition would become lighter than original biomass since the production of CO from biomass burning is enhanced during smoldering stage. From this study it follows that the KIE for CO isotopes from biomass burning should be considered. The effect for ^{13}C depends not only on the type of plants, but also on smoldering or flaming. For ^{18}O, the $\delta^{18}O$ of the cellulose, which depends on that of precipitation and humidity, adds an additional complication, whereas the effect of smoldering or flaming also has to be considered.

5-2 Cigarette burning

Cigarette is easier to burn under controlled condition. The purpose of this experiment is to know which factor determine the isotopic compositions of CO from biomass burning. However, the results are unexpected and cannot answer the above question.

5-2-1 Experiments

Experimental setup of cigarette burning is shown in Figure 5-4. A cigarette was connected on a movable inlet tube in a glass tube (diameter is 1 inch, length is 24 cm) and air was injected through a cigarette with mass flow controllers (MFC). The inlet side of the glass tube was closed and the other side had a sampling hole for a syringe and a small draught for over flow. Samples were taken with 50 mL syringes. When the air flow was fast enough, excess flow passed through as overflow. When the air flow was slow, the injector was pulled slowly to avoid sucking air from the laboratory. Oxygen concentration in the injected air was controlled by mixing air and nitrogen using two MFCs, but total flow rates were kept constant at 4.2, 8.5 and 16.6 $cm^3 s^{-1}$. Temperatures at burning place were measured at different air flow rate and oxygen concentration. For the measurement of the temperature, a Pt thermo-couple sensor was inserted in a cigarette and the highest temperature was read when the burning zone passed. Cigarettes were from commercial products (Marlboro) and were dried in an oven (120 °C) over a night before use.

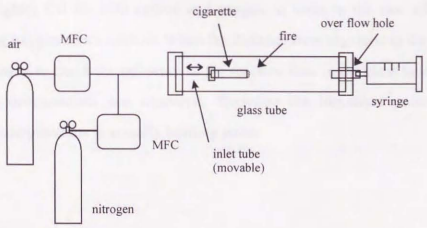

Figure 5-4. Experimental set up of cigarette burning experiments

5-2-2 Results

The results of changing the injected air flow rate are shown in Figure 5-5a and b for carbon and oxygen, respectively. The $\delta^{13}C$ values at slower flow are around -28 ‰ and at higher flow they become lighter near -31 ‰. The $\delta^{18}O$ values is about 24 ‰ at maximum, which is close to ambient atmospheric oxygen isotopic composition, and decrease to around 12 ‰ at faster flow rate. Slower air flow rate makes heavier CO and faster flow makes lighter CO both for carbon and oxygen. These trends are clearer for oxygen since the extent of isotopic ratio change is larger. The correlation of $\delta^{13}C$ and $\delta^{18}O$ is shown in Figure 5-6 with the regression line (solid line). The regression line (arrow) of biomass burning experiment for C_3 plants (Figure 5-3) is also shown by a dotted line. The cigarette data shows same trend as plant burning; heavier carbon accompanies heavier oxygen and lighter carbon accompanies lighter oxygen. However, the slope of the solid line is much steeper than that of the dotted line; only small $\delta^{13}C$ shift accompanies larger $\delta^{18}O$ shift in the cigarette burning. The results under different oxygen concentration are also shown in Figure 5-7a and b for carbon and oxygen, respectively. Total flow rates were kept constant at 4.2, 8.5 and 16.6 $cm^3\ s^{-1}$ and their symbols are squares (□), triangles (△) and circles (○), respectively. At each air flow rate, oxygen concentration is changed from 10 to 21 %, but at the same flow rate, there is no trend of oxygen concentration dependence for the observed isotopic compositions. The trend, faster flow makes lighter CO for both carbon and oxygen, is same in the case of the data without changing oxygen concentration. When the distance from cigarette to the sampling syringe was changed to check the influence of the reaction time in the glass tube, no difference of isotopic compositions was observed. Therefore the important point for determining isotope compositions is actually burning point.

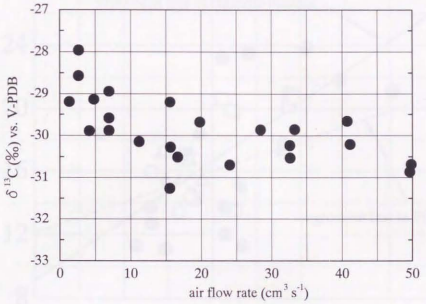

Figure 5-5a. $\delta^{13}C$ of CO from cigarette burning vs. air flow rate

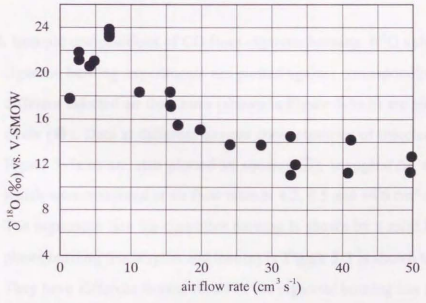

Figure 5-5b. $\delta^{18}O$ of CO from cigarette burning vs. air flow rate

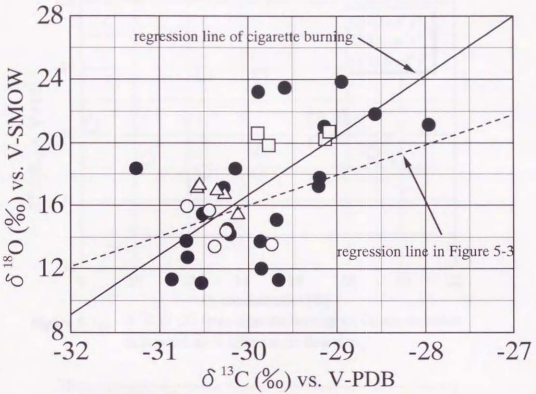

Figure 5-6. Isotopic compositions of CO from cigarette burning. $\delta^{18}O$ values of CO from cigarette burning experiments are plotted against corresponding $\delta^{13}C$. Data at different injected air flow rates (shown in Figure 5-5a,b) are plotted with solid circle (●). Data at different oxygen concentrations of injected air (shown in Figure 5-7a,b) are also plotted as squares(□), triangles(△) and circles(○), which were measured at air flow rates at 4.2, 8.5 and 16.6 $cm^3\ s^{-1}$, respectively. The regression line for cigarettes burning is shown by a solid line, and for C_3 plants burning (eucalyptus and leaves) in Figure 5-3 is shown by a dotted line. They have different slopes; result of the cigarette burning has a steeper slope, little $\delta^{13}C$ change makes large $\delta^{18}O$ change.

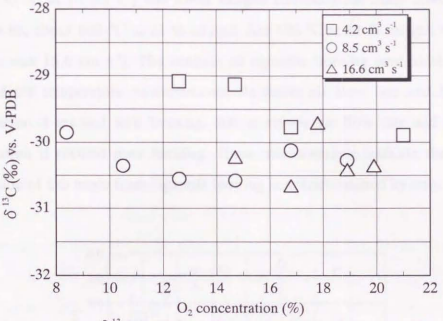

Figure 5-7a. $\delta^{13}C$ of CO from cigarette burning vs. O_2 concentration of injected air at different air flow rate

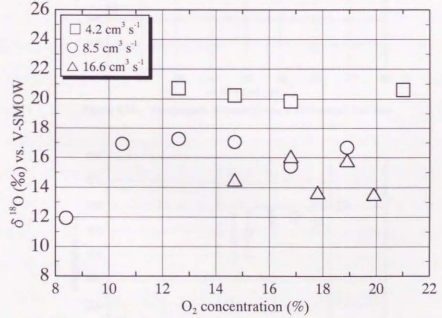

Figure 5-7b. $\delta^{18}O$ of CO from cigarette burning vs. O_2 concentration of injected air at different air flow rate

As expected, faster flow made higher temperature (Figure 5-8a, about 750 °C at 50 cm s^{-1} and 550 °C at 10 cm s^{-1}) and lower oxygen concentration made lower temperature (Figure 5-8b, about 600 °C at 21 % oxygen and 450 °C at 11 % oxygen when the total flow rate was 16.6 cm s^{-1}). The outlook of cigarette burning was consistent with the results of the temperature measurements. At faster air flow rate and higher oxygen concentration it seemed well burning, and at slower air flow rate and lower oxygen concentration it seemed poor burning. These measurements indicate that the isotopic composition of CO made from cigarette burning is not determined by only temperature.

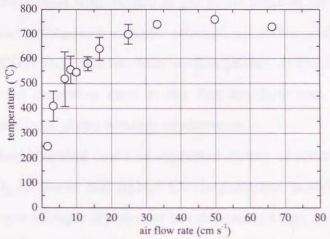

Figure 5-8a. Temperature of burning zone at different air flow rate

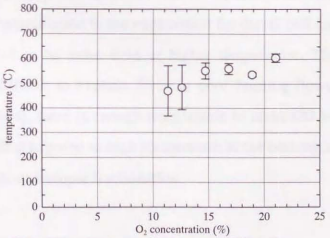

Figure 5-8b. Temperature of burning zone at different O_2 concentration in injected air

5-2-3 Discussion

The purpose of cigarette experiments is to find which factor is controlling the isotopic compositions of CO from biomass burning. Temperature of fire had been expected as the factor, since flaming burning has high temperature and makes a small KIE. The cigarette experiments show unexpected results. Temperature is not important for the isotopic compositions of CO, but flow rate is the key factor. This contradiction suggests that the actual biomass burning can not be explained by only experiments of small scale burning like cigarettes. During flaming phase, the biomass is pyrolyzed at first and then the decomposed molecules react with oxygen as gas phase reaction. In smoldering phase, on the other hand, the atmospheric oxygen attacked to active surface of biomass and oxidized carbons (CO, CO_2) come out from surface [*Baker*, 1983]. Cigarette experiments would be smoldering condition even at the fast air flow rate, and it has different oxidation mechanism from plants burning experiments.

The results of plants burning could be explained simply as follows. The produced CO is oxidized to CO_2 in flame and lighter CO is preferred in this reaction. Therefore remained CO becomes isotopically heavier in the flaming stage. In the smoldering stage, CO production from plants surface prefers lighter isotopes and lighter CO is produced. Here the KIE of CO oxidation reaction need to be positive for both carbon and oxygen. This would be in contradiction to the explanation for diesel fuel combustion; the KIE of CO+OH is assumed to be same even at higher temperature. The results of cigarette burning is more difficult to explain. Even at poor burning (lower flow rate or lower oxygen concentration), there is enough temperature to make CO which accompanies no KIE. But enough time exposed to high temperature in the burning zone would be needed to produce CO without isotopic fractionation.

Chapter 6
Measurements in urban area

In this chapter, isotopic measurements of atmospheric CO in a middle-scale city, Mainz, are demonstrated. $\delta^{18}O$ values are very good indicator to see pollution from car exhaust. Also preliminary measurements in a big city, Tokyo, are presented.

6-1 Mainz air

6-1-1 Experiment

Ambient air in Mainz was collected through a 1/2 inch PFA tube from the roof of a Max Planck Institute for Chemistry building in Mainz (50°N, 8°E). Sample air was dried with about 1 L molecular sieve (13X) at the sampling inlet and introduced to the CO extraction line as shown in Figure 3-2a. Mainz has about 200,000 inhabitants and is located about 30 km southwest of Frankfurt (am Main). The institute's three-storied building is located on the Mainz university campus, which is surrounded by roads with considerable traffic. Measurements were made on June 11,13,16 , October 14,17 and December 2,3,4 in 1997. Samples were collected 4 to 6 times a day. For convenience the three sampling periods are called "summer", "autumn" and "winter". Sampling flow rate was set at about 3 L min^{-1} and about 300 L air was processed in each measurement.

6-1-2 Results

In Figure 6-1a, CO concentration is plotted without distinguishing the difference of days. During the whole sampling period the CO concentrations varied from 186 ppb to 1741 ppb; lower concentrations appeared mostly in summer and higher concentrations in winter. The higher concentrations in winter would be caused by the stagnation of air because of the inversion layer, while in summer the mixing layer would be much higher to result in the lower CO concentration near the ground. This mixing would be very

effective since CO concentration of around 200 ppb during summer is quite low for urban areas, which is comparable to the value at a remote site in the northern hemisphere during winter [*Derwent et al.*, 1998]. A diurnal change of CO concentration was also noted; in the morning and evening CO concentration was higher in most of the days. This can be explained simply by enhanced automobile traffic during these hours. In Figure 6-1 b and c, $\delta^{18}O$ and $\delta^{13}C$ values are plotted. Data in these figures are scattered and it is difficult to read any trend. However, when oxygen and carbon isotopic compositions of CO are plotted against reciprocal of CO concentration as shown in Figures 6-2 a and b, a clear correlation is observed. A good linear correlation of $\delta^{18}O$ and 1/[CO] over a wide range of isotopic value (9 to 20 ‰) can be seen in Figure 6-2 a. For $\delta^{13}C$, there is also linear correlation as seen in Figure 6-2 b, but not so clear as $\delta^{18}O$.

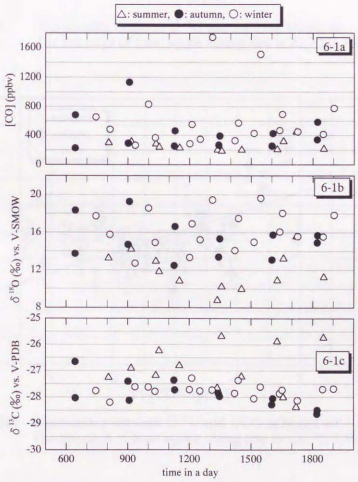

Figure 6-1. Ambient air Measurements in Mainz

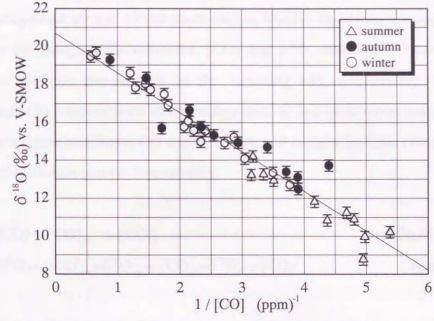

Figure 6-2a. Relationship between $\delta^{18}O$ and 1/CO in Mainz air. The intercept of least squair fitting line is 20.7±0.3‰.

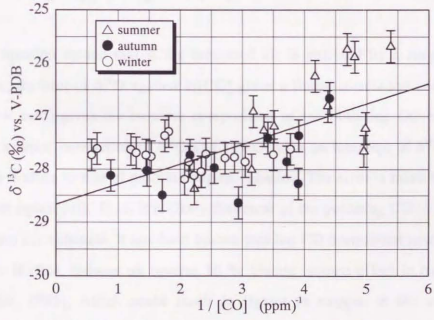

Figure 6-2b. Relationship between $\delta^{13}C$ and 1/CO in Mainz air. The intercept of least squair fitting line is -28.7±0.3‰.

6-1-3 Discussion

The $\delta^{18}O$ of the atmospheric CO will be explained here as mixing of the $\delta^{18}O$ values of the background air and of the local source. Similar equations are applicable for carbon simply by changing the notations. [CO] and $\delta^{18}O$ represent CO concentration and its oxygen isotopic composition at the sampling site, respectively. $[CO]_{bg}$ and $\delta^{18}O_{bg}$ represent CO concentration in the background air and its isotopic composition. $[CO]_s$ and $\delta^{18}O_s$ represent additional CO concentration and oxygen isotopic composition of CO due to local pollution source, respectively.

$$[CO] = [CO]_{bg} + [CO]_s \qquad \text{(Eq.6-1)}$$

$$\delta^{18}O = ([CO]_{bg} \times \delta^{18}O_{bg} + [CO]_s \times \delta^{18}O_s) / [CO] \qquad \text{(Eq.6-2)}$$

Substituting Eq.6-1 in Eq.6-2, one gets the following equation.

$$\delta^{18}O = \{[CO]_{bg} \times (\delta^{18}O_{bg} - \delta^{18}O_s)\} / [CO] + \delta^{18}O_s \qquad \text{(Eq.6-3)}$$

This equation means that if the measured air is polluted by a single category of CO source, the plot of $\delta^{18}O$ against 1/[CO] gives a linear correlation and the intercept (1 / [CO] = zero) gives the isotopic composition of the polluting CO source. Figure 6-2a gives a linear correlation of $\delta^{18}O$ and 1/[CO] with an intercept of $\delta^{18}O = 20.7 \pm 0.3$ ‰, which is close to that of gasoline engine exhausts. The error is taken from standard error of least squares fit. Thus, it is likely that most of the polluting CO in Mainz comes from gasoline car exhausts. It has been known that the CO destruction reaction, $CO + OH \rightarrow CO_2 + H$ (R6), induces an inverse 10 ‰ kinetic isotope effect in oxygen [*Stevens and Wagner*, 1989], which could result in lighter in oxygen in the atmospheric CO as compared to the source CO. However, CO from automobile exhaust does not travel for long enough time to make large isotopic fractionation before sampling of the atmospheric CO measurement in Mainz. For example, assuming the OH concentration at 10^6 molecules cm^{-3} and using $k_{CO+OH} = 2.8 \times 10^{-13}$ cm^3 $molecule^{-1}$ s^{-1}, about 4 days are needed

to decrease 1 ‰ from original $\delta^{18}O$ of car exhausts, which is much longer than the expected traveling time of CO within a city.

In the above analysis, considerable seasonal changes of isotopic compositions and concentration in background CO could happen. The seasonal variation of background air would disturb a correlation found in Figure 6-2a, because the slope of Eq.6-3 is not constant in this case, and it will be difficult to make a single line found in Figure 6-2a especially at low CO concentration. Using Eq.6-3, this influence can be estimated. For example, the background CO concentration is constant at 150 ppb and its oxygen isotopic composition changes from 3 to 9 ‰, the observation of $\delta^{18}O$ will show about 5 ‰ difference at 1/[CO] = 5 (Figure 6-3). Also when the isotopic composition of background CO is constant ($\delta^{18}O_{bg}$ = 6 ‰) and background CO concentration changes from 110 to 160 ppb, the observation of $\delta^{18}O$ will show about 4 ‰ difference at 1/[CO] = 5 (Figure 6-4). In those calculations, the isotopic composition of CO source is assumed as $\delta^{18}O_s$ = 20.7 ‰. Assuming suitable background CO concentration and isotopic composition for each season in the Mainz measurements, relations between $\delta^{18}O$ and 1/[CO] are calculated. $[CO]_{bg}$ and $\delta^{18}O_{bg}$ are assumed as 110, 145 and 155 ppb, and 3, 6 and 8.5 ‰ in summer, autumn and winter, respectively. Here, background CO concentrations are quoted from the data at Mace Head (53°N, 10°W) [*Derwent et al.*, 1998], and CO isotopic compositions are estimated from the measurement at Happo (38°N, 138°E, in chapter 7). Figure 6-5 shows the results of calculation with the least square fitting line in Figure 6-2a. These plots in three seasons make only a small difference (about 1‰ at 1/[CO] = 5). Therefore the contribution of CO background concentration and isotopic composition can be canceled and it gives a single line as shown in Figure 6-2a within a range of scattering of data in spite of seasonal variation of background air

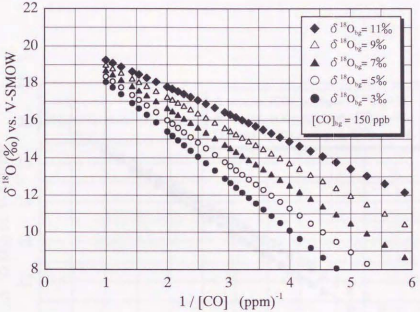

Figure 6-3. Calculation at different background $\delta^{18}O$

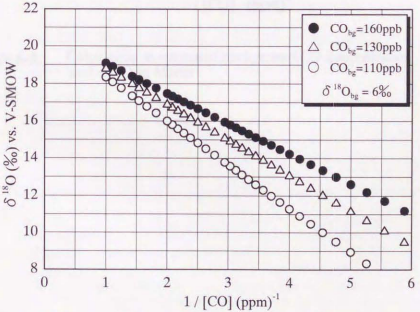

Figure 6-4. Calculation at different background CO concentration

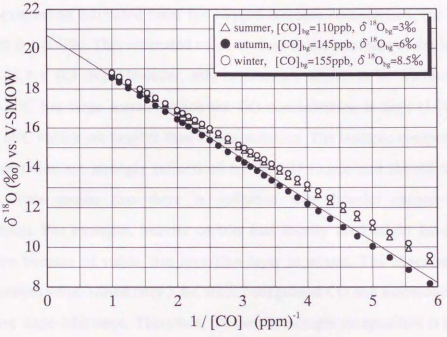

Figure 6-5. Calculation at estimated background CO concentration and $\delta^{18}O$ in Mainz

The $\delta^{18}O$ values estimated by the intercept in Figure 6-2a is slightly lower than that of gasoline exhaust. The isotopic values of estimated pollution source and of measured car exhausts are listed in Table 6-1. If one tries to explain the lower $\delta^{18}O$ by mixing gasoline and diesel exhausts, 14 ± 7 % of CO needs to come from diesel exhausts.

This discussion is also applied to $\delta^{13}C$ values. If 14 % of diesel exhaust mixes into gasoline exhaust as estimated from the oxygen isotopic composition, the resulted $\delta^{13}C$ will be -28.8 ± 0.4 ‰. This estimated value is close to the intercept of the least square fit ($\delta^{13}C$ = -28.7 ± 0.3 ‰). However, this consistence seems to be accidental since the observed $\delta^{13}C$ has large scatter. When the CO concentration is high ($1/[CO] < 2$), the observed $\delta^{13}C$ values are heavier than the expectation. The isotopic compositions at high CO concentration are strongly influenced by the CO source and should reflect it more correctly. This means that there is pollution with heavier carbon at high CO concentration. For example, heavier carbon fuel locally used might have affected the observation because of stable thin inversion layer in winter. The observed atmospheric carbon isotopic value varied only 3 ‰, since background CO and automobile exhaust CO do not have large difference. Therefore, the carbon isotopic composition is not a sensitive indicator for assessing the contribution of CO from car exhaust. In contrast, oxygen isotopic composition has been found to be a useful indicator of pollution from automobiles.

Table 6-1. Isotopic values of estimated pollution source and of measured car exhausts.

	estimated values by intercept (Figure 6-2a, b)	gasoline car (chapter 4)	diesel car (chapter 4)	contribution of diesel car
$\delta^{18}O$	20.7 ± 0.3 ‰	22.3 ± 0.3 ‰	10.9 ± 0.8 ‰	14 ± 7 %
$\delta^{13}C$	-28.7 ± 0.3 ‰	-29.9 ± 0.3 ‰	-22.2 ± 1.1 ‰	
calculated from $\delta^{18}O$	(-28.8 ± 0.4 ‰)			(14 %)

6-2 Tokyo air

This measurements in Tokyo is just a preliminary results. Even only a few data, it is interesting to see the different from the measurements in Mainz.

6-2-1 Experiments

Sampling setup is same as Mainz air measurements. Air was taken from the roof top of the building No.56 in Research Center for Advanced Science and Technology, in Komaba, Tokyo. That is a five-storied building and there are much traffic, industrial activity around the sampling place. Air samples were taken during May to August in 1998. Isotope mass spectrometer in Tsukuba was used for analysis of the isotopic compositions.

6-2-2 Results and discussion

In Figures 6-6 a and b, the isotopic compositions are plotted against reciprocal of CO concentration for oxygen and carbon, respectively. The measurements in Mainz are also plotted here. The four data around 1/[CO] = 4 were measured in a day. Except for these four measurements, it seemed that air made less daily variation both in CO concentration and isotopic ratios in Tokyo. $\delta^{18}O$ shows similar value at high CO concentration (around 1/[CO] = 1.5). This means that the main CO source is also car exhaust in Tokyo. But at low CO concentration, $\delta^{18}O$ is higher than Mainz air. This may be caused from heavier $\delta^{18}O$ of background air in Tokyo. It may be difficult to define the "background air" in such a big, polluted city. However, the latitudinal gradient of isotopic compositions measured by airplane [*Mak,* 1998] shows maximum $\delta^{18}O$ at around 40°N and high $\delta^{18}O$ in back ground air may be possible. In the case of carbon, $\delta^{13}C$ is heavier than Mainz data at high CO concentration. This may be reflecting the heavier fuel used in Tokyo. This heavier $\delta^{13}C$ (around -26 ‰) may also be affected by more diesel fuel combustion from trucks.

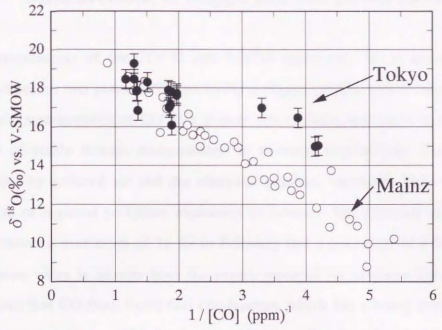

Figure 6-6a. $\delta^{18}O$ of ambient air CO in Tokyo

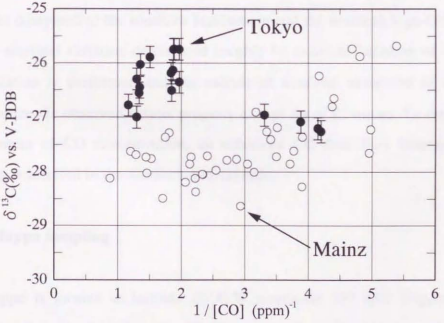

Figure 6-6b. $\delta^{13}C$ of ambient air CO in Tokyo

Chapter 7

Measurement at Happo and box model calculation

Measurements of the $^{13}C/^{12}C$ and $^{18}O/^{16}O$ ratios and ^{14}C of atmospheric CO were carried out for two years (1997 and 1998) at Happo (1840m asl) in Japan. This is the first isotopic measurement of CO at a remote site in Asia, and there is no published time series of stable isotope compositions in northern mid-latitude. The $^{18}O/^{16}O$ ratio is sensitive to polluted air and the observed seasonal variations have some fluctuations because of regional pollution, especially in summer. The seasonal cycle of the $^{18}O/^{16}O$ ratio shows a maximum of 11 ‰ in February and a minimum of 0 ‰ in August. This minimum value is heavier than the values reported for northern high-latitude and this indicates that CO from fossil fuel combustion, which has a heavy isotopic composition, affects the northern mid-latitudes considerably. On the other hand, the $^{13}C/^{12}C$ ratio shows a clear seasonal variation with little scatter; maximum -24.5 ‰ in April and minimum -29 ‰ in August. The seasonal variation at Happo has different values and phases compared to the southern hemisphere and the northern high-latitude. ^{14}CO shows clear seasonal variation determined roughly by seasonal variation of OH. A box model calculation is performed and the calculated seasonal variations of the isotope ratios reproduce the observed results properly except for $\delta^{13}C$ values. To reproduce the spring maximum of CO concentration, an enhanced CO flux from biomass burning during spring is inferred in the northern mid-latitude.

7-1 Happo sampling

Happo is located in latitude 36°41'N, longitude 137°48'E (Figure 7-1), at 25 km distance from the Sea of Japan with the nearest city is Shinano-omachi, 25 km south. The sampling site is on a mountain slope (Happo-one, 1840 m above sea level), where the 1998 winter Olympic Game (down hill and jump) took place. Because of its elevated location and short distance from the sea, it is expected that the air at this sampling place

is above the boundary layer and the sampled air is basically free from local pollution. The sampling compressor is kept in a commercial lodge (Happo-ike-sansou) which is near a terminal of ski lifts. The acid rain monitoring station owned by Japan Environmental Agency is about 50 m from the lodge and Akimoto research group has been measured CO concentration continuously by NDIR method there.

Air samples for CO isotope measurements had been taken about every 2 weeks by the improved 3 stage RIX compressor [*Mak and Brenninkmeijer*, 1994] into 5.9 L aluminum air cylinders (Scott-Marrin Inc.) at about 100 bar. The filled air cylinders were sent to the Max Planck Institute in Germany and processed there. Details of sampling method and analysis method are explained in chapter 3. The air had been sampled from February in 1997 to January in 1999. Analyzed results for CO concentration, $\delta^{18}O$, $\delta^{13}C$ and ^{14}CO are listed in Table 7-1. Reciprocal CO concentration and air mass origin in Table 7-1 are used for discussion in chapter 8.

Figure 7-1. Location of Happo (36.4°N 137.5°E) and Oki island (36.2°N, 133.1°E).

Table 7-1. List of the analyzed results of Happo measurements

Date	[CO] (ppb)	1/CO (1/ppm)	d13C (per mil)	d18O (per mil)	14CO (molecule/cm3)	air mass origin
10-Feb-97	228.6	4.4	-25.2	11.0	21.2	W
17-Feb-97	214.5	4.7	-26.0	10.4	22.8	N,NW
25-Feb-97	252.7	4.0		11.3	18.0	W
3-Mar-97	163.1	6.1	-26.8	8.7	21.7	N,NW
11-Mar-97	225.3	4.4	-25.5	10.9	21.3	N,NW
17-Mar-97	166.4	6.0	-26.2	8.9	22.3	N,NW
8-Apr-97	223.6	4.5	-24.5	9.4	19.0	W
14-Apr-97	210.5	4.7	-25.1	8.4	18.3	W
22-Apr-97	219.9	4.5	-25.3	9.7	20.2	W
29-Apr-97	186.9	5.4	-24.6	8.3	18.2	W
14-May-97	170.8	5.9	-25.5	5.4	18.8	S,SE
26-May-97	210.2	4.8	-24.7	7.7	18.6	JP
9-Jun-97	222.5	4.5	-25.4	8.7	14.8	JP
23-Jun-97	219.5	4.6	-26.4	8.3	11.4	W
8-Jul-97	111.0	9.0	-28.1	3.0	8.6	SW
22-Jul-97	230.3	4.3	-27.4	7.9	12.7	JP
4-Aug-97	215.3	4.6	-28.2	7.3	8.8	JP
19-Aug-97	139.0	7.2	-28.9	4.9	9.4	S,SE
1-Sep-97	226.1	4.4	-28.1	7.7	9.4	W
15-Sep-97	120.7	8.3	-28.0	3.2	10.9	S,SE
29-Sep-97	142.1	7.0		6.3	12.8	N,NW
13-Oct-97	134.3	7.4	-27.6	4.9	15.2	N,NW
27-Oct-97	156.4	6.4	-27.4	7.5	15.2	N,NW
14-Nov-97	294.6	3.4	-25.6	12.3	13.4	JP
25-Nov-97	207.5	4.8	-26.4	9.0	15.4	W
8-Dec-97	177.5	5.6	-25.5	7.4	14.0	W
19-Jan-98	157.8	6.3	-26.2	8.8	19.6	N,NW
29-Jan-98	170.9	5.9	-26.1	9.1	22.1	N,NW
2-Feb-98	159.3	6.3	-26.0	7.6	20.0	W
23-Feb-98	210.5	4.8	-25.9	9.7	21.1	N,NW
28-Feb-98	382.2	2.6	-24.9	13.0	20.0	JP
13-Mar-98	261.0	3.8	-24.6	10.1	25.0	W
4-Apr-98	165.4	6.0	-24.8	6.8	22.9	W
13-Apr-98	174.3	5.7	-25.7	5.6	11.6	S,SE
29-Apr-98	236.8	4.2	-24.9	8.7	17.9	W
13-May-98	221.7	4.5	-24.8	8.6	18.6	N,NW
29-May-98	209.3	4.8	-25.3	7.2	16.8	SW
15-Jun-98	160.1	6.2	-25.8	3.6	14.0	JP
30-Jun-98	137.2	7.3	-27.2	0.3	13.2	N,NW
13-Jul-98	138.0	7.2	-26.2	2.3	10.5	N,NW
28-Jul-98	108.7	9.2	-29.0	0.4	8.1	SW
11-Aug-98	148.8	6.7	-27.4	3.0	9.2	SW
7-Sep-98	101.0	9.9	-27.3	7.3	5.3	W
18-Sep-98	300.3	3.3	-26.9	9.9	13.4	JP
1-Oct-98	133.6	7.5	-27.5	3.6	8.7	S,SE
16-Oct-98	84.1	11.9	-25.6	7.4	4.8	S,SE
22-Oct-98	135.5	7.4	-27.3	3.9	12.4	N,NW
2-Nov-98	126.7	7.9	-27.1	2.6	14.4	W
17-Nov-98	274.3	3.6	-24.3	10.8		W
1-Dec-98	131.5	7.6	-26.2	4.6		W
14-Dec-98	182.0	5.5	-26.0	7.8		W
28-Dec-98	240.6	4.2	-26.2	9.2		W
12-Jan-99	183.1	5.5	-26.2	8.1		
29-Jan-99	204.1	4.9	-25.7	9.4		

7-2 Seasonal cycle

In Figure 7-2 the CO concentration measured by the extraction method (measurements for isotope analysis) is plotted by circles. Since the CO concentration has some scatter, especially during summer, outliers are plotted by open circles. CO concentration is also measured continuously at Happo since 1996 with an NDIR CO analyzer (Kimoto Model 540S, NDIR means non dispersive infrared). The CO data measured this way from 1996 to 1998, given as median values to reduce the effect of data affected by pollution, are also plotted in Figure 7-2 by open triangles. In spite of totally different measurement methods, it can be said that the difference is not so large. Some CO data measured by extraction method have large deviation from NDIR data, since they represent the CO concentration at a given moment during sampling (average of about 1 hour) and the NDIR data points represent monthly average CO concentration.

At other remote sites in Japan, the CO concentration has a maximum in April and minimum in August (Oki island, shown in Figure 7-1) [*Pochanart et al.*, 1996; 1999]. In August there is large scatter in the Happo data, and this is a character of this site. Since Japan is under the Pacific marine air mass during summer, air masses pass over the mainland of Japan are polluted occasionally. Air polluted by regional CO sources can be distinguished clearly by high CO concentration. When ignoring the higher CO data, one can see a similar CO seasonal cycle as at Oki island. The maximum CO concentration of about 230 ppbv appears in April. Then CO concentration decreases rapidly and the lowest CO concentration of about 120 ppbv appears in August. After that CO concentration increases gradually to the spring peak in the next year. Except for the later spring peak, this seasonal variation is same as other remote sites in the mid- and high latitude in the northern hemisphere as shown in Figure 1-2 [*Novelli et al.*, 1998].

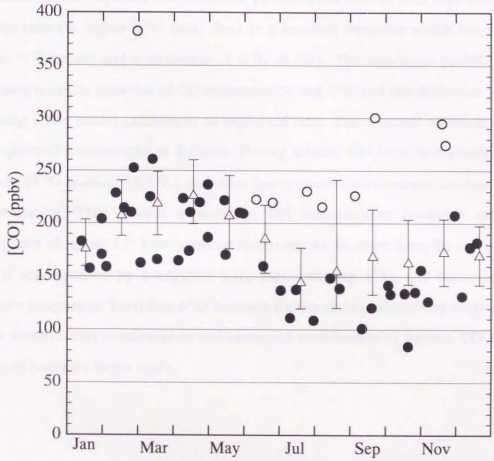

Figure 7-2. CO concentration at Happo in 1997 and 1998. Open circles represent data affected by pollution. CO concentrations measured by NDIR are also plotted by open triangles. They are given as median and the error bars indicate the 25 % and 75 % spread.

In Figure 7-3, the result of $C^{18}O$ measurements is plotted by circles. Open circles are data affected by pollution. These data show similar seasonal variation as the CO concentration; high during winter-spring and low during summer. Also, higher $\delta^{18}O$ values appear corresponding to higher CO concentrations, generally polluted air. This indicates that the expected CO source for pollution has heavier $\delta^{18}O$ than clean air CO. If one ignores the higher $\delta^{18}O$ data, there is a seasonal variation which has a maximum 11 ‰ in February and a minimum of 0 ‰ in July. The maximum period appeared in February is earlier than that of CO concentration and $\delta^{13}C$ and this difference is explained by using a box model calculation as explained later. The seasonal variation of $\delta^{18}O$ can be explained qualitatively as follows. During winter, CO from isotopically heavy car exhaust ($\delta^{18}O$ is about 23.5 ‰) and other heavy sources accumulates because of low OH concentration. Then toward to summer, OH concentration increases and enhances production of lighter CO from methane oxidation. At the same time, the reaction of CO + OH is accompanied by a negative KIE, then reducing $\delta^{18}O$. CO becomes lighter as reaction progresses. Therefore $\delta^{18}O$ becomes lighter during summer by these two factors. After summer, OH concentration decreases and contribution of heavier CO sources (car exhaust) becomes larger again.

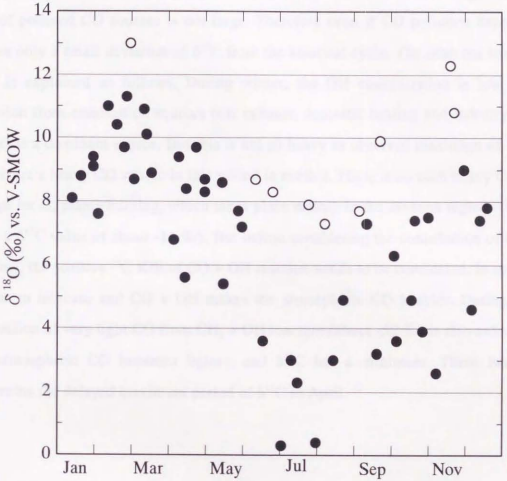

Figure 7-3. $\delta^{18}O$ of CO measured at Happo in 1997 and 1998. Open circles represent data affected by pollution.

The results of the measurements of ^{13}CO are shown in Figure 7-4. There is a very clear seasonal cycle with a maximum of about -25 ‰ around April, and a minimum of -28.5 ‰ around August. In spite of some CO polluted measurements found in Figure 7-2 and Figure 7-3, there is only small deviation from in the seasonal variation curve of $\delta^{13}C$. This is explained that the difference between the $\delta^{13}C$ value of CO in background air and that of polluted CO sources is not large. Therefore even if CO pollution happens, this causes only a small deviation of $\delta^{13}C$ from the seasonal cycle. The seasonal variation of $\delta^{13}C$ is explained as follows. During winter, the OH concentration is low and CO emission from combustion sources (car exhaust, domestic heating and industry; about -27 ‰) is a dominant source. But this is not so heavy as observed maximum of -24.5 ‰. Therefore a heavy CO source in this period is needed. There is no such heavy CO source except for C_4 plants burning, which takes place mainly in the savanna regions (C_4 plants have a $\delta^{13}C$ value of about -11 ‰). But before considering the contribution of C_4 plants burning, the positive ^{13}C KIE of CO + OH reaction needs to be considered. In spring, OH begins to increase and CO + OH makes the atmospheric CO heavier. During summer production of very light CO from CH_4 + OH reaction (about -52 ‰) is also enhanced and the atmospheric CO becomes lighter, and $\delta^{13}C$ has a minimum. These two factors determine the delayed maximum period of $\delta^{13}C$ in April.

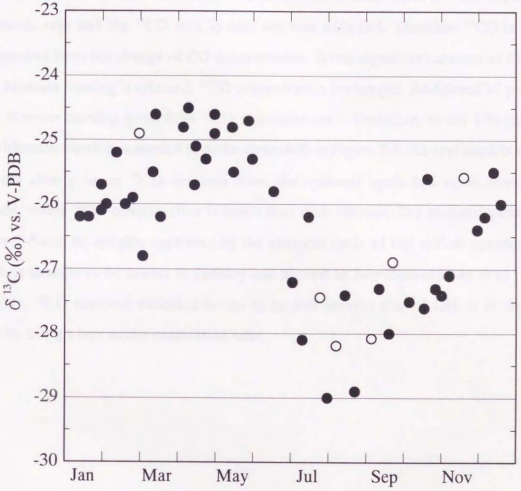

Figure 7-4. $\delta^{13}C$ of CO measured at Happo in 1997 and 1998. Open circles represent data affected by pollution.

The results of ^{14}CO measurements are shown in Figure 7-5. Except for some lower data, there is a clear seasonal variation. The maximum is about 23 molecules cm^{-3} in February (or March) and minimum is about 9 molecules cm^{-3} in July. The maximum of ^{14}CO appears earlier than that of CO concentration and $\delta^{13}C$. ^{14}CO values have small deviations from the seasonal cycle, even for polluted air measurements. Most of ^{14}CO is produced by cosmic rays and the ^{14}CO sink is only reaction with OH. Therefore ^{14}CO is almost independent from the change of CO concentration. When significant amount of CO from local biomass burning is affected, ^{14}CO concentration is changed. Additional 10 ppbv CO from biomass burning gives 0.38 ^{14}CO molecules cm^{-3}. Therefore, to say 100 ppbv CO from biomass burning is needed to make clear shift in Figure 7-5. As explained in chapter 8-3, the clearly lower ^{14}CO deviated from the seasonal cycle had come from lower latitude, where ^{14}CO concentration is lower than mid- latitude. The seasonal variation in Figure 7-5 can be roughly explained by the seasonal cycle of OH radical concentration, which is thought to be lowest in January and highest in July [*Spivakovsky et al.*, 1990]. Roughly, ^{14}CO seasonal variation seems to be just inverse that of OH. It is discussed more by using a box model calculation later.

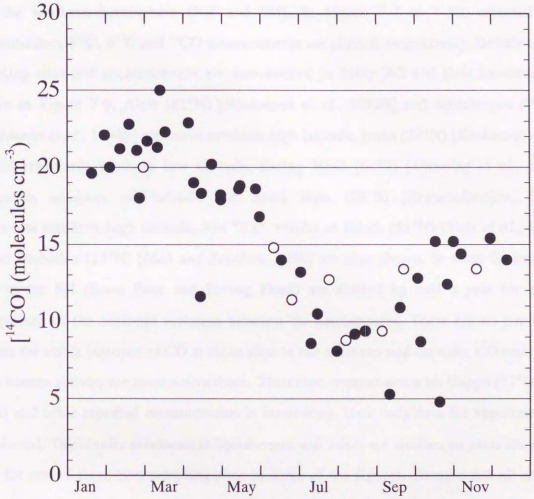

Figure 7-5. ^{14}CO measured at Happo in 1997 and 1998. Open circles represent data affected by pollution.

7-3 Comparison with other isotopic measurements of CO

There is only a limited number of published time series for atmospheric CO isotopes at fixed remote sampling stations. Here I will group the data for the northern hemisphere and the southern hemisphere (NH and SH). In Figure 7-7 to 7-10, reported CO concentration, $\delta^{18}O$, $\delta^{13}C$ and ^{14}CO measurements are plotted, respectively. Details of the sampling sites and measurements are summarized in Table 7-2 and their locations are shown in Figure 7-6. Alert (81°N) [*Röckmann et al.*, 1998b] and Spitsbergen (79°N) [*Röckmann et al.*, 1998b] represent northern high latitude, Izaña (28°N) [*Röckmann et al.*, 1998b] represents northern low latitude, Baring Head (41°S) [*Manning et al.*, 1997] represents southern mid-latitude and Scott Base (78°S) [*Brenninkmeijer*, 1993] represents southern high latitude. For ^{14}CO, results at Jülich (51°N) [*Volz et al.*, 1981] and at Barbados (13°N) [*Mak and Southon*, 1998] are also shown. In these figures, the date in the SH (Scott Base and Baring Head) are shifted by half a year for easier comparison of the seasonal variation between the hemispheres. There are no published reports for stable isotopes of CO at clean sites in the northern mid-latitude. CO emissions from human activity are most active there. Therefore, comparison with Happo (37°N, this work) and other reported measurements is interesting. Here only data for unpolluted air are plotted. The results measured at Spitsbergen and Alert are similar, so plots are given only for one of these two sampling sites in some of the figures. Because not all reports give the original data, some data were read from the figures, and there may be small errors in the reading procedure. Also some data are averaged over a month. The measurements at Illinois [*Stevens et al.*, 1972] are not used since it is difficult to read values from their figures and considerable pollution by local fossil fuel exhaust is suspected during winter; high CO concentration and heavy $\delta^{18}O$ were similar to CO from car exhaust.

Table 7-2. Sampling sites for continuous CO isotopic measurements

site	latitude	location	sampling period	reference
Scott Base	78°S	Antarctica	July, 1991 - Feb., 1992	*Brenninkmeijer,* 1993
Baring Head	41°S	New Zealand	June, 1989 - June, 1995	*Manning et al,* 1997
				Brenninkmeijer, 1993
				Brenninkmeijer et al., 1992
Barbados	13°N	Barbados	Jul,1996-	*Mak and Southon,* 1998
Izaña	28°N	Spain	Nov., 1996 -	*Röckmann et al,* 1998b
Happo	37°N	Japan	Feb., 1997 - Jan., 1999	This work
Jülich	51°N	Germany	May, 1977 - Sep., 1978	*Volz et al.*, 1981
Spitsbergen	79°N	Norway	Apl., 1995- Jun., 1995	*Röckmann and Brenninkmeijer,* 1997
			Nov., 1996 -	*Röckmann et al,* 1998b
				Röckmann et al, 1998a
Alert	81°N	Canada	Nov., 1996 -	*Röckmann et al,* 1998b
				Röckmann et al, 1998a

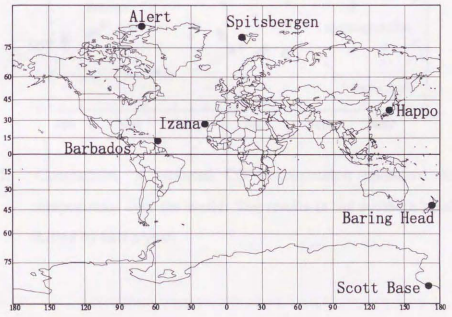

Figure 7-6. Location of sampling sites for isotopic measurements of CO.

From Figure 7-7, one can find that CO concentrations are much lower in the SH and show smaller seasonal variations. This is a well known fact. Spitsbergen and Alert data are about 30 ppbv lower than the Happo measurements. Izaña and Barbados are located at low latitude and seem to have a near constant CO concentration of 100 ppb with slightly lower concentration during summer. The difference between the NH and the SH is largest in February-March (winter in the NH) and minimum in July-August (summer in the NH).

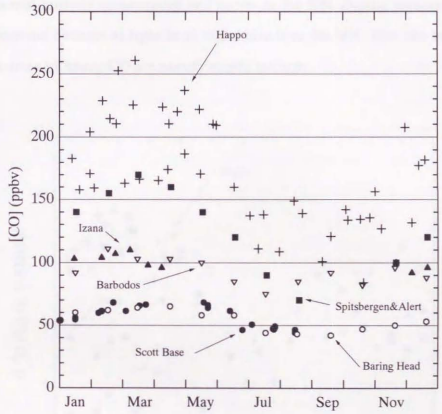

Figure 7-7. Comparison of reported CO concentration measured for isotopic compositions over the world. The results in the southern hemisphere are shifted by half a year.

As shown in Figure 7-8, there is large difference of $\delta^{18}O$ between the NH and the SH. Especially during winter, the difference becomes very large. The interhemispheric difference is smaller during summer, and $\delta^{18}O$ at northern high-latitude approaches that of the SH. Most of the heavy CO (at about 23.5 ‰) from combustion is emitted in the NH, and this causes the interhemispheric difference of $\delta^{18}O$. In the northern high-latitude, $\delta^{18}O$ is comparable to northern mid-latitude during winter and spring. Because OH concentrations are low in winter and only a small fraction of CO reacts, polluted air emitted in mid-latitude accumulates and mixes in the NH. During summer, $\delta^{18}O$ at mid latitude does not become as light as at high latitude in the NH. This can be explained in that the sources of heavy CO are mostly at mid latitude.

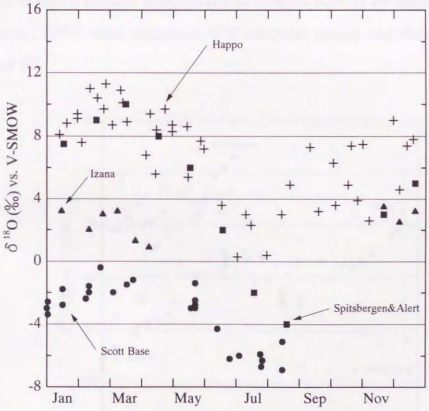

Figure 7-8. Comparison of reported $\delta^{18}O$ of CO over the world.

Seasonal variations of $\delta^{13}C$ are shown in Figure 7-9. No seasonal variation has been published in the NH except for short period measurements at Spitsbergen [*Röckmann and Brenninkmeijer*, 1997]. $\delta^{13}C$ is heavier in the NH than in the SH most of the time. This can be explained that CO emissions from combustion (-27 ‰) are smaller in the SH, whereas the isotopically very light CO from CH_4 (-52 ‰) is about the same in both hemisphere. The $\delta^{13}C$ maximum at Happo appears in April, but in the northern high-latitudes (Spitsbergen) there is a steep $\delta^{13}C$ increase during polar sunrise period. *Röckmann et al.* [1997] explained this rapid $\delta^{13}C$ increase as the result of the KIE of CO oxidation by OH. In this explanation, CO formation from CH_4 oxidation by OH, which is very depleted in $\delta^{13}C$ by about -52 ‰, is not considered. This light CO source seems to contradict their explanation for the rapid $\delta^{13}C$ increase. There should be another reason for this. In the SH, the $\delta^{13}C$ maximum is just before summer (December in the SH). This shift of peak period is thought to be caused by biomass burning [*Brenninkmeijer*, 1993; *Manning et al.*, 1997]. After maximum, $\delta^{13}C$ decreases rapidly and shows minimum in March in the SH.

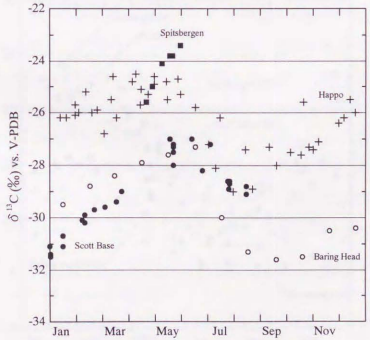

Figure 7-9. Comparison of reported $\delta^{13}C$ of CO over the world.

In Figure 7-10 ^{14}CO measurements over the world are shown. ^{14}CO production is affected by the 11 year solar cycle, but here this factor is not considered and all data are just plotted together. The data for Baring Head are the average values from *Brenninkmeijer* [1993]. In spite of latitudinal and solar cycle difference, measurements in the middle and high northern hemisphere have similar values and seasonal cycles, and well mixing of tropospheric air in those latitudes is expected. The maximum appears in February, and minimum appears in July. The measurements in the Tropics, Barbados, show lowest ^{14}CO. *Mak and Southon* [1998] explained that these low ^{14}CO were still higher during winter than expected values by modeling studies and ^{14}CO transportation from higher latitude was expected. In the SH the maximum and minimum period is almost same as in the NH, but the ^{14}CO concentration is lower, especially the winter maximum in the SH. Because the ^{14}CO production by cosmic rays is nearly symmetric in both hemispheres [*Jöckel et al.*, 1999], *Brenninkmeijer et al.*, [1992] had pointed out the interhemispheric asymmetry of average OH concentration; higher in the SH than in the NH.

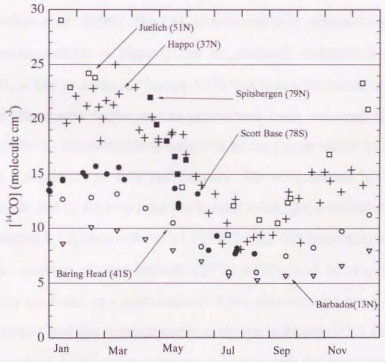

Figure 7-10. Comparison of reported ^{14}CO over the world.

7-4 Box Model calculation in northern mid latitude

Box model calculations are performed for the CO concentration, $\delta^{18}O$, $\delta^{13}C$ and ^{14}CO. No model calculation has been reported for stable isotopes in the NH and there is a two dimensional calculation only for $\delta^{13}C$ in the SH [*Manning et al.*, 1997]. The parameters for the calculations conform the conditions basically at northern mid-latitude and 2 km altitude. The respective CO sources are fossil fuel combustion (FF), biomass burning (BB), oxidation of non methane hydrocarbons (NMHC) and oxidation of CH_4. The values used for these CO sources are listed in Table 7-3. The fluxes of FF, BB and NMHC are calculated from the global estimation (640, 520 an 320 TgCO yr^{-1} [*Novelli et al.*, 1998]) and these flux are portioned to NH (94, 63 and 72 %), referring to [*Logan et al.*, 1981]. Seasonal variations of CO source fluxes are shown in Figure 7-12. Because BB is enhanced during spring in the NH (for example [*Cahoon Jr. et al.*, 1994]), 7/10 of total BB flux is just proportioned equally over year and 3/10 of total BB flux is added on the base as Gaussian manner at the peak in April with the width of about 3 months. NHMC is distributed as average profile from 10°N to 90°N derived from fluxes of isoprene and terpenes [*Guenther et al.*, 1995]. The CH_4 concentration is assumed constant at 1830 ppb (taken from measurements at Happo) and its seasonal variation is ignored. The rate constant of CH_4 + OH is $2.45\times10^{-12}\times\exp(-1775/T[K])$ ($cm^3molecule^{-1}s^{-1}$) [*DeMore et al.*, 1997] and the conversion factor of CO production from oxidized CH_4 is used as 0.8 [*Logan et al.*, 1981]. Temperature is assumed to be a sine curve at 277 ± 8 K with a maximum and a minimum in July and January. The temperature is representing to the about 2km altitude and is the lower than at ground level. OH concentrations are estimated from the estimation by *Spivakovsky et al.* [1990]. The OH concentration in 4 season are taken from the average of mid-latitude (28°N-60°N), and of troposphere (1000-300 mbar). Then they are fitted by a combination of two sine curves ($y = a + b\times\sin(2\pi(x-c)/d) + e\times\cos(2\pi(x-f)/g)$), and the resulted curve is shown in Figure 7-12. Daily average of the maximum value is 14.3×10^5 (molecules cm^{-3}) in July and the minimum value is 1.8×10^5 (molecules cm^{-3}) in January. The rate constant of the sink reaction CO + OH is $1.5\times10^{-13}\times(1+0.6\times P)$ ($cm^3molecule^{-1}s^{-1}$) [*DeMore et al.*, 1997]. P indicates the pressure in the

unit of atm. In this model P is assumed at 0.79 atm (800 hPa), representing the altitude of the sampling site of Happo. The direct emission from ocean and plants, uptake by soil are not considered here. $\delta^{18}O$ and $\delta^{13}C$ values for CO sources are 23.5 ‰ (atmospheric oxygen isotopic composition) and -27.4 ‰ [*Stevens et al.* 1972] for FF. For BB, 18 ‰ [*Stevens and Wagner,* 1989] and -27 ‰ (about same value as C_3 plants) are used. There is no actual measurement of CO from NMHC oxidation, but here $\delta^{18}O$ is assumed to be 5 ‰ (*Brenninkmeijer and Röckmann* [1997] proposed 0 ‰) and $\delta^{13}C$ = -30 ‰, which is slightly lighter than $\delta^{13}C$ of isoprene (-27.9 ‰ [*Stevens*, 1993] and -29.4 ‰ [*Sharkey et al.*, 1991]). For CH_4 oxidation, $\delta^{18}O$ is assumed as 0 ‰ estimated by *Brenninkmeijer and Röckmann* [1997] and $\delta^{13}C$ = -52 ‰ deduced from isotopic composition of CH_4 (-47.2 ‰) [*Lowe et al.*, 1994] and the KIE of CH_4 + OH (5.4 ‰) [*Cantrell et al.*, 1990]. The values of the KIE used are 0.990 for oxygen and 1.005 for carbon [*Stevens and Wagner*, 1989]. The latter value has pressure dependence as shown in Figure 2-1, and it decreases at high altitude (lower pressure). When the pressure is 1 atm and 0.8 atm, the KIE is about 1.006 and 1.004, respectively [*Stevens et al.*, 1980]. In this box model calculation the value of 1.005 is used. The ^{14}CO production rate is taken from the average value in the solar maximum period [*Jöckel et al.*, 1999] and discussed later. The calculation step is one day and calculations starts from 1 January. The initial conditions are taken from Happo measurements, but they are not important because the results become almost stable in the calculated cycle in the second year and do not depending on initial value. The results in the third year are used for discussion.

Table 7-3. Flux and isotopic compositions of CO sources used for the box model calculation

	Fossil Fuel	Biomass Burning	NMHC	CH_4 oxidation
flux [a)]	640×0.94	520×0.63	320×0.72	
$\delta^{18}O$	23.5 ‰	18 ‰	5 ‰	0 ‰
$\delta^{13}C$	-27 ‰	-27 ‰	-30 ‰	-52 ‰

a) Unit is [TgCO yr^{-1}]. Later factor is multiplied for representing the proportion in the northern hemisphere.

The calculated results are shown in Figure 7-11a,b,c,d for CO concentration, $\delta^{18}O$, $\delta^{13}C$ and ^{14}CO, respectively. The observed data at Happo are also plotted by open circles excluding the polluted measurements. The postulated OH concentration and CO source fluxes (FF, BB, NMHC oxidation and CH_4 oxidation) are also shown in Figure 7-12. In spite of using a simple one box model, it can be said that the calculations reproduce well the observed data of CO, $\delta^{18}O$ and ^{14}CO. For $\delta^{13}C$, the phase of the seasonal cycle is reproduced, but the amplitude of the seasonal variation is not enough. The calculated CO maximum appears in April and minimum appears in August, reproducing the observed seasonal cycle as NDIR method. But this calculated spring peak is produced by adding the enhanced flux of biomass burning in spring. When there is no seasonal variation of the BB source (constant over a year), the maximum appears in February, as discussed later. The calculated $\delta^{18}O$ simulate the observations well; the maximum appears in February, earlier than CO concentration or $\delta^{13}C$, and the minimum appears in July-August. For $\delta^{13}C$, the phase of the seasonal variation is simulated; higher in late spring and lower in summer. But the amplitude of the seasonal variation is smaller and there is a discussion for this issue later. The lower values in summer are caused by combination of the KIE and light CO from CH_4. For ^{14}CO, agreement of the phase of the seasonal variation could indicate that proper OH seasonal variation is assumed. But agreement of the absolute value is rather accidental as discussing later.

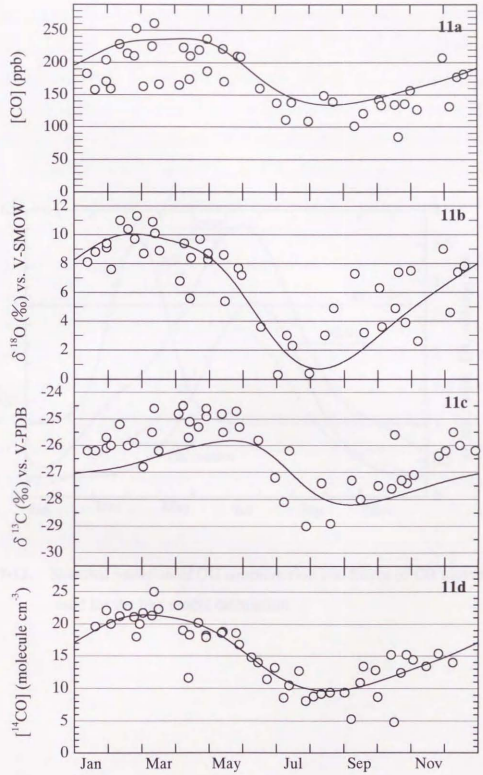

Figure 7-11. The results of the box model calculation.

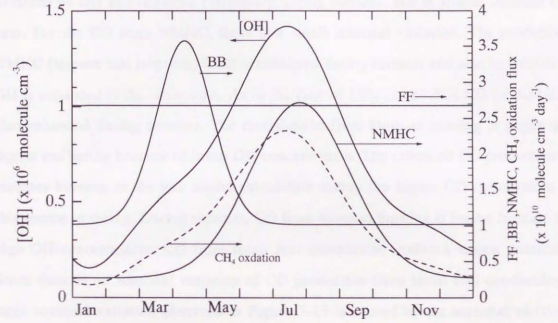

Figure 7-12. Seasonal variation of OH concentration and fluxes of CO sources used for the box model calculation.

From the results of this box model calculation, CO concentration from each CO sources at a given date can be calculated. In Figure 7-13 the seasonal variations of CO concentration from four main CO sources are shown. Note that the proportions of CO concentrations are different from that of the CO fluxes, since produced CO is also removed by OH radicals. CO from CH_4 oxidation is almost constant over a whole year. CO production from CH_4 has considerable seasonal variation and enhanced by high OH concentration during summer. However, the CO produced from CH_4 oxidation is also oxidized by OH and removed intensively during summer, and is almost constant over a year. For the CO from NMHC, there is a small seasonal variation. The production of NMHC (terpene and isoprene) itself is enhanced during summer and also its oxidation by OH is enhanced at the same time. As in the case of CH_4, removal of CO by oxidation is also enhanced during summer. The contribution from biomass burning is larger during winter and spring because of lower OH concentration. The enhanced CO production from biomass burning in the box model calculation makes the higher CO contribution from this source in spring. During summer, CO from biomass burning is lowest because of the high OH concentration. CO from fossil fuel combustion makes a largest contribution. Since there is no seasonal variation of CO production from fossil fuel combustion, the large seasonal variation observed in Figure 7-13 is caused by the seasonal variation of OH. The contribution of fossil fuel combustion is considerable during winter.

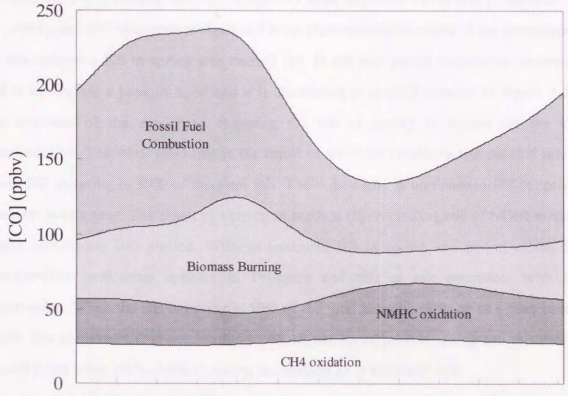

Figure 7-13. Labeled CO concentration for each CO source (a) and the seasonal variation of CO sink reaction (CO+OH) in the box model calculation.

Since data of seasonal variation of biomass burning (BB) in the mid- northern latitude are not available, model enhanced BB in spring is postulated in the box model calculation. This is more realistic situation than no seasonal variation of BB. In lower northern latitude, BB takes place in March (for example in Thailand, [*Pochanart et al.*, submitted]). BB in Siberia has been recognized as an important CO source [*Cahoon Jr. et al.*, 1994], and it is enhanced in April and May. Here sensitivity check of the contribution of this enhanced BB in spring was carried out. In the box model calculation, enhanced BB in Spring has a peak in April and it is distributed in about 3 months. In Figure 7-14, the response of the model to changing the BB in spring is shown for the CO concentration. The thick solid line is the result of the basic condition and the thin line is when BB in spring is 50% of the total BB. The dotted line is no enhance BB in spring, constant over a year. The result of extraction method (open circles) and of NDIR method (solid circles) are also plotted. Without enhanced BB in spring, the period of the CO concentration maximum appears in February and this is not consistent with the observation. When the BB in spring is 50% of the total amount, there arise a peak in late April. The observed CO concentration by NDIR has broad peak in spring and this profile is well fitted when 30% of BB in spring is assumed as in the basic run.

In Figure 7-15, the period of BB peak is shifted. When the BB flux peak is appeared at middle of March as shown by a thin solid line, CO concentration peak appears earlier in late March. The maximum value become over 250 ppbv and it is too high. When the period of BB peak is in May as shown by a dotted line, the peak is still in February and no peak is produced in May. In May, OH concentration has started to increase and additional CO from BB is removed quickly, so it makes less effect than emitted in March. The additional CO flux during spring makes "Spring peak" of CO concentration, and this is sensitive to the peak period of the additional CO flux. The peak period in April postulated in the box model calculation would be reasonable from the calculated results and also from the fact that the period of BB shifts from March to May as latitude increases.

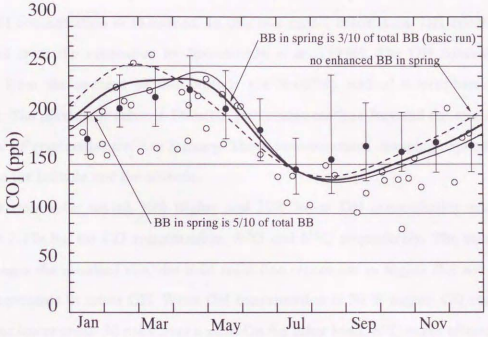

Figure 7-14. Model results when changing CO flux in spring from biomass burning

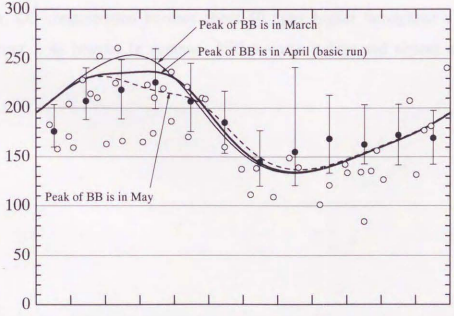

Figure7-15. Model result when chaning the peak period of biomass burning in spring

OH concentration is a very important factor for CO model, but the OH concentration distribution itself is not yet well defined. Here sensitivity of the box model calculation for OH concentration is examined. In this box model calculation, OH concentration is derived from the estimation by *Spivakovsky et al.* [1990]. The OH concentration are taken from the average of mid-latitude (28°N-60°N), and of troposphere (1000-300 mbar). The maximum value is 14.3×10^5 (molecules cm^{-3}) in July and the minimum value is 1.8×10^5 (molecules cm^{-3}) in January. These concentrations changing depending how to choose the latitude and the altitude.

The results for taking 30% higher and 30% lower OH concentration are shown in figure 7-17a,b,c for CO concentration, $\delta^{18}O$ and $\delta^{13}C$, respectively. The thin solid line represents the standard run, the bold solid line represents in higher OH and the dotted line represents in lower OH. When OH concentration is 30 % higher, CO concentration become lower about 30 ppbv over a year. On the other hand, $\delta^{18}O$ is not affected so much and becomes about 1 ‰ lighter in summer. $\delta^{13}C$ becomes lighter, especially during summer by the enhanced production of light CO from CH_4. When OH concentration is 30% lower, CO concentration become about 50 ppbv higher throughout a year. $\delta^{18}O$ become about 1 ‰ heavier in summer. $\delta^{13}C$ become lighter and almost no seasonal variation.

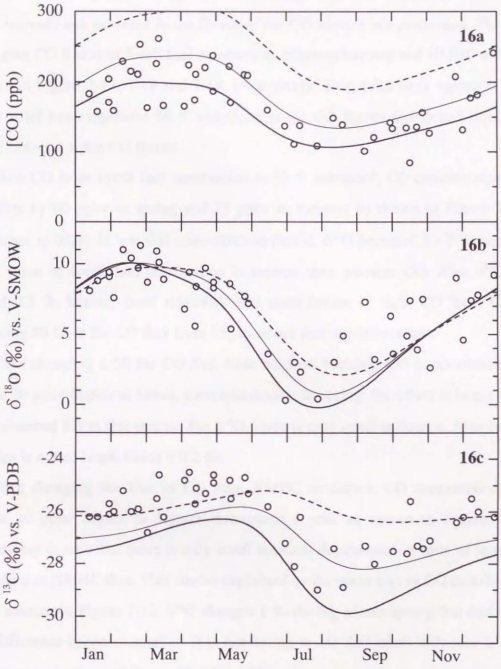

Figure 16. Model results of higher and lower OH concentration. Thin solid lines represent the basic run, thick solid lines represent higher OH concentration and dotted lines represents lower OH concentration.

The uncertainty of the estimation of the fluxes of CO sources has large. Here the influence of changing these CO fluxes are examined. The calculation when changing 50% increase and decrease in the fluxes of the CO sources are performed. The results of changing CO fluxes of fossil fuel combustion, biomass burning and NMHC oxidation are shown in Figure 7-17, 7-18 and 7-19, respectively. Thin solid lines represent basic run, thick solid lines represent 50 % enhanced in the CO fluxes and dotted lines represent 50 % reduced in the CO fluxes.

When CO from fossil fuel combustion is 50 % enhanced, CO concentration becomes increase by 60 ppbv in spring and 25 ppbv in summer as shown in Figure 7-17a. The influence is larger in low OH concentration period. $\delta^{18}O$ becomes 1 - 2 ‰ heavier since $\delta^{18}O$ value of fossil fuel combustion is heavier than ambient CO. Also $\delta^{13}C$ becomes about 0.3 ‰ heavier from relatively less contribution of light CO from CH_4. When reducing 50 % of the CO flux from FF, there are just opposite results.

When changing ± 50 for CO flux from biomass burning, CO concentration becomes about 20 ppbv higher or lower, correspondingly. In spring, the effect is larger because of the enhanced BB in this season. For $\delta^{18}O$, there is only small influence. Also for $\delta^{13}C$, the change is not so large, about ± 0.2 ‰.

When changing the flux of CO from NMHC oxidation, CO concentration becomes about 20 ppbv higher or lighter throughout a year as shown in Figure 7-19. It is interesting to note that there is only small seasonal dependence in spite of large seasonal variation of NMHC flux. This can be explained by the same way as CO contribution from each sources in Figure 7-12. $\delta^{18}O$ changes 1 ‰ during winter-spring, but during summer the difference becomes smaller. It is interesting to see that small influence is derived in the season of enhanced flux in NMHC. $\delta^{13}C$ is affected by only small extent.

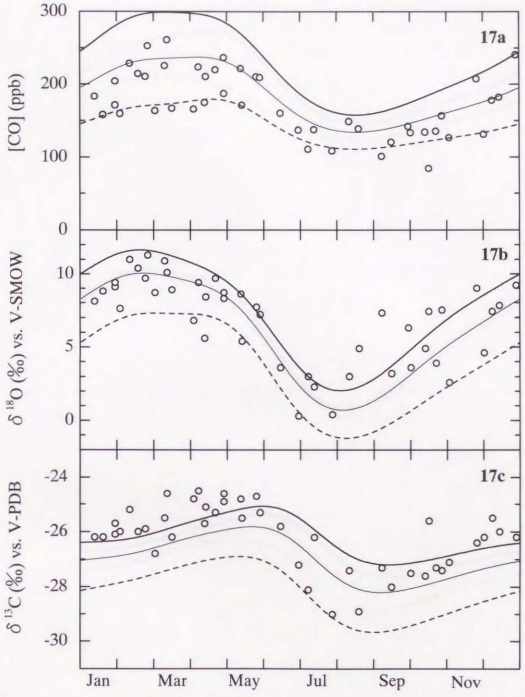

Figure 7-17. Model results of more and less CO flux from fossil fuel combustion. Thin solid lines represent the basic run, thick solid lines represent 50 % more flux and dotted lines represents 50 % less flux.

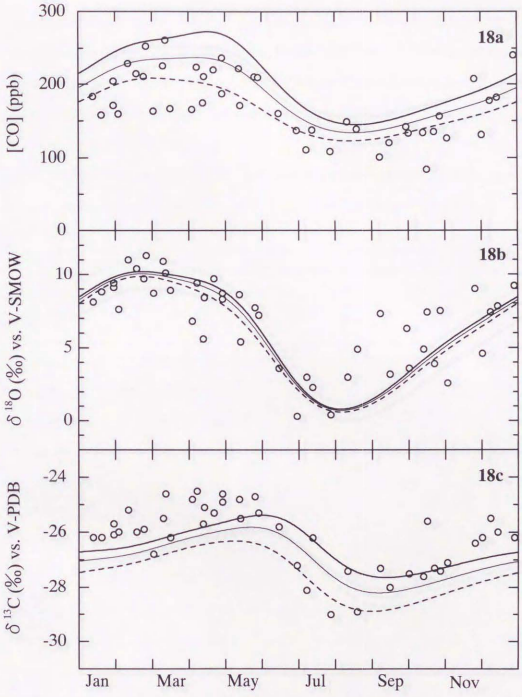

Figure 7-18. Model results of more and less CO flux from biomass burning. Thin solid lines represent the basic run, thick solid lines represent 50 % more flux and dotted lines represents 50 % less flux.

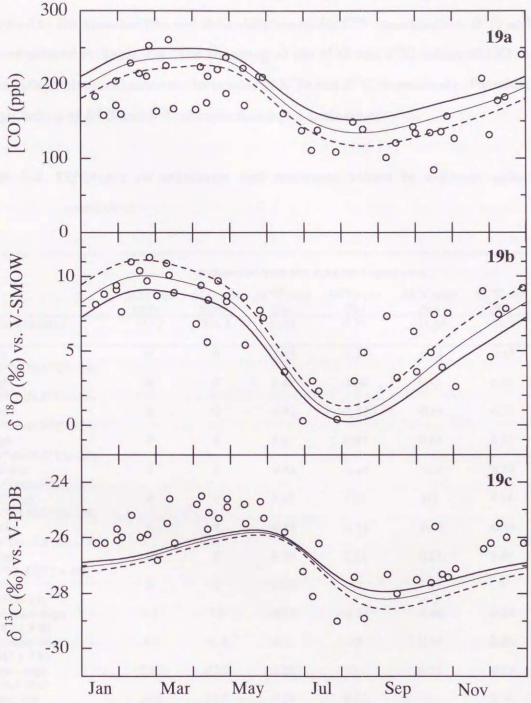

Figure 7-19. Model results of more and less CO flux from NMHC oxidation. Thin solid lines represent the basic run, thick solid lines represent 50 % more flux and dotted lines represents 50 % less flux.

The influences of changing the isotopic compositions of the CO sources are examined here. Also other parameters, temperature and pressure etc. are changed. Their results are compared to the standard run and their differences for CO concentration, $\delta^{18}O$ and $\delta^{13}C$ are summarized in Table 7-4. The changing of the $\delta^{18}O$ and $\delta^{13}C$ values of CO sources makes independent influence to the results of $\delta^{18}O$ and $\delta^{13}C$ respectively. Therefore, low or high values of $\delta^{18}O$ and $\delta^{13}C$ are calculated at a same time.

Table 7-4. Difference of maximum and minimum values in different calculation conditions.

	difference from the standard condition					
	ΔCO-max (ppbv)	ΔCO-min (ppbv)	$\Delta\delta^{18}O$-max (‰)	$\Delta\delta^{18}O$-min (‰)	$\Delta\delta^{13}C$-max (‰)	$\Delta\delta^{13}C$-min (‰)
standard condition	237.2	134.3	10.05	0.71	-25.81	-28.2
FF-low ($\delta^{18}O$=20,$\delta^{13}C$= -28)	0	0	-1.89	-1.21	-0.45	-0.35
FF-high ($\delta^{18}O$=26,$\delta^{13}C$= -26)	0	0	1.36	0.86	0.45	0.36
BB-low ($\delta^{18}O$=14,$\delta^{13}C$= -29)	0	0	-0.86	-0.69	-0.64	-0.31
BB-high ($\delta^{18}O$=22,$\delta^{13}C$= -25)	0	0	0.87	0.67	0.64	0.32
NMHC-low ($\delta^{18}O$=0,$\delta^{13}C$= -32)	0	0	-0.61	-1.24	-0.2	-0.54
NMHC-high ($\delta^{18}O$=10,$\delta^{13}C$= -28)	0	0	0.62	1.21	0.2	0.54
CH_4-low ($\delta^{18}O$= -5,$\delta^{13}C$= -54)	0	0	-0.55	-1.14	-0.27	-0.45
CH_4-high ($\delta^{18}O$=5,$\delta^{13}C$= -50)	0	0	0.56	1.13	0.27	0.45
CH_4 -high ($\delta^{18}O$= 15)	0	0	1.67	3.4	0	0
Temperature -high (287 ± 8 K)	6.5	7.3	-0.56	-0.54	-0.66	-0.97
Temperature -low (267 ± 8 K)	-5.6	-6.4	0.51	0.5	0.64	0.91
Pressure - high (1013 hPa)	-15.3	-12.1	0.23	-0.1	0.09	-0.13
Pressure -low (600 hPa)	16.6	13.6	-0.24	0.12	-0.1	0.14
Low conversion of CO from CH_4 (α = 0.7)	-3.3	-3.9	0.3	0.3	0.37	0.55
[CH4] -low (1730 ppb)	-1.5	-1.7	0.13	0.13	0.16	0.24

When FF has lighter isotopic values, the maximum and minimum of $\delta^{18}O$ and $\delta^{13}C$ become lighter. The influence is larger for maximum of $\delta^{18}O$, in spring when the contribution from FF is larger. Also heavier FF makes heavier results. In the case of BB, the results have more impact for the maximum values. NMHC gives larger influence for the minimum values in summer, since this CO source is enhanced in summer. CO from oxidation of CH_4 is also more effective in summer same as NMHC.

About the oxygen isotopic composition of CO from CH_4 oxidation and NMHC oxidation, only limited information is available. *Stevens and Wagner* [1989] estimated $\delta^{18}O$ = 15 ‰ from the dilution plots on Illinois measurements. The other estimate was proposed by *Brenninkmeijer and Röckmann* [1997]. Judging from the atmospheric observation in the SH, light CO with a $\delta^{18}O$ of nearly 0 ‰ from CH_4 oxidation is needed to balance the observed results. They applied 0 ‰ and 10 ‰ for isotopic composition of NMHC oxidation and stated that the former was more proper value. In this box model calculation, this light isotopic composition from CH_4 oxidation (0 ‰) is used. But for NMHC, 5 ‰ is used because there may be a contribution from NHMC oxidized by ozone, which should produce very heavy oxygen [*Röckmann et al.*, 1998a]. When the heavier $\delta^{18}O$ (15‰) is assumed, the calculated $\delta^{18}O$ becomes 3.4 ‰ heavier in summer. Therefore it is certain that the CO produced from CH_4 oxidation is not so heavy, around zero as proposed by *Brenninkmeijer and Röckmann* [1997].

The temperature influences to some extent for the results of CO concentration and isotopic compositions. In this box model, temperature dependence is used only the CO production reaction from CH_4 ($k=2.45\times10^{-12}\times\exp(-1775/T[K])$ ($cm^3molecule^{-1}s^{-1}$)) [*DeMore et al.*, 1997]. When temperature is higher, CH_4 oxidation is enhanced and CO concentration becomes higher. Since CO from CH_4 oxidation has light $\delta^{18}O$ and $\delta^{13}C$, the calculated results become lighter in $\delta^{18}O$ and $\delta^{13}C$. When temperature is lower, it becomes to opposite situations.

When pressure is changed, CO concentration are influenced about 15 ppbv. On the other hand, isotopic values are not so influenced. In the box model calculation, pressure

dependence is applied in the reaction of CO oxidation by OH ($k=1.5\times10^{-13}\times(1+0.6\times P)$ ($cm^3molecule^{-1}s^{-1}$) [*DeMore et al.*, 1997]). At higher pressure, CO oxidation is enhanced and CO concentration becomes lower. In lower pressure, CO concentration becomes higher because of less oxidation reaction.

The lower conversion factor of CO production from CH_4 oxidation (from 0.8 to 0.7) does not affect so much. In the model calculation in the southern hemisphere [*Manning et al.*, 1997], the conversion factor from CH_4 is a sensitive factor for $\delta^{13}C$ values. In the northern hemisphere, the contribution of CO from CH_4 is lower because of large contribution of FF. When the CH_4 concentration is lower, the CO production by CH_4 oxidation is enhanced. But there are only small influence on the results.

The KIE value of CO+OH for carbon has pressure dependence as shown Figure 2-1. When the pressure is at the ground level, KIE = 1.006 and it decreases as pressure decreases. The standard calculation employed KIE = 1.005. When changing the KIE value to 1.006 or 1.004, the calculated $\delta^{13}C$ values shift lighter or heavier as shown in Figure 7-20. They shift about 0.8 ‰ throughout a year. The standard run (KIE = 1.005) has less amplitude of spring maximum and summer minimum than the observation. Only changing the KIE value makes systematic shifts and does not make up for the differences of the maximum and the minimum at a same time. From Table 7-4, the change of isotopic values for FF and BB give larger influence to the maximum values, and for NMHC and CH_4 give larger influence to the minimum values. But they also influence to the less affected period about half the value of more affected period. Therefore, amplitude of the seasonal variation can not be increased easily. Changing of OH concentration gives large influence to the seasonal variation of $\delta^{13}C$ as shown in Figure 7-16c. In Figure 7-20, the results when KIE = 1.006 and higher OH concentration (1.3 times higher) are shown. The amplitude of the seasonal variation becomes larger. Higher OH concentration also affects CO concentration and $\delta^{18}O$ value. CO concentration becomes too low in this case. Also, KIE = 1.006 means CO oxidation takes place mostly in ground surface atmosphere.

There is a difficulty for the amplitude of the seasonal variation of $\delta^{13}C$, but it can be said that its seasonal variation is reproduced by the box model calculation.

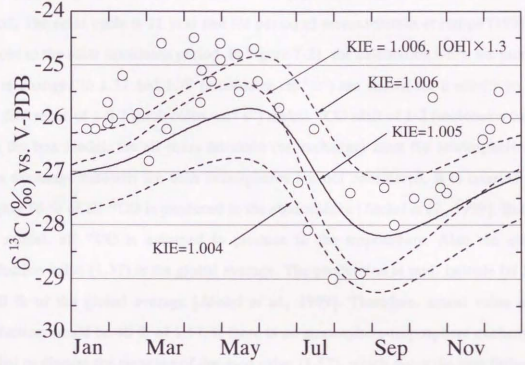

Figure 7-20. Model results by changing the KIE of CO+OH value and OH concentration.

The results of ^{14}CO is discussed here. The best result of the production rate of ^{14}CO is 1.57 (molecules cm^{-2} s^{-1}) in the box model calculation. This value is taken from the global average production rate for solar maximum period [*Jöckel et al.,* 1999]. But this good agreement is rather accidental. ^{14}C production is minimum in the solar maximum period, and its production rate becomes 2.495 (molecules cm^{-2} s^{-1}) in the solar minimum period. The solar cycle is 11 year and the period of measurements at Happo (1997-1998) is close to the solar maximum period. In Figure 7-21, the calculation when the production rate is changed to 1.37 and 1.77 (molecules cm^{-2} s^{-1}) are shown for a sensitivity check. The difference of ± 0.2 (molecules cm^{-2} s^{-1}) makes ^{14}CO shift of 1-2 (molecules cm^{-3}).

In the box model, the air mass intrusion (or exchange) from the stratosphere and air mass exchange between the both hemispheres are not considered. It is considered that roughly 50 % of all ^{14}CO is produced in the stratosphere [*Jöckel et al.,* 1999]. But in this box model, all ^{14}CO is assumed to produce in the troposphere. Also the employed production value (1.57) is the global average. The production at mid- latitude (at Happo) is 80 % of the global average [*Jöckel et al.,* 1999]. Therefore, actual value of ^{14}CO production would be 40 % of 1.57, if there is no stratosphere-troposphere exchange. It is needed to discuss the meaning of the used value (1.57), which gives the best fitting to the observed ^{14}CO line in the box model calculation.

When 40 % of 1.57 is employed for the ^{14}CO production in the box model calculation, the results become too low. In the higher latitude, the production of ^{14}CO is larger. If air in the troposphere are well mixing and the higher ^{14}CO production in high latitude affect the ^{14}CO at Happo, this discrepancy could be explained. *Mak and Southon* [1998] also suggested faster mixing of tropospheric air from the comparison between the observation and 2D model calculation in tropic. Also small difference of observed ^{14}CO between Spitsbergen (79°N) and Happo (37°N) shown in Figure 7-10 supports this explanation.

The ^{14}CO production has no seasonal variation, but the intrusion of stratospheric air would have seasonal variation. The box model calculation did not include any seasonal change for ^{14}CO production. The good agreement between the observed ^{14}CO concentration and the result of the box model calculation indicated that the seasonal

variation of ^{14}CO intrusion is not large or OH seasonal variation used for the box model calculation need modification.

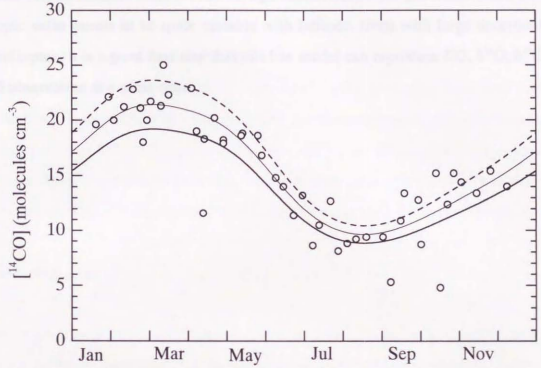

Figure 7-21. Model results of more and less ^{14}CO production. Thin solid lines represent the basic run (1.57), thick solid lines represent 1.77 and dotted lines represents 1.37 molecules cm^{-2} s^{-1}.

Box model calculations reproduce the observed results rather well. It is indicated that CO from biomass burning is enhanced in spring. The $\delta^{18}O$ value of CO from CH_4 oxidation and NMHC oxidation would be around zero. There is some limitation to a simple box model. There is a difficulty to choose suitable representative values for parameters. For more accurate descriptions, 2D or 3D model calculations should be needed. At this moment there are not enough measurements for detailed models, because isotopic value seems to be quite variable with latitude. Even with large uncertainty of model inputs, it is a good first step that this box model can reproduce CO, $\delta^{18}O$, $\delta^{13}C$ and ^{14}CO observation at a same time.

Chapter 8

Discussion using dilution plot and trajectory analysis at Happo

Using the plot of $\delta^{18}O$ and $\delta^{13}C$ against the reciprocal of CO concentration (dilution plot), CO sources are discussed from the intercepts of their regression lines. For all the seasons good correlation is observed. However it is due to just the normal seasonal cycle of the isotopic compositions of CO. For only limited season, the intercept would represent the isotopic compositions of CO sources. Also data affected by pollution in the Happo measurements are discussed. ^{14}CO is not affected by pollution from fossil fuel CO and higher CO polluted by this source can be distinguished easily. Backward trajectory analysis is applied for the Happo measurements and higher CO concentration and isotope ratios are found for westerly air mass, indicating enhanced human activity in that area. The lower ^{14}CO measurements are found to come mainly from the lower latitude.

8-1 Dilution plots

When plotting $\delta^{18}O$ and $\delta^{13}C$ against reciprocal CO (dilution plots), their intercept of least square fitting lines will give the isotopic composition of CO source, as explained in chapter 6-1-3. This analysis often used for the isotopic measurements and is applied to the Happo data. In Figure 8-1, $\delta^{18}O$ is plotted against reciprocal CO for all Happo data. Data affected by pollution are plotted by crosses. Negative correlation can be seen for the all measurements; $\delta^{18}O$ is lighter at lower CO concentration and heavy at higher CO concentration. In Figure 8-2, $\delta^{13}C$ values are plotted against reciprocal CO concentrations. Most of the data affected by pollution, shown by crosses, are clear outlier in this figure. Except for these data, there is a good negative correlation between $\delta^{13}C$ and 1/[CO]. The regression line for these clean measurements is given in Figure 8-2.

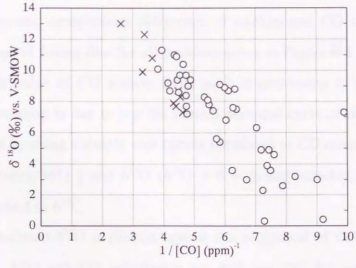

Figure 8-1. Dilution plot for $\delta^{18}O$ of all Happo measurements. Data affected by pollution are plotted by crosses.

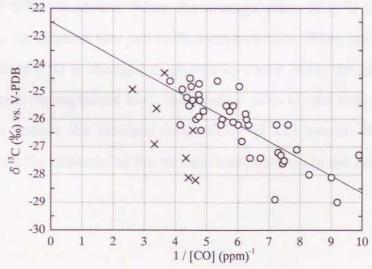

Figure 8-2. Dilution plot for $\delta^{13}C$ of all Happo measurements. Data affected by pollution are plotted by crosses. The regression line for clean air is given by a solid line.

In general the analysis using dilution plots can be applied for a short period when the concentration and isotopic composition difference of background CO can be ignored. Therefore the intercept of fitting line for all measurements in Figure 8-1 and 8-2 do not represent the isotopic value of CO source. Even so it is interesting to find their good correlation. This correlation is due to just the natural seasonal cycle of the CO isotopes. Here this is explained by using a simple sine curves simulated to CO concentration ([CO] = 170 + 60×sin(2×π×day/365)) and $\delta^{18}O$ ($\delta^{18}O$ = 6 + 5×sin(2×π×day/365)). Similar discussion can be applied to $\delta^{13}C$.

In Figure 8-3a, simulated $\delta^{18}O$ is plotted against the reciprocal of CO concentration. When the phase of $\delta^{18}O$ and CO calculation are different (30 day and 60 day), the seasonal cycle makes a loop as shown by dotted lines. The swelling becomes larger as the difference of the phase becomes larger. Further, the line of the seasonal cycle becomes almost circle and then forms a line with totally opposite trend when the phase difference is maximum (π or 182.5 day).

In Figure 8-3b, the results changing the average value of $\delta^{18}O$ and amplitude of the seasonal variation of $\delta^{18}O$ are shown. When the average value of $\delta^{18}O$ is changed as plotted by solid lines, the dilution plot just shifts systematically. When the amplitude of the seasonal variation of $\delta^{18}O$ is changed as plotted by doted lines, the gradient of the dilution plot is changed. As explained here, the dilution plots for the time series over a whole year does not deduce the isotopic composition of CO source. However, this analysis could represent the character of the isotopic compositions in the sampling sites.

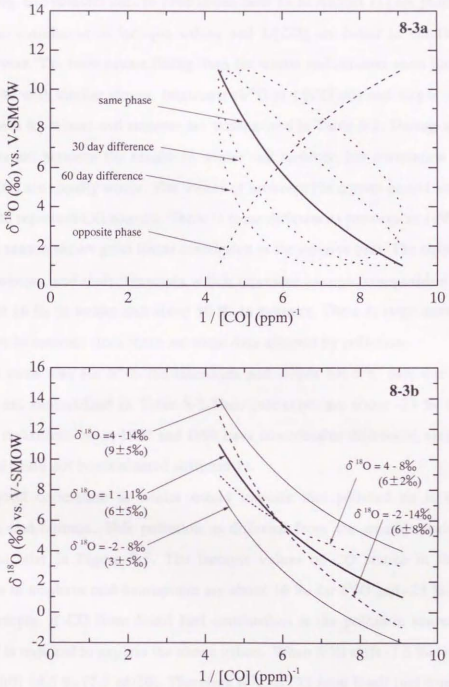

Figure 8-3. Dilution plot for simulated CO and $\delta^{18}O$. Phases of the seasonal variations of CO and $\delta^{18}O$ are changed (a). $\delta^{18}O$ values are changed in same phase (b).

The dilution plots can be applied for a certain season. In Figure 8-4 winter data in 1997 (from February 10 to March 17) are plotted by square (□), which have very little scatter (R^2= 0.99), and summer data in 1998 (from June 15 to August 11) are plotted by triangle (△). The correlation of isotopic values and 1/[CO] are better in certain season than whole a year. The least square fitting lines for winter and summer seem just to be shifted about 6 ‰ with similar slopes. Intercepts ($\delta^{18}O$ at 1/[CO]=0) and slopes of least square fitting lines for winter and summer are summarized in Table 8-1. During spring and fall, intercepts are between the results in winter and summer, but correlation between $\delta^{18}O$ and 1/[CO] are usually worse. The values of intercept for certain period shown in Figure 8-4 would represent CO sources. There is some differences between in 1997 and in 1998, but each season shows good linear correlation in the dilution plot. The slope is about -1.1 for all seasons, and their intercepts which represent isotopic composition of CO source are about 16 ‰ in winter and about 10 ‰ in summer. There is large uncertainty on the intercepts in summer since there are some data affected by pollution.

In the same way for $\delta^{18}O$, the intercepts and slopes for $\delta^{13}C$ data during winter and summer are summarized in Table 8-2.Their intercepts are about -23 ‰ in winter. The summer measurements in 1997 and 1998 have considerable difference, since the effect of pollution could not be eliminated sufficiently.

The good correlation in winter would indicate that polluted air is well mixed in northern mid-latitude. This pollution is different from the smaller scale pollution as explained later in Figure 8-5. The isotopic values of CO source in this large scale pollution in northern mid-hemisphere are about 16 ‰ for $\delta^{18}O$ and -23 ‰ for $\delta^{13}C$ from the intercepts. If CO from fossil fuel combustion is the pollution source, the KIE by CO+OH is required to explain the above values. When $\delta^{18}O$ shift -7.5 ‰ (16 - 23.5), $\delta^{13}C$ should shift +4.5 ‰ (7.5 ×6/10). Therefore $\delta^{13}C$ of CO from fossil fuel combustion needs to be -27.5 ‰ (-23-4.5), which is close to that of CO from fossil fuel combustion. Therefore, it is a persuasive explanation that CO from fossil fuel combustion is well mixed in the northern mid-latitude in winter. For the intercepts in summer, however the error would be large, lighter $\delta^{18}O$ and heavier $\delta^{13}C$ in 1998 are consistent with above explanation.

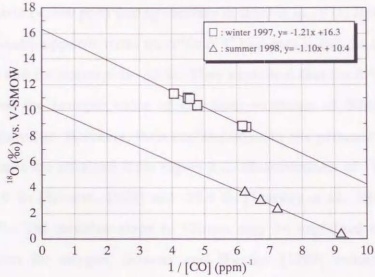

Figure 8-4. Dilution plot of $\delta^{18}O$ in winter and in summer

Table 8-1. Characters of the regression lines for $\delta^{18}O$ data

	intercept	slope	R^2	period
winter 97	16.3±0.3	-1.21±0.05	0.993	Feb.10 - Mar. 17, 1997
summer 97	12.8±0.5	-1.08±0.07	0.977	Jun. 23 - Sep. 15, 1997
winter 98	15.3±1.13	-1.14±0.22	0.870	Jan. 19- Mar. 13, 1998
summer 98	10.4±0.37	-1.10±0.05	0.996	Jun.15 - Aug. 11, 1998*

* except for the data of June 30

Table 8-2. Characters of the regression lines for $\delta^{13}C$ data

	intercept	slope	R^2	period
winter 97	-22.7±1.0	-0.62±0.19	0.793	Feb.10 - Mar. 17, 1997
summer 97	-25.0±2.0	-0.38±0.26	0.525	Jun. 23 - Sep. 15, 1997*
winter 98	-23.6±0.5	-0.40±0.11	0.755	Jan. 19- Mar. 13, 1998
summer 98	-20.1±2.3	-0.95±0.31	0.729	Jun.15 - Aug. 11, 1998

* except for the data affected by pollution.

Stevens and Wagner [1989] showed the dilution plots for the measurements of only low concentration data (< 200 ppb) during summer in Illinois in 1971. But interestingly, their results show totally opposite trend for $\delta^{13}C$; $\delta^{13}C$ becomes lighter as increase of CO (decrease of 1/CO) and its intercept is -32 ‰. They explained that the $\delta^{13}C$ value of the intercept represented the isotopic value of CO from oxidation of NMHC and some researchers used this value. However, their explanations are not persuasive enough and totally different results are obtained from Figure 8-2. Measurements of $^{13}C/^{12}C$ ratio for isoprene show -27.9 ‰ [*Stevens*, 1993] and -29.4 ‰ [*Sharkey et al.*, 1991], which are heavier than -32 ‰. The positive slope in Illinois may be explained by the KIE as discussed later. Also for oxygen, *Stevens and Wagner* [1989] estimated from the intercept that $\delta^{18}O$ of CO from NMHC and CH_4 oxidation was about 15‰. As demonstrated by the box model calculation (chapter 7-4), these values should be much lighter (5 ‰ for NMHC and 0‰ for CH_4 oxidation).

Some data affected by pollution are analyzed here. In Figure 8-5a, $\delta^{18}O$ values of the CO source for the pollution are estimated. Some data affected by pollution during summer (August-September) and winter (February) are plotted by solid circles. The open circles are the data without pollution, which are estimated from the seasonal cycle of the observed Happo measurements (Figure 7-11) for the period corresponding to the data affected by pollution. If pollution did not happen, solid circles should locate at open circles. The intercepts of the fitting lines for these data (shown by solid lines) should represent the isotope ratio of the polluted CO source. $\delta^{18}O$ for summer samples are about 13 ‰, and winter samples have about 17 ‰. These values are clearly lower than the $\delta^{18}O$ value of car exhausts. Also for $\delta^{13}C$, data affected by pollution are analyzed in Figure 8-5b in a similar way. The dotted line is the regression line for the clean air in Figure 8-2. $\delta^{13}C$ values of CO sources are about -28 ‰ and -25 ‰ for summer and winter, respectively.

Summer samples are thought to be polluted during traveling over Japan, where car exhaust is the main CO source. $\delta^{13}C$ values (-28 ‰) are consistent with this expectation, but $\delta^{18}O$ values (13 ‰) are significantly lighter than CO from car exhaust. These data are measured in summer, so enhanced reaction with OH may provide light CO by the large KIE for $\delta^{18}O$, but $\delta^{13}C$ also needs to be changed by the KIE at the same time. If $\delta^{18}O$ shifts 10 ‰ (23.5 → 13.5 ‰), $\delta^{13}C$ needs to shift about 6 ‰ heavier and becomes -21 ‰ (-27 ‰ + 6 ‰). Therefore the data affected by pollution during summer cannot be explained as car exhaust. If there is enough OH concentration, the winter data can be explained as car exhaust modified by the KIE, about half extent of the above KIE shift.

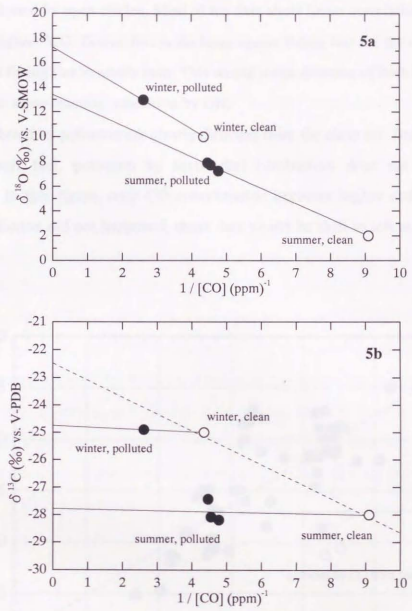

Figure 8-5. Source estimation plots (dilution plots) on some data affected by pollution of Happo data for $\delta^{18}O$ (5a) and $\delta^{13}C$ (5b). Open circles are estimated from the seasonal cycle for clean air. The dotted line in 5b is the regression line for clean air shown in Figure 8-2.

^{14}CO concentration is plotted against CO concentration in Figure 8-6.Data affected by pollution are plotted by open circles. Most of the data show linear correlation, higher CO accompanies higher ^{14}CO. Dotted line is the least square fitting line for the clean air. The intercept of the fitting line is nearly zero. This would mean decrease of both CO and ^{14}CO is caused by the same reaction; oxidation by OH.

The data affected by pollution are clearly different from the clean air. Because there is no ^{14}C in fossil fuel, pollution by fossil fuel combustion does not affect ^{14}CO concentration. In this figure, only CO concentration becomes higher and ^{14}CO is not affected. If pollution did not happened, those data would be shift to left as indicated by an arrow.

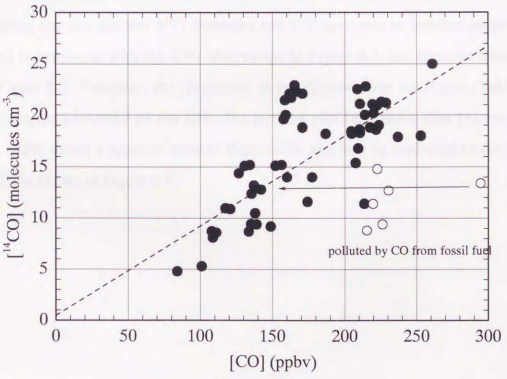

Figure 8-6. Correlation between ^{14}CO concentration and CO concentration. Data affected by pollution are plotted by open circles. The dotted line is the least square fitting for the clean air.

8-2 KIE calculation

It has been explained that isotopic compositions are changed by CO mixing from CO sources. There is another factor to change the isotopic ratios of atmospheric CO; the KIE of CO sink reaction (CO + OH). In Figure 8-7 and 8-8, the calculated δ values using the Rayleigh's Equation (Eq.2-8) are shown for $\delta^{18}O$ and $\delta^{13}C$, respectively.

$$\delta_{fin} = \delta_{ini} + (1000 + \delta_{ini}) \times (1/\alpha - 1) \times \log([CO]_{fin}/[CO]_{ini}) \quad \text{(Eq.2-8)}$$

Here, the initial CO concentrations are assumed as 1 ppm (●), 05 ppm (△) and 0.3 ppm (□) and initial $\delta^{18}O$ is 24 ‰ and initial $\delta^{13}C$ is -27 ‰ (urban air). If one wants to start from different initial $\delta^{18}O$ and $\delta^{13}C$, the curves are just shifted in vertical direction. In these figures, one can see that $\delta^{18}O$ decreases and $\delta^{13}C$ increases as reaction progresses. This trend is consistent with the $\delta^{18}O$ observation in Figure 8-1, but opposite trends for $\delta^{13}C$ in Figure 8-2. Therefore, the correlation in the dilution plots for Happo (Table 8-1 and 8-2) can not explained by the KIE. The dilution plot for Illinois data [*Stevens and Wagner*, 1989] shows a opposite trend to Happo data, and may be explained by the effect of the KIE as shown in Figure 8-8.

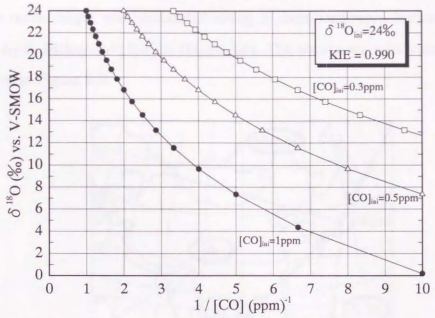

Figure 8-7. Calculated $\delta^{18}O$ change caused by the KIE of CO+OH

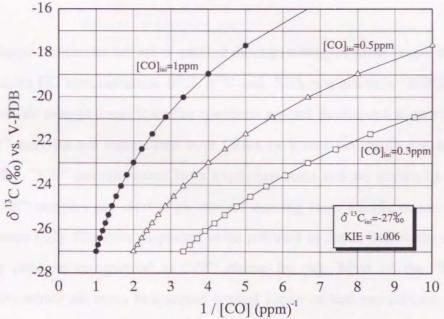

Figure 8-8. Calculated $\delta^{13}C$ change caused by the KIE of CO+OH

8-3 Trajectory analysis

The air mass origin was calculated using 5 days isentropic backward trajectory [provided by S. Maksyutov] for the Happo data. The air masses were categorized into 4 areas shown in Figure 8-9.

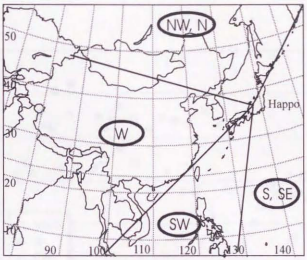

Figure 8-9. Air mass categories for backward trajectory analysis.

The Happo measurements are re-plotted distinguishing air mass origin in Figure 8-10a, b, c and d for CO concentration, $\delta^{18}O$, $\delta^{13}C$ and ^{14}CO, respectively. "NW,N" samples are continental air masses come from the continent around Russia and shown by open circles (○). "W" samples are transported over China or Korea peninsula and shown by solid circles (●). "SW" samples come from south-east Asia and are shown by open triangles (△). "S,SE" samples are marine air masses coming from Pacific ocean and shown by open squares (□). The data suspected to be polluted in Japan before the air reached the sampling site are categorized as "JP" shown by (×). Most of the "JP" data have trajectories which air mass had stayed around Japan or had passed over Japan. During winter, Siberian high pressure is dominant, and most air masses come from NW,N and W. During summer, Pacific high pressure is dominant and most air masses come from S,SE and crossing Japan island. Therefore some data are polluted in Japan. In Figure 8-10a, it can be seen that there are two trend in summer; high CO concentration are W or JP and low CO concentration are other air masses. This different trends are more clear for $\delta^{18}O$

in Figure 8-10b. In this way the back trajectory categorization can explain the CO concentration fluctuation, especially in summer. In Figure 8-10d, the lower ^{14}CO measurements from the seasonal variation as labeled by arrows originated from S,SE. This result is consistent with the fact that ^{14}CO concentration is lower in low latitude than mid-latitude.

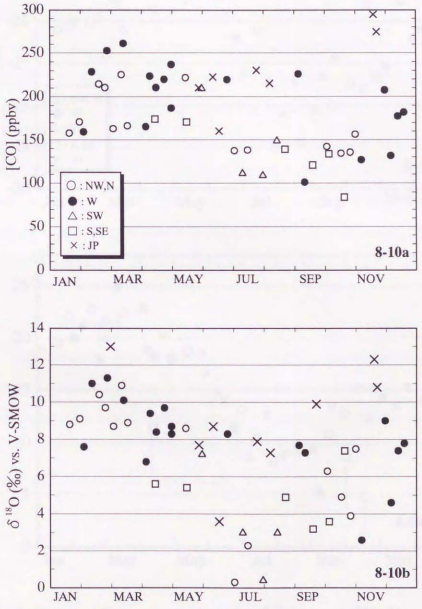

Figure 8-10ab. Trajectory analysis for CO concentration (a) and $\delta^{18}O$ (b)

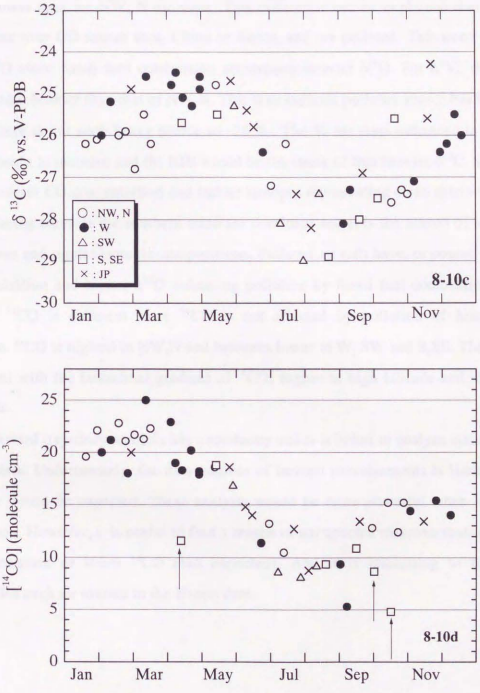

Figure 8-10cd. Trajectory analysis for $\delta^{13}C$ (c) and ^{14}CO (d). Arrows indicate low ^{14}CO from S,SE.

The average of categorized values for CO concentration, $\delta^{18}O$, $\delta^{13}C$ and ^{14}CO are summarized in Table 8-3, and are compared in Figure 8-11. CO concentration is higher for W air mass than for NW, N air mass. This difference can be explained that W air masses come over CO source area, China or Korea, and are polluted. This trend is also seen in $\delta^{18}O$ since fossil fuel combustion accompany heavier $\delta^{18}O$. For $\delta^{13}C$, the data from W is also heavier than that of NW,N. This may indicate polluted source has heavier $\delta^{13}C$, but there is not such heavy source as -26 ‰. The W air mass enhanced in spring when OH begin to increase and the KIE would be the cause of this heavier $\delta^{13}C$. SW and S,SE have lower CO concentration and lighter isotopes representing clean marine air. In addition, during summer the southern wind are dominant and it is the season of low CO concentration and lighter isotopic compositions. Polluted air (JP) have, of course, higher CO concentration and higher $\delta^{18}O$ indicating pollution by fossil fuel combustion. The results on ^{14}CO is different since ^{14}CO is not affected by pollution of fossil fuel combustion. ^{14}CO is highest in NW,N and becomes lower to W, SW and S,SE. This trend is consistent with the latitudinal gradient of ^{14}CO; higher in high latitude and lower in low latitude.

The backward trajectory analysis has uncertainty and it is better to analyze statistically for many data. Unfortunately, the data number of isotope measurements is limited and some error would be expected. These analysis would be more powerful when limiting only a season. However, it is useful to find a reason of unexpected measurements (higher CO concentration or lower ^{14}CO than expected). And it is interesting to find the difference for each air masses in the Happo data.

Table 8-3. Average of CO, $\delta^{18}O$, $\delta^{13}C$ and ^{14}CO for different air mass origins

	NW, N	W	SW	S, SE	JP
(n)	(14)	(20)	(4)	(6)	(8)
[CO] (ppb)	169.6	197.7	144.5	137.1	251.9
standard deviation	32.8	45.5	50.6	32.6	67.6
$\delta^{18}O$ (‰ V-SMOW)	7.2	8.2	3.4	5.0	8.8
standard deviation	3.2	2.0	3.4	1.7	3.0
$\delta^{13}C$ (‰ V-PDB)	-26.4	-25.8	-27.5	-26.9	-26.1
standard deviation	0.8	1.0	1.9	1.5	1.1
^{14}CO (molecule cm^{-3})	17.8	16.9	10.7	10.7	14.5
standard deviation	4.3	5.1	4.7	2.7	3.1

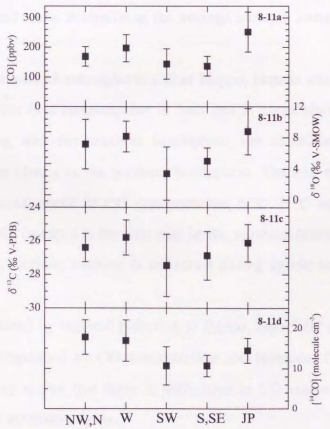

Figure 8-11. Comparison of averaged CO, $\delta^{18}O$, $\delta^{13}C$ and ^{14}CO for the different air mass categories. Error bars are for 1 σ deviation.

Summary and Conclusion

Isotopic measurements of atmospheric CO offer more information on CO sources and CO behavior in the atmosphere. Since isotopic information of CO sources is not enough, exhaust from gasoline cars, diesel cars and natural gas buses have been measured. Their isotopic compositions are different reflecting their fuels and combustion processes. From the atmospheric CO measurements at urban area, Mainz, the pollution of CO from car exhaust can be seen clearly using $\delta^{18}O$ values. Isotopic measurements, especially $\delta^{18}O$, are good indicators to assess CO pollution from car exhaust.

Biomass burning is one of the most important CO sources. The stable isotopic compositions of CO from biomass burning experiments are measured and observed large isotopic fluctuation as burning becomes smoldering condition. This large fluctuation should be considered when determining the average isotopic compositions of CO from biomass burning.

Isotopic compositions of atmospheric CO at Happo, remote site in Japan, have been measured. This is the first measurement in Asia and in clean sites in the northern mid latitude. Comparing with the southern hemisphere, the contribution from fossil fuel exhaust can be seen clearly in the northern hemisphere. The box model calculation can reproduce the seasonal cycle of CO concentration, $\delta^{18}O$, $\delta^{13}C$ and ^{14}CO. This model calculation for stable isotopes is the first trial in the northern hemisphere. It is expected that CO flux from biomass burning is enhanced during spring to explain the "spring peak".

Some air is affected by regional pollution at Happo, especially during summer. They can be clearly distinguished by CO concentration and isotopes. The categorization by back ward trajectory shows that there is difference in CO concentration and isotopic values for different air mass origins.

References

Akimoto, H., H. Nakane, and Y. Matsumoto, The chemistry of oxidant generation: Tropospheric ozone increase in Japan, in Chemistry of the atmosphere: The impact of global change, *edited by J. Carvert, Blackwell Science Publications*, 261-273, 1994.

Akimoto, H., H. Mukai, M. Nishikawa, K. Murano, S. Hatakeyama, C.-M. Liu, M. Buhr, K.J. Hsu, D.A. Jaffe, L. Zhang, R. Honrath, J.T. Merrill, and R. E. Newell, Long-range transport of ozone in the East Asian Pacific rim region, *Journal of Geophysical Research*, *101* (D1), 1999-2010, 1996.

Akimoto, Tropospheric ozone production and transport at Northwest Asia and pacific rim region (Japanese), *Chikyu- Kankyo*, *2* (1), 21-31, 1997.

Baker, R.R., Formation of carbon oxides during tobacco combustion: Pyrolysis studies in the presence of isotopic gases to elucidate reaction sequence, *Journal of Analytical and Applied Pyrolysis*, *4*, 297-334, 1983.

Bates, T.S., K.C. Kelly, J.E. Johnson, and R.H. Gammon, Regional and seasonal variations in the flux of oceanic carbon monoxide to the atmosphere, *Journal of Geophysical Research*, *100* (D11), 23093-23101, 1995.

Bergamaschi, P., C. Brühl, C.A.M. Brenninkmeijer, G. Saueressig, J.N. Crowley, J.U. Grooss, H. Fischer, and P.J. Crutzen, Implications of the large carbon kinetic isotope effect in the reaction CH_4 + Cl for the $^{13}C/^{12}C$ ratio of stratospheric CH_4, *Geophysical Research Letters*, *23* (17), 2227-2230, 1996.

Bergamaschi, P., C.A.M. Brenninkmeijer, M. Hahn, T. Röckmann, N.F. Elansky, I.B. Belikov, N. Trivett, and D. Worthy, Isotope analysis based source identification for atmospheric CH_4 and CO sampled across Russia using the Trans-Siberian railroad, *Journal of Geophysical Research*, *103* (D7), 8227-8235, 1998.

Brenninkmeijer, C.A.M., Deuterium, oxygen-18 and carbon-13 in tree rings and peat deposits in relation to climate, *Doctoral thesis, University of Groningen, The Netherlands*, 1983.

Brenninkmeijer, C.A.M., P. Kraft, and W.G. Mook, Oxygen isotope fractionation between CO_2 and H_2O, *Isotope Geoscience*, *1*, 181-190, 1983.

Brenninkmeijer, C.A.M., Robust, high-efficiency, high-capacity cryogenic trap, *Anal. Chem.*, *63*, 1182-1184, 1991.

Brenninkmeijer, C.A.M., M.R. Manning, D.C. Lowe, G. Wallace, R.J. Sparks, and A. Volz-Thomas, Interhemispheric asymmetry in OH abundance inferred from measurements of atmospheric ^{14}CO, *NATURE*, *356* (5 March), 50-52, 1992.

Brenninkmeijer, C.A.M., Measurement of the abundance of ^{14}CO in the atmosphere and the $^{13}C/^{12}C$ and $^{18}O/^{16}O$ ratio of atmospheric CO with applications in New Zealand and Antarctica, *Journal of Geophysical Research*, *98* (D6), 10595-10614, 1993.

Brenninkmeijer, C.A.M., and P.A. Roberts, An air-driven pressure booster pump for aircraft-based air sampling, *Journal of Atmospheric and Oceanic Technology*, *11*, 1664-1671, 1994.

Brenninkmeijer, C.A.M., D.C. Lowe, M.R. Manning, R.J. Sparks, and P.F.J. Velthoven, The ^{13}C, ^{14}C, and ^{18}O isotopic composition of CO, CH_4, and CO_2 in the higher southern latitudes lower stratosphere, *Journal of Geophysical Research*, *100* (D12), 26163-26172, 1995.

Brenninkmeijer, C.A.M., R. Müller, P.J. Crutzen, D.C. Lowe, M.R. Manning, R.J. Sparks, and P.F.J. Velthoven, A large ^{13}CO deficit in the lower Antarctic stratosphere due to "ozone hole" chemistry : Part 1, observations, *Geophysical Research Letters*, *23* (16), 2125-2128, 1996.

Brenninkmeijer, C.M.A., and T. Röckmann, Russian doll type cryogenic traps: Improved design and

isotope separation effects, *Anal. Chem.*, *68*, 3050-3053, 1996.

Brenninkmeijer, C.A.M., and T. Röckmann, Principal factors determining the $^{18}O/^{16}O$ ratio of atmospheric CO as derived from observations in the southern hemispheric troposphere and lowermost stratosphere, *Journal of Geophysical Research*, *102* (D21), 25477-25485, 1997.

Brenninkmeijer, C.A.M., T. Röckmann, M. Bräunlich, P. Jöckel, and P. Bergamaschi, Review of progress in isotope studies of atmospheric carbon monoxide, *Chemosphere*, in press (1999).

Cahoon Jr, D.R., B.J. Stocks, J.S. Levine, W.R. Cofer III, and P.J. M., Satellite analysis of the severe 1987 forest fires in northern China and southern Siberia, *Journal of Geophysical Research, 99* (D9), 18627-18638, 1994.

Cantrell, C.A., R.E. Shetter, A.H. McDaniel, J.G. Calvert, J.A. Davidson, D.C. Lowe, S.C. Tyler, R.J. Cicerone, and J.P. Greenberg, Carbon kinetic isotope effect in the oxidation of Methane by the Hydroxyl radical, *Journal of Geophysical Research*, *95* (D13), 22455-22462, 1990.

Chan, W.H., W.M. Uselman, J.G. Calvert, and J.H. Shaw, *Chemical Pysics Letter*, *45*, 240, 1977.

Cliff, S.S., and M.H. Thiemens, The $^{18}O/^{16}O$ and $^{17}O/^{16}O$ ratios in atmospheric nitrous oxide: a mass-independent anomaly, *Science*, *278*, 1774-1775, 1997.

Conny, J.M., and L.A. Currie, The isotopic characterization of methane, non-methane hydrocarbons and formaldehyde in the troposphere, *Atmospheric Environment*, *30* (4), 621-638, 1996.

Conny, J.M., R.M. Verkouteren, and L.A. Currie, Carbon 13 composition of tropospheric CO in Brazil: A model scenario during the biomass season, *Journal of Geophysical Research*, *102* (D9), 10683-10693, 1997.

Conny, J.M., The isotopic characterization of carbon monoxide in the troposphere, *Atmospheric Environment*, *32*, 2669-2683, 1998.

Craig, H., Isotopic standards for carbon and oxygen and correction factors for mass spectrometric analysis of carbon dioxide, *Geochim. Cosmochim. Acta*, *12*, 133-149, 1957.

Crutzen, P.J., L.E. Heidt, J.P. Krasnec, W.H. Pollock, and W. Seiler, Biomass burning as a source of atmospheric gases CO, H_2, N_2O, NO, CH_3Cl and COS, *Nature*, *282* (15), 253-256, 1979.

Crutzen, P.J., and M.O. Andreae, Biomass burning in the tropics impact on atmospheric chemistry and biogeochemical cycles, *Science*, *250*, 1669-1678, 1990.

Crutzen, P.J., and P.H. Zimmermann, The changing photochemistry of the troposphere, *Tellus*, *43AB*, 136-151, 1991.

Crutzen, P.J., N.F. Elansky, M. Hahn, G.S. Golitsyn, C.A.M. Brenninkmeijer, D.H. Scharffe, I.B. Belikov, M. Maiss, P. Bergamaschi, T. Röckmann, A.M. Grisenko, and V.M. Sevostyanov, Trace gas measurements between Moscow and Vladivostok using trains-Siberian railroad, *Journal of Atmospheric Chemistry*, *29*, 179-194, 1998.

Currie, L.A., G.A. Klouda, J. Schjoldager, and T. Ramdahl, The power of ^{14}C measurements combined with chemical characterization for tracing urban aerosol in Norway, *Radiocarbon*, *28* (2A), 673-680, 1986.

Davidson, J.A., C.A. Cantrell, S.C. Tyler, R.E. Shetter, R.J. Cicerone, and J.G. Calvert, Carbon kinetic isotope effect in the reaction of CH_4 with HO, *Journal of Geophysical Research*, *92* (D2), 2195-2199, 1987.

DeMore, W.B., S.P. Sander, D.M. Golden, R.F. Hampson, M.J. Kurylo, C.J. Howard, C.J. Ravishankara, C.E. Kolb, and M.J. Molina, Chemical kinetics and photochemical data for use in stratospheric modeling, *JPL publication 97-4, Evaluation Number 12*, 1997.

Derwent, R.G., P.G. Simmonds, S. Seuring, and C. Dimmer, Observation and interpretation of the seasonal cycles in the surface concentrations of ozone and carbon monoxide at Mace Head, Ireland from 1990 to 1994, *Atmospheric Environment*, *32* (2), 145-157, 1998.

Felton, C.C., J.C. Sheppard, and M.J. Campbell, measurements of the diurnal OH cycle by a ^{14}C-

tracer method, *Nature, 335*, 53-55, 1988.

Felton, C.C., J.C. Sheppard, and M.J. Campbell, The radiochemical hydroxyl radical measurement method, *Environmental Science and Technology, 24*, 1841-1847, 1990.

Gemery, P.A., M. Trolier, and J.W.C. White, Oxygen isotope exchange between carbon dioxide and water following atmospheric sampling using glass flasks, *Journal of Geophysical Research, 101* (D9), 14415-14420, 1996.

Gonfiantini, R., Standards for stable isotope measurements in natural compounds, *Nature, 271* (9 February), 534-536, 1978.

Greenberg, J.P., D. Helming, and P.R. Zimmerman, Seasonal measurements of nonmethane hydrocarbons and carbon monoxide at the Mauna Loa Observatory during the Mauna Loa Observatory Photochemistry Experiment 2, *Journal of Geophysical Research, 101* (D9), 14581-14598, 1996.

Gruenther, A., C.N. Hewitt, D. Erickson, R. Fall, C. Geron, T. Graedel, P. Harley, L. Klinger, M. Lerdau, W.A. McKay, T. Pierce, B. Scholes, R. Steinbrecher, R. Tallamraju, J. Taylor, and P. Zimmerman, A global model of natural volatile organic compound emissions, *Journal of Geochemical Research, 100* (D5), 8873-8892, 1995.

Gupta, M.L., M.P. McGrath, R.J. Cicerone, F.S. Rowland, and M. Wolfsberg, $^{12}C/^{13}C$ kinetic isotope effects in the reactions of CH_4 with OH and Cl, *Geophysical Research Letters, 24* (22), 2761-2764, 1997.

Haan, D., P. Martinerie, and D. Raynaud, Ice core data of atmospheric carbon monoxide over Antarctica and Greenland during the last 200 years, *Geophysical Research Letters, 23* (17), 2235-2238, 1996.

Huff, A.H., and M.H. Thiemens, $^{17}O/^{16}O$ and $^{18}O/^{16}O$ isotope measurements of atmospheric carbon monoxide and its sources, *Geophysical Research Letters, 25* (18), 3509-3512, 1998.

Jaffe, D.A., R.E. Honrath, L. Zhang, H. Akimoto, A. Shimizu, H. Mukai, K. Murano, S. Hatakeyama, and J. Merrill, Measurements of NO, NO_y, CO and O_3 and estimation of the ozone production rate at Okilsland, Japan, during PEM-West, *Journal of Geophysical Research, 101* (D1), 2037-2048, 1996.

Jaffe, D., A. Mahura, J. Kelley, and J. Atkins, Impact of Asian emissions on the remote North Pacific atmosphere: Interpretation of CO data from Shemya, Guam, Midway and Mauna Loa, *Journal of Geophysical Research, 102* (D23), 28627-28635, 1997.

Jöckel, P., M.G. Lawrence, and C.A.M. Brenninkmeijer, Simulations of cosmogenic ^{14}CO using the three-dimensional atmospheric model MATCH: effects of ^{14}C production distribution and the solar cycle, *Journal of Geophysical Research*, in press (1999).

Johnson, B.J., and G.A. Dawson, Collection of Formaldehyde from clean air for Carbon isotope analysis, *Environmental Science and Technology, 24* (6), 898-902, 1990.

Johnson, J.E., and T.S. Bates, Source and sink of carbon monoxide in mixed layer of the tropical South Pacific Ocean, *Global Biogeochemical Cycles, 10* (2), 347-359, 1996.

Johnston, J.C., and M.H. Thiemens, The isotopic composition of tropospheric ozone in the environments, *Journal of Geophysical Research, 102* (D21), 25395-25404, 1997.

Kajii, Y., H. Akimoto, Y. Komazaki, S. Tanak, H. Mukai, K. Murano, and H.T. Merrill, Long-range transport of ozone, carbon monoxide, and acidic trace gases at Oki Island, Japan, during PEM-WEST B / PEACAMPOT B campaign, *Journal of Geophysical Research, 102* (D23), 28637-28649, 1997.

Kajii, Y., K. Someno, H. Tanimoto, J. Hirokawa, and H. Akimoto, Evidence for the seasonal variation of photochemical activity of tropospheric ozone: Continuous observation of ozone and CO at Happo, Japan, *Geophysical Research Letters, 25* (18), 3505-3508, 1998.

Kato, N., and H. Akimoto, Anthropogenic emissions of SO_2 and NO_x in Asia: Emission inventories, *Atmospheric Environment*, *26A*, 2997-3017, 1992.

Kato, S., H. Akimoto, M. Bräunlich, T. Röckmann, and C.A.M. Brenninkmeijer, Measurements of stable carbon and oxygen isotopic compositions of CO in automobile exhausts and ambient air from semi-urban Mainz, Germany, *Geochemical Journal*, *33*, 73-77, 1999.

Kato, S., H. Akimoto, T. Röckmann, M. Bräunlich, and C.A.M. Brenninkmeijer, Stable isotopic compositions of carbon monoxide from biomass burning experiments, *Atmospheric Environment*, in press (1999).

Kaye, J.A., Mechanisms and observations for isotope fractionation of molecular species in planetary atmospheres, *Reviews of Geophysics*, *25* (8), 1609-1658, 1987.

Khalil, M.A.K., and R.A. Rasmusssen, Carbon monoxide in the Earth's atmosphere: Increasing trend, *Science*, *224*, 54-56, 1984.

Khalil, M.A.K., and R.A. Rasmussen, Carbon monoxide in the Earth's atmosphere: Indications of a global increase, *Nature*, *332*, 242-245, 1988.

Khalil, M.A.K., and R.A. Rasmussen, Global decrease in atmospheric carbon monoxide, *Nature*, *370*, 639-641, 1994.

Klouda, G.A., L.A. Currie, D.J. Donahue, A.T.J. Jull, and M.H. Naylor, Urban atmospheric ^{14}CO and $^{14}CH_4$ measurements by accelerator mass spectrometry, *Radiocarbon*, *28* (2A), 625-633, 1986.

Klouda, G.A., L.A. Currie, R.M. Verkouteren, W. Einfeld, and B.D. Zak, Advances in microradiocarbon dating and the direct tracing of environmental carbon, *Journal of Radioanalytical and Nuclear Chemistry, Articles*, *123* (1), 191-197, 1988.

Krankowsky, D., F. Bartecki, G.G. Klees, K. Mauersberger, K. Schellenbach, and J. Stehr, Measurement of heavy isotope enrichment in tropospheric ozone, *Geophysical Research Letters*, *22* (13), 1713-1716, 1995.

Kroopnick, P., and H. Craig, Atmospheric oxygen: isotopic composition and solubility fractionation, *Science*, *175*, 54-55, 1972.

Lee, S., H. Akimoto, H. Nakane, S. Kurnosenko, and Y. Kinjo, Lower tropospheric ozone trend observed in 1989-1997 at Okinawa, Japan, *Geophysical Research Letters*, *25* (10), 1637-1640, 1998.

Lobert, J.M., D.H. Scharfe, W.M. Hao, and P.J. Crutzen, Importance of biomass burning in the atmospheric budget of nitrogen containing gases, *Nature*, *346*, 552-554, 1990.

Logan, J.A., M.J. Prather, S.C. Wofsy, and M.B. McElroy, Tropospheric chemistry: A global perspective, *Journal of Geophysical Research*, *86*, 7210-7254, 1981.

Lowe, D.C., C.A.M. Brenninkmeijer, S.C. Tyler, and E.J. Dlugkencky, Determination of the isotope composition of atmospheric methane and its application in the Antarctic, *Journal of Geophysical Research*, *96* (D8), 15455-15467, 1991.

Lowe, D.C., C.A.M. Brenninkmeijer, G.W. Brailsford, K.R. Lassey, and A.J. Gomez, Concentration and ^{13}C records of atmospheric methane in New Zealand and Antarctica: Evidence for changes in methane source, *Journal of Geophysical Research*, *99* (D8), 16913-16925, 1994.

MacKey, C., M. Pandow, and R. Wolfgang, On the chemistry of natural radiocarbon, *Journal of Geophysical Research*, *68* (13), 3929-3931, 1963.

Mak, J.E., Evidence for a missing carbon monoxide sink based on tropospheric measurements of ^{14}CO, *Geophysical Research letters*, *19* (14), 1467-1470, 1992.

Mak, J.E., C.A.M. Brenninkmeijer, and J. Tamaresis, Atmospheric ^{14}CO observations and their use for estimating carbon monoxide removal rates, *Journal of geophysical Research*, *99* (D11), 22915-22922, 1994.

Mak, J.E., and C.A.M. Brenninkmeijer, Compressed air sample technology for isotopic analysis of

atmospheric carbon monoxide, *Journal of Atmospheric and Oceanic Technology*, *11* (2), 425-431, 1994.

Mak, J.E., and C.A.M. Brenninkmeijer, Measurement of ^{13}CO and $C^{18}O$ in the free troposphere, *Journal of Geophysical Research*, *103* (D15), 19347-19358, 1998.

Mak, J.E., and J.R. Southon, Assessment of tropical OH seasonality using atmospheric ^{14}CO measurements from Barbados, *Geophysical Research Letters*, *25* (15), 2801-2804, 1998.

Manning, M.R., C.A.M. Brenninkmeijer, and W. Allen, Atmospheric carbon monoxide budget of the southern hemisphere: Implications of $^{13}C/^{12}C$ measurements, *Journal of Geophysical Research*, *102* (D9), 10,673-10,682, 1997.

Müller, R., C.A.M. Brenninkmeijer, and P.J. Crutzen, A large ^{13}CO deficit in the lower Antarctic stratosphere due to "ozone hole" chemistry : Part 2, Modeling, *Geophysical Research Letters*, *23* (16), 2129-2132, 1996.

Narita, D., P. Pochanart, J. Matsumoto, K. Someno, H. Tanimoto, J. Hirokawa, Y. Kajii, H. Akimoto, M. Nakao, T. Katsuno, and Y. Kinjo, Seasonal variation of carbon monoxide at remote sites in Japan, *Chemosphere*, in press (1999).

Novelli, P.C., L.P. Steele, and P.P. Tans, Mixing ratio of carbon monoxide in the troposphere, *Journal of Geophysical Research*, *97*, 20731-20750, 1992.

Novelli, P.C., K.A. Masarie, P.P. Tans, and P.M.L. Lang, Recent change in atmospheric carbon monoxide, *Science*, *263*, 1587-1590, 1994.

Novelli, P.C., K.A. Masarie, and P.M. Lang, Distributions and recent changes of carbon monoxide in the lower troposphere, *Journal of Geophysical Research*, *103* (D15), 19015-19033, 1998.

Pacyna, J.M., and T.E. Graedel, Atmospheric emissions inventories: Status and prospects, *Annu. Rev. Energy Environ.*, *20*, 265-300, 1995.

Pochanart, P., J. Hirokawa, Y. Kajii, and H. Akimoto, Surface ozone and carbon monoxide measurement at Oki islands, Japan, during March 1994 to February 1996, *Atmospheric Ozone, Proceedings of the XVII Quadrennial Ozone Symposium, edited by R.D. Bojkov and G. Visconti*, 571-574, 1996.

Pochanart, P., Characteristics of surface ozone and carbon monoxide in East Asia: The impact of long-range transport and anthropogenic activity, *Doctoral thesis, the University of Tokyo*, 1998.

Pochanart, P., J. Hirokawa, Y. Kajii, H. Akimoto, and M. Nakao, Influence of regional scale anthropogenic activity in Northeast Asia on seasonal variations of surface ozone and carbon monoxide observed at Oki, Japan, *Journal of Geophysical Research, 104*, 3621-3631, 1999.

Pochanart, P., J. Hirokawa, Y. Kajii, H. Akimoto, J. Kreasuwun, N. Chansombut, P. Sukasem, and M.S. Tabucanon, Tropical tropospheric ozone observed in Thailand, submitted to *Geophysical Research Letters*.

Prinn, R., D. Cunnold, P. Simmonds, F. Alyea, R. Boldi, A. Crawford, P. Fraser, D. Gutzler, D. Hartley, R. Rosen, and R. Rasmussen, Atmospheric trends in Methylchloroform and the global average for the OH radical, *Science*, *238*, 945-950, 1987.

Quay, P.D., S.L. King, J. Stutsman, D.O. Wilbur, L.P. Steele, I. Fung, R.H. Gammon, T.A. Brown, G.W. Farwell, P.M. Grootes, and F.H. Schmidt, Carbon isotopic composition of atmospheric CH_4: Fossil and biomass burning source strengths, *Global Biogeochemical Cycles*, *5* (1), 25-47, 1991.

Röckmann, T., and C.A.M. Brenninkmeijer, CO and CO_2 isotopic composition in Spitsbergen during the 1995 ARCTOC campaign, *Tellus*, *49B*, 455-465, 1997.

Röckmann, T., and C.A.M. Brenninkmeijer, The error in conventional reported $^{13}C/^{12}C$ ratios of atmospheric CO due to the presence of mass independent oxygen isotope enrichment, *Geophysical Research Letters*, *25* (16), 3163-3166, 1998.

Röckmann, T., C.A.M. Brenninkmeijer, P. Neeb, and P.J. Crutzen, Ozonolysis of nonmethane hydrocarbons as a source of the observed mass independent oxygen isotope enrichment in tropospheric CO, *Journal of Geophysical Research, 103* (D1), 1463-1470, 1998a.

Röckmann, T., C.A.M. Brenninkmeijer, G. Saueressig, P. Bergamaschi, J.N. Crowley, H. Fischer, and P.J. Crutzen, Mass-independent oxygen isotope fractionation in atmospheric CO as a result of the reaction CO + OH, *Science, 281*, 544-546, 1998b.

Röckmann, T., C.A.M. Brenninkmeijer, P.J. Crutzen, and U. Platt, Short-term variations in the $^{13}C/^{12}C$ ratio of CO as a measure of Cl activation during tropospheric ozone depletion events in the Arctic, *Journal of Geophysical Research, 104* (D1), 1691-1697, 1999.

Rotty, R.M., Estimates of seasonal variation in fossil fuel CO_2 emissions, *Tellus, 39B*, 184-202, 1987.

Rudolph, J., D.C. Lowe, R.J. Martin, and T.S. Clarkson, A novel method for compound specific determination of $\delta^{13}C$ in volatile organic compounds at ppt levels in ambient air, *Geophysical research Letters, 24* (6), 659-662, 1997.

Sakugawa, H., and I.R. Kaplan, Radio- and stable-isotope measurements of atmospheric carbon monoxide in Los Angeles, *Geochemical Journal, 31*, 75-83, 1997.

Saurer, M., S. Borella, and M. Leuenberger, $\delta^{18}O$ of tree rings of beech (Fague silvatica) as a record of $\delta^{18}O$ of the growing season precipitation, *Tellus, 49B*, 80-92, 1997.

Saueressig, G., P. Bergamaschi, J.N. Crowley, H. Fischer, and G.W. Harris, Carbon kinetic isotope effect in the reaction of CH_4 with Cl atoms, *Geophysical Research Letters, 22* (10), 1225-1228, 1995.

Schütze, M., Ein neues Oxidationsmittel für die quantitative Ueberfuerung von Kohlenoxyd in Kohlendioxyd, *Ein Beitrag zur Chemie des Jodpentoxyds, Ber. Dtsch. Chem. Ges., 77B*, 484-487, 1949.

Schüler, B., J. Morton, and K. mauersberger, Measurements of isotopic abundances in collected stratospheric ozone samples, *Geophysical Research Letter, 17*, 1295-1298, 1990.

Seilaer, W., and R. Conard, Contributions of tropical ecosystems to the global budgets of trace gases especially CH_4, H_2, CO and N_2O, *Geophysiology of Amazonia, edited by R. Dickinson, John Wiley, New York*, 133-162, 1987.

Smit, H.G.J., A. Volz, D.H. Ehhalt, and H. Knappe, The isotope fractionation during the oxidation of carbon monoxide by hydroxyl-radical and its implication for the atmospheric CO-cycle, *Stable Isotopes*, 147-152, 1982.

Sharkey, T.D., F. Loreto, C.F. Delwiche, and I.W. Treichel, Fractionation of carbon isotopes during biogenesis of atmospheric isoprene, *Plant Physiol., 97*, 436-466, 1991.

Springer-Young, M., D.J. Erickson III, and T.P. Carsey, Carbon monoxide gradients in the marine boundary layer of the North Atlantic Ocean, *Journal of Geophysical Research, 101* (D2), 4479-4484, 1996.

Spivakovsky, C.M., R. Yevich, J.A. Logan, S.C. Wofsy, and M.B. McElroy, Tropospheric OH in a three dimensional chemical tracer model: An assessment based on observations of CH_3CCl_3, *Journal of Geophysical Research, 95*, 18441-18471, 1990.

Stevens, C.M., and L. Krout, Method for the determination of the concentration and of the carbon and oxygen isotopic composition of atmospheric carbon monoxide, *International Journal of Mass Spectrometry and Ion Physics, 8*, 265-275, 1972.

Stevens, C.M., L. Krout, D. Walling, A. Venters, A. Engelkemeir, and L.E. Ross, The isotopic composition of atmospheric carbon monoxide, *Earth and Planetary Science Letters, 16*, 147-165, 1972.

Stevens, C.M., L. Kaplan, R. Gorse, S. Durkee, M. Compton, S. Cohen, and K. Bielling, The kinetics

isotope effect for carbon and oxygen in the reaction CO + OH, *International Journal of Chemical Kinetics*, *12*, 935-948, 1980.

Stevens, C.M., and A. Engelkemeir, Stable carbon isotopic composition of Methane from some natural and anthropogenic sources, *Journal of Geophysical Research*, *93* (D1), 725-733, 1988.

Stevens, C.M., and A.F. Wagner, The role of isotope fractionation effects in atmospheric chemistry, *Z. Naturforsch.*, *44a*, 376-384, 1989.

Stevens, Private communication with Conny mentioned in [Conny et al., 1996], 1993.

Thompson, A.M., The oxidation capacity of the Earth's atmosphere: Probable past and future changes, *Science*, *256*, 1157-1165, 1992.

Volz, A., D.H. Ehhalt and R.G. Derwent, Seasonal and latitudinal variation of ^{14}CO and the tropospheric concentration of OH radicals, *Journal of Geophysical Research*, *86* (C6), 5163-5171, 1981.

Wahlen, M., N. Tanaka, R. Henry, B. Deck, J. Zeglen, J.S. Vogel, J. Southon, A. Shemesh, R. Fairbanks, and W. Broecker, Carbon-14 in methane source and in atmospheric methane: The contribution from Fossil carbon, *Science*, *245*, 286-290, 1989.

Weinstock, B., Carbon monoxide: residence time in the atmosphere, *Science*, *166*, 224-225, 1969.

Weinstock, B., and H. Niki, Carbon monoxide balance in nature, *Science*, *176*, 290-292, 1972.

Weinstock, B., and T.Y. Chang, The global balance of carbon monoxide, *Tellus*, *26*, 108-115, 1974.

Zhao, Y., Y. Kondo, F.J. Murcray, X. Liu, M. Koike, K. Kita, H. Nakajima, I. Murata, and K. Suzuki, Carbon monoxide column abundances and tropospheric concentrations retrieved from high resolution ground-based infrared solar spectra at 43.5N over Japan, *Journal of Geophysical Research*, *102* (D19), 23403-23411, 1997.

Zimmerman, P.R., R.B. Chatfield, J. Fishman, P.J. Crutzen, and P.L. Hanst, Estimates on the production of CO and H_2 from the oxidation of hydrocarbon emissions from vegetation, *Geophysical Research Letters*, *5* (8), 679-682, 1978.

Acknowledgment

At first I would like to express my deep gratitude and sincerity to my academic supervisor, Professor Hajime Akimoto and to Dr. Carl A. M. Brenninkmeijer. This work would not realize without their comprehension and generosity. I am also deeply grateful to Professor Yoshizumi Kajii and Dr. Jun Hirokawa for their helps in measurements management and scientific discussion.

I would like to thank members of Max Planck Institute for Chemistry in Germany, especially Dr. Thomas Röckmann, Maya Bräunlich and Rolf Hofmann. I also grateful to Wolfgang Hanewacker for operation of the isotope mass spectrometer and construction of the air compressor, and Dr. Osamu Horie and Michael Hahn for comfortable staying in Germany.

I would like to thank Nagano Research Institute for Health and pollution, especially Takao Katsuno, and Happo-ike Sanso lodge for keeping the compressor and Sakurao Wakamatsu for air sampling at Happo.

I appreciate National Institute for Environmental Studies (NIES) for helping mass spectrometric measurements of Tokyo air. I also thanks to Dr. Nobu Ohte in Kyoto University for carbon isotopic measurements of plants.

Grateful acknowledgment is given to CREST (Core Research for Evolutional Science and Technology) of the Japan Science and Technology Corporation (JST) for funding this research.

I also cannot miss to extend my thanks to the members of Akimoto research group. They offer nice friendship and always encourage me, sometimes using special liquid.

And at last, I would like to thank my parents and sister for financial and mental support for a long time.

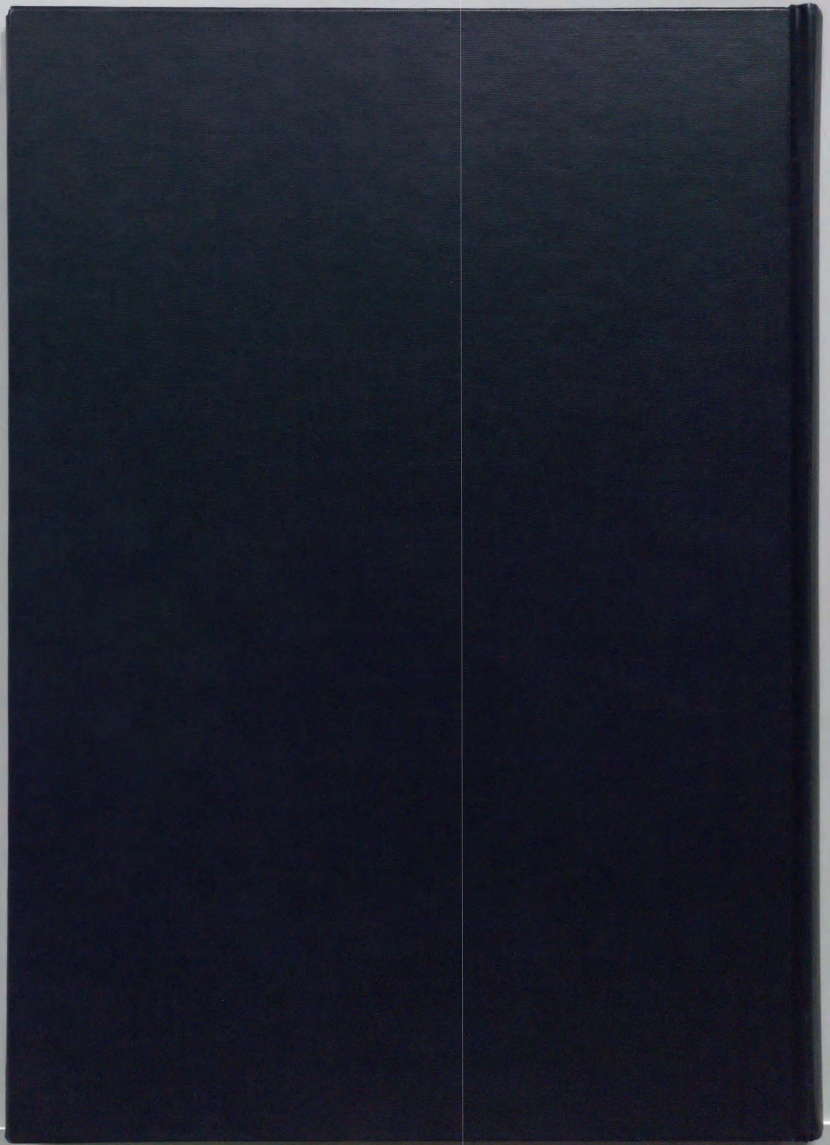

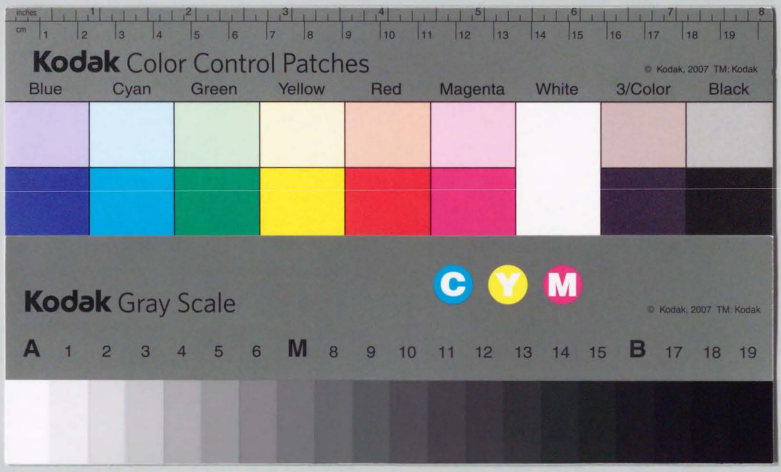
inches
cm
Kodak Color Control Patches
© Kodak, 2007 TM: Kodak
Blue
Cyan
Green
Yellow
Red
Magenta
White
3/Color
Black
Kodak Gray Scale
C
Y
M
© Kodak, 2007 TM: Kodak
A 1 2 3 4 5 6 M 8 9 10 11 12 13 14 15 B 17 18 19